LAPPEENRANTA UNIVERSITY OF TECHNOLOGY
LUT School of Engineering
Degree Program of Chemical Engineering

Jere Elfving

CHARACTERIZATION OF AMINE-BASED CO_2 ADSORBENT FOR DIRECT AIR CAPTURE

Examiners: Assoc. Prof. Satu-Pia Reinikainen
Ph. D Cyril Jose E. Bajamundi

ABSTRACT

Lappeenranta University of Technology
LUT School of Engineering
Degree Program of Chemical Engineering

Jere Elfving

Characterization of amine-based CO_2 adsorbent for Direct Air Capture

Master's thesis

2015

81 pages, 28 figures, 6 tables and 7 appendices

Examiners: Assoc. prof. Satu-Pia Reinikainen
Ph. D Cyril Jose E. Bajamundi

Keywords: Characterization, CO_2 adsorbent, direct air capture

Direct air capture technologies extract CO_2 from air at a concentration of as low as 400ppm. The captured CO_2 can be used for the production of synthetic methane or liquid fuels. In the literature survey of this thesis, results related to direct air capture by using solid sorbents are presented and critically discussed. In the experimental part, a proprietary amine functionalized resin is characterized for direct air capture. Structural comparison is also made to a commercial resin of similar type.

Based on the literature survey, the most important parameters in direct air capture process are low adsorption and desorption temperatures, good cyclic stability in dry and humid conditions, high CO_2 outlet purity and a high working capacity. Primary amine functionalized solid sorbents are found to often have good qualities for direct air capture, but overall process performance is rarely studied exhaustively.

Based on FTIR spectra, both resin adsorbents are found to be consisted of polystyrene functionalized with primary amine, and capture CO_2 by forming carbamate. The commercial resin is more porous, has a slightly higher particle size and contains fewer impurities. Important physical parameters are gained of the proprietary resin, such as internal porosity and median particle size. The resin's amine group is found to endure thermal treatment reasonably well. CO_2 adsorption capacity gained by thermal gravimetry from 400ppm CO_2 is highest at 25^oC, and is found to be reasonable compared to values presented in literature. Thus, the resin is stated to exhibit promising qualities for direct air capture.

TIIVISTELMÄ

Lappeenrannan teknillinen yliopisto
LUT School of Engineering
Kemiantekniikan koulutusohjelma

Jere Elfving

Amiinipohjaisen CO_2 adsorbentin karakterisointi hiilidioksidin talteenottoon ilmasta

Diplomityö

2015

81 sivua, 28 kuvaa, 6 taulukkoa ja 7 liitettä

Työn tarkastajat: Tutkijaopettaja Satu-Pia Reinikainen
FT Cyril Jose E. Bajamundi

Avainsanat: Karakterisointi, CO_2 adsorbentti, hiilidioksidin talteenotto ilmasta

Direct air capture- teknologioilla erotetaan hiilidioksidia suoraan ilmasta jopa vain 400ppm:n konsentraatiosta. Talteen otettua hiilidioksidia voidaan käyttää synteettisen metaanin tai nestemäisten polttoaineiden tuotantoon. Diplomityön kirjallisuuskatsauksessa esitetään erilaisilla direct air capture sorbenteilla saatuja keskeisimpiä tuloksia, ja tarkastellaan niitä kriittisesti. Kokeellisessa osuudessa yksityisomistuksellinen amiinilla funktionalisoitu hartsi karakterisoidaan direct air capture- prosessia varten. Lisäksi verrataan tämän hartsin rakennetta samantyyppiseen kaupalliseen hartsiin.

Kirjallisuuskatsaukseen perustuen, direct air capture- prosessin tärkeimmät parametrit ovat alhaiset adsorptio- ja desorptiolämpötilat, hyvä syklinen stabiliteetti kuivissa ja kosteissa olosuhteissa, korkea CO_2:n ulostulovirran puhtausaste, sekä korkea desorptiokapasiteetti. Primäärisellä amiinilla funktionalisoiduilla sorbenteilla on usein hyvät ominaisuudet direct air capture- prosesseja varten, mutta suorituskykyä kokonaisuudessaan tutkitaan harvoin kattavasti.

FTIR-spektreihin perustuen, kumpikin adsorbentti koostuu primäärisellä amiinilla funktionalisoidusta polystyreenistä, ja kaappaavat hiilidioksidia muodostaen karbamaattia. Kaupallinen hartsi on huokoisempi, sillä on hieman suurempi partikkelikoko, ja se sisältää vähemmän epäpuhtauksia. Tärkeitä fysikaalisia parametreja saadaan yksityisomistuksellisesta hartsista, kuten sisäinen huokoisuus ja mediaanipartikkelikoko. Hartsin amiiniryhmän todetaan kestävän lämpökäsittelyä kohtalaisen hyvin. Lämpögravimetrisellä analyysillä saatu adsorptiokapasiteetti 400ppm:n CO_2:sta on suurin 25^oC:n lämpötilassa, ja arvon havaitaan olevan kohtuullinen verrattuna kirjallisuuden arvoihin. Kyseisellä hartsilla todetaan siis olevan lupaavia ominaisuuksia direct air capture- prosessia varten.

FOREWORD

First, thanks to Pasi Vainikka and Cyril Bajamundi for giving me the opportunity of conducting my thesis work at VTT in a group of skilled scientists about a subject both intriguing and challenging. To be able to work towards something bigger than one person gives vigour even in these dark winter days.

Thanks to Cyril and Satu-Pia Reinikainen for your valuable feedback and support through the whole thesis. Thanks also to all other kind people at VTT and LUT who helped me through my experiments.

Five and a half years passed by fast in LUT with good friends that I was lucky to find. I gained willpower and support from these friends as well as from my family. I'm grateful for all these bonds newly forged and those old as I.

Taimi my dearest, you came with me so I could make my thesis here, and have been to support me every day of this process. I'm extremely grateful.

Jere Elfving
Jyväskylä, 30.11.2015

Table of Contents

Acronyms

AEC	Alkaline Electrolysis
APS	American Physical Society
APTMS	3-aminopropyltrimethoxysilane
BET	Brunauer-, Emmet-, Teller- adsorption isotherm
CCS	Carbon Capture and Storage / Carbon Capture and Sequestration
DAC	Direct Air Capture
DEA	Diethanolamine
DETA	Diethylenetriamine
DSC	Differential Scanning Calorimetry
EDA	Ethylenediamine
EDS	Energy-Dispersive X-ray spectroscopy
ES	Equilibrium Section / Equilibrium Zone
HAS	Hyperbranched Aminosilica
HIPE	High Internal Phase Emulsion
IAST	Ideal Adsorption Solution Theory
LES	Length of Equilibrium Zone
LUB	Length of Unused Bed
MEA	Monoethanolamine
MDEA	N-methyldiethanolamine
MOF	Metal-Organic Framework
MTZ	Mass-Transfer Zone
NFC	Nanofibrillated Cellulose
PAA	Polyallylamine
PCC	Post-Combustion Capture
PEI	Polyethyleneimine
PEMEC	Polymer Electrolyte Membrane Electrolysis
PP	Polypropylene

PPN	Porous Polymer Network
PSA	Pressure-Swing-Adsorption
PtG	Power-to-Gas
PtL	Power-to-Liquid
PVEC	Photovoltaic Electrolysis
SEM	Scanning Electron Microscopy
SOEC	Solid Oxide Electrolysis
STA	Simultaneous Thermal Analysis
TCS	Temperature-Concentration-Swing-Adsorption
TGA	Thermogravimetric analysis
TSA	Temperature-Swing-Adsorption
TVS	Temperature-Vacuum-Swing-Adsorption
UB	Unused Bed
VSA	Vacuum-Swing-Adsorption
WES	Width of Equilibrium Zone
WUB	Width of Unused Bed
XRF	X-ray Fluorescence
mmen	Dimethylethylenediamine
ppm	parts per million (by volume)

1 Introduction

The monthly average of the concentration of CO_2 in the atmosphere has risen from about 316ppm to about 404ppm from March of 1958 until May of 2015 [1]. A large portion of emitted CO_2 is caused by other than concentrated point sources such as coal-powered power plants [2]. About third of total emissions is caused by transport, residential and other sources (Figure 1). These fragmented carbon emission sources are usually hard or nearly impossible to control, and public awareness of the greenhouse effect has been the "weapon of choice" against them.

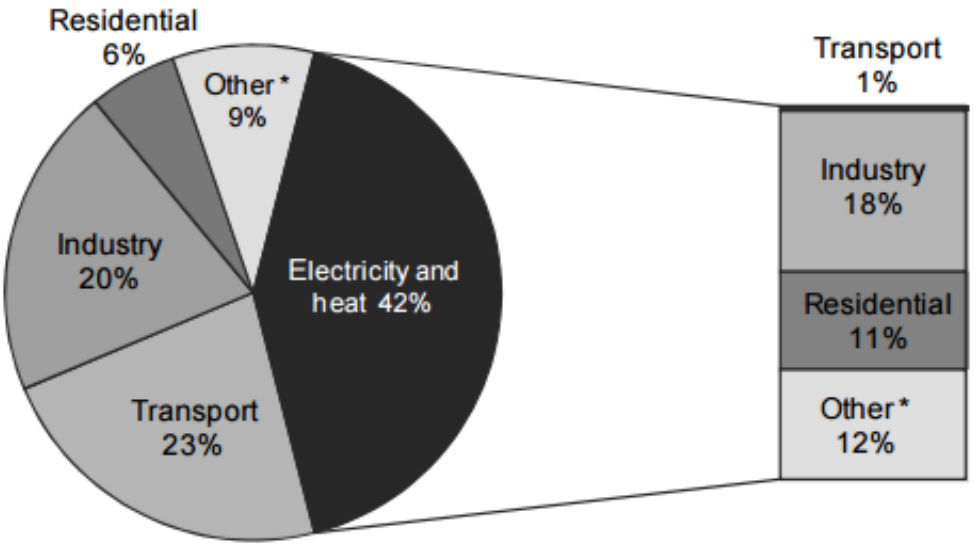

FIGURE 1 Global CO_2 emissions by sector in 2012. Other includes areas such as commercial/public services, agriculture/forestry and energy industries other than electricity. [2]

One focus of the study in the mitigation of greenhouse effect in recent years has been Carbon Capture and Storage (CCS). CCS involves technologies that aim at capturing CO_2 from different industrial process stages. One possibility is to capture CO_2 from post-combustion gases with high concentrations of CO_2, which is referred to as Post-Combustion Capture (PCC). In CCS, the captured CO_2 is pressurized, transferred to a storage site and stored there into stable geological formations, for example. Means of CO_2 capture include scrubbing of coal power flue gases with aqueous amine solutions, using ionic liquids as solvents of CO_2, calcining CO_2 into carbonates, using solid adsorbents, or alternative fuel burning processes such as Oxyfuel, where recycled flue gas is burned with

oxygen stream. Although CCS may be one of the only plausible ways to effectively limit CO_2 emissions of the industry, it faces significant difficulties, such as high cost of CO_2 transportation and injection into underground storages and leaking of the CO_2 from them. [3] Using PCC technologies in CCS ignore the CO_2 already emitted into the atmosphere. On the other hand, CCS could also be argued to be a waste of precious raw material for fuels. Direct air capture presents a possible solution to these problems, while striving towards carbon neutrality.

This thesis was conducted as a part of the NeoCarbon Energy project. The project is focused on designing the foundation for an energy system where only renewable sources are utilized. One main goal is creating energy storage solutions for excess electricity generated by wind- and solar power. One solution to energy storage problem is to produce renewable fuels using excess electricity and DAC as the carbon source.

1.1 Why Direct Air Capture?

Direct air capture (DAC) refers to chemical methods and materials used to specifically capture CO_2 from atmospheric air [4–7]. The capture of CO_2 from atmospheric air is more expensive than from concentrated point sources, and can be evaluated with the ideal minimum work needed in the capture process [4,6]. The ideal minimum work needed to capture CO_2 from atmospheric air is about 20 kJ/mol CO_2, which is about 3.4 times more than from an industrial flue gas containing 10% CO_2 by volume [6]. Keith et al.[4] argued in 2006, that the cost of DAC will be comparable to carbon capture from large fixed sources. Costs including energy, capital costs and maintenance with a system using NaOH were evaluated to be between \$55-\$136/tCO_2. Lackner et al.[7] estimated in 2009, that even \$30/tCO_2 would be achievable in the near future and was a reasonable target. However, Ranjan et al.[6] presented much more pessimistic figures in 2010, with only energy costs reaching as high as \$420-\$630/tCO_2, depending on thermodynamic efficiency. House et al. (2011)[8] also presented cost figures of more than \$1000/tCO_2.

It is clear from these cost figures that the cost of CO_2 capture is not easy to evaluate, but if the more pessimistic figures are to be believed, the cost needs to come down. However, these cost evaluations are for CCS, and treat CO_2 as expenditure, only. These kinds of evaluations usually have not taken into account the potential of DAC being integrated in Power-to-Gas (PtG) systems or Power-to-Liquid (PtL) systems. One such example is a

synthetic diesel co-operation pilot plant by Audi and Sunfire, that is located in Dresden [9–11] (Figure 2).

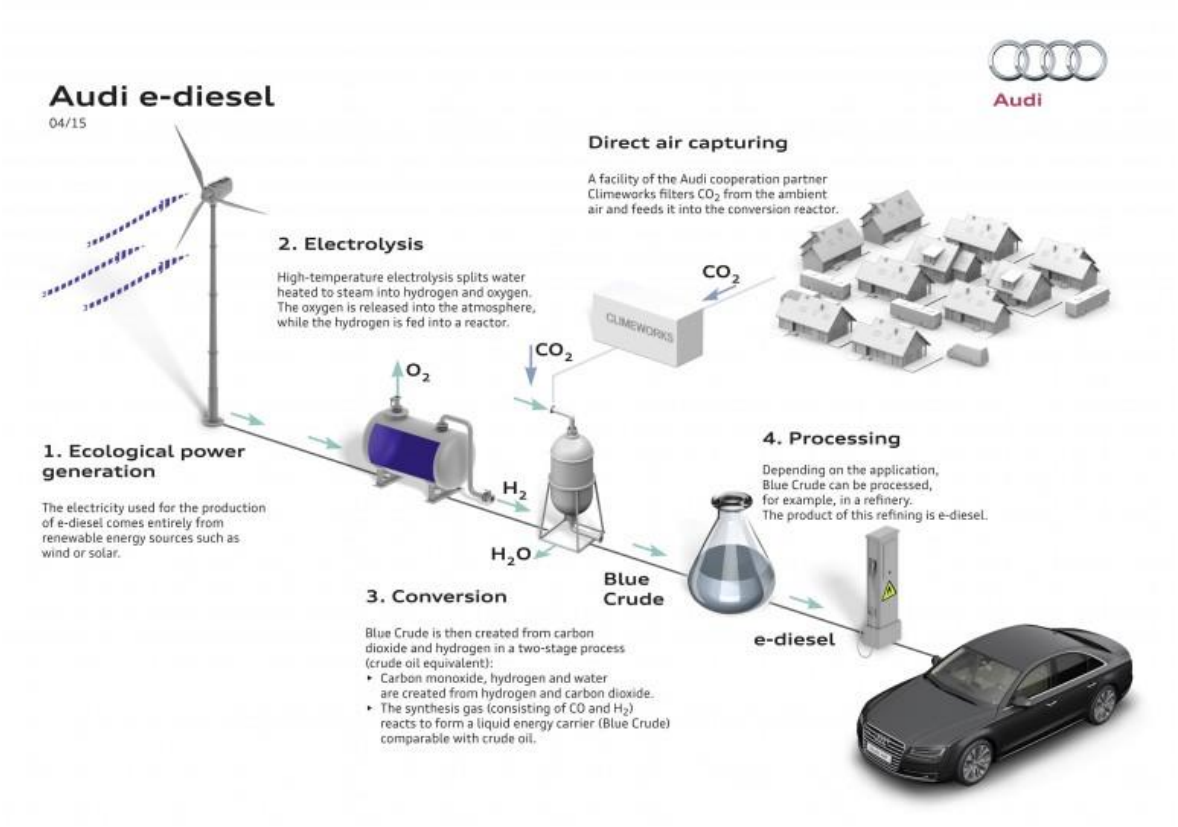

FIGURE 2 Process illustration of the Audi e-diesel production [9].

CO_2 needed in the Audi PtL process is intended to be provided by a DAC system by Climeworks (Figure 2). The purpose of this chapter is to introduce the reader into the PtG and PtL processes and justify the use and study of DAC.

1.1.1 Power-to-Gas and Power-to-Liquids concepts

The amount of power plants providing renewable energy such as wind turbines and solar plants will increase significantly in the following century in the Europe [12]. The power generated especially by wind turbines and photovoltaic is very fluctuating due to weather changes and time of day [13]. Power demand does not always correspond to power generation, and the capacity of the electricity grid may also be limited, leading to excess energy being generated [14]. One option to remedy these fluctuations is to expand the electricity grid [13]. Another is to use the generated excess electricity for the production of transport fuels [14].

Power-to-Gas (PtG) is a solution for the utilization of excess renewable electricity. PtG involves the production of hydrogen gas in a water electrolysis plant. Oxygen is generated as a by-product. The hydrogen produced can be used as a raw material for chemical, petrochemical or metallurgical industries, or as a fuel. Oxygen can also be used as a raw material, or be simply released into the atmosphere. Methanation is an optional process step in PtG. The main product is then synthetic methane, produced from carbon dioxide and the hydrogen generated from the water electrolysis. [14]

The idea of Power-to-Liquids (PtL) is basically the same as in PtG: to convert excess electricity into chemicals that can be used as fuels or raw materials. The difference is that whereas in PtG the end-product is gaseous methane, in PtL the products are chemicals in liquid form at room temperature, such as methanol, petrol, diesel and kerosene. The raw materials are CO_2 and H_2 such as in PtG. [15]

1.1.2 Water electrolysis & methanation processes

The basic principle of water electrolysis is to introduce voltage and direct current through electrodes into an electrolyte solution consisting mostly water. Water is dissociated into hydrogen and oxygen by redox reactions on the surface of the oppositely charged electrodes. Oxidation and oxygen gas generation takes place on the positively charged anode, reduction and hydrogen gas generation on the negatively charged cathode. Four main types of electrolyses are alkaline electrolysis (AEC), polymer electrolyte membrane electrolysis (PEMEC), solid oxide electrolysis (SOEC) and photovoltaic (PV) electrolysis. The most common of these is AEC, whereas PEMEC has the highest efficiency. [16]

In AEC, the electrolyte solution is a potassium- or sodium hydroxide solution. Anodic and cathodic regions are separated by a microporous diaphragm. OH^--ions generated in the cathode reaction travel through the diaphragm from the cathode side to the anode. The product gas is separated from the electrolyte, which is pumped back into the cell. The greatest difference between AEC and PEMEC is that in PEM electrolyzers a solid membrane replaces the electrolyte solution. H_2-ions travel through the membrane from the anode side to the cathode side. The technologies have their own advantages and drawbacks. For example, AEC cannot be operated under high pressures causing bulkiness, has low dynamics caused by the liquid electrolyte, and suffers from lower product purity. On the other hand, PEMEC is more expensive to implement and has durability issues. [17]

As already stated, the hydrogen generated by water electrolysis described above can then be used in the methanation process. The basic principles and process conditions of chemical methanation are discussed below. Biological methanation processes also exist [14], but are out of the scope of this thesis.

The general chemical formula of methanation using CO_2 and H_2 at temperature of 25°C is presented in the following equation [18].

$$CO_{2\,(g)} + 4H_{2\,(g)} \leftrightarrow CH_{4\,(g)} + 2H_2O_{(g)} \qquad \Delta H_R^0 = -165.0kJ/mol \qquad (1)$$

Methanation is strongly exothermic (Equation 1). To balance high conversion, yield and selectivity, and on the other hand fast reaction kinetics, the operation temperature must be kept within certain limits in the process. Methanation reaction temperature of 200°C provided higher CO_2 conversion, methane selectivity and yield compared to higher temperatures in a thermodynamic study of methanation reactions [18]. Higher operation pressure also yielded higher conversion, selectivity and yield. Naturally, the reaction kinetics is more unfavourable in lower temperatures. Therefore, to provide both fast kinetics and high conversion, yield and selectivity, nickel- based catalysts are usually used in methanation reactions with high temperatures [19,20].

Some components in the input gases can negatively affect the methanation reaction and the catalysts. In the thermodynamic study [18], it was found that water vapour did not affect the results significantly. Oxygen and other hydrocarbons were found to hinder methanation, however. Sulphur-based contaminants such as H_2S [20] and SO_2 [21] also act as poisons for the catalysts. Thus, H_2 and CO_2 input gases have their own quality requirements for methanation process in Table I. However, for example sulphur resistant catalysts for methanation processes have been developed [22].

TABLE I Necessary gas quality for methanation [14].

Component	Unit	Value for methanation input	Value for CO_2 stream
H_2	Vol.%	35–80	–
CO_2	Vol.%	0–30	0–100
CO	Vol.%	0–25	0–100
CH_4	Vol.%	0–10	0–50
N_2	Vol.%	<3	<15
O_2	Vol.%	n.s.	n.s.
H_2O	Vol.%	0–10	0–50
Particles	mg/scbm	<0.5	<2.5
Tar	mg/scbm	<0.1	<0.5
Na, K	mg/scbm	<1	<5
NH_3, HCN	mg/scbm	<0.8	<4
H_2S	mg/scbm	<0.4	<2
NO_x	mg/scbm	n.s.	n.s.
SO_x	mg/scbm	n.s.	n.s.
Halogens	mg/scbm	<0.06	<0.3

n.s.: not specified, *scbm:* standard cubicmeter (20 °C, 0.1 MPa)

The most common chemical methanation process is fixed-bed methanation [19]. The fixed-bed methanation process setup consists of several reactors with beds of catalyst in a cascade-type process [14]. In the process, gas cooling, gas recycling and reaction heat recovery steps alternate. Known power-to-methane plants are for example the Werlte plant delivered by ETOGAS to Audi and Stuttgart plant by Fraunhofer & IWES [23].

One might question the reasonability of methanation, when hydrogen is already a viable product. Hydrogen itself is an energy storage option, and can be used for example in fuel cells in cars [24]. Germany, for example, has already invested in hydrogen infrastructure, such as refuelling stations [24]. However, the use of hydrogen in a large scale needs large investments in hydrogen infrastructure and in the end-use technologies, especially in countries with no existing infrastructure [25]. Safety also needs special focus when dealing with hydrogen as an energy source, such as need for safety sensors [26]. On the other hand, the infrastructure and technology for the use of methane already exists, and is increasing especially in the northern Europe [27]. As an energy source, methane can be used in power plants to produce electricity [27], for heating [28], or as a transport fuel [29]. Like hydrogen, methane is also an important raw material for chemical industry, such as for the production of methanol [28].

1.1.3 Utilization of DAC in Power to Gas systems

Using DAC to fulfil the CO_2 need for methanation has advantages that CO_2 capture from concentrated sources cannot provide. Because DAC uses air as the CO_2 source, it can be operated almost anywhere. Climeworks is a company that provides mobile DAC-units that produce high-purity (>99%) CO_2 from ambient air [30]. The DAC-units are transported in containers, and can be scaled up on location to produce CO_2 continuously. This provides convenience and a steady supply of CO_2 for the methanation. Also, because methanation is highly exothermic (see 1.1.2), the waste heat could be used for the regeneration of the DAC sorbent material on location. The energy released in methanation (Eq. 1) is up to 70% of the total thermal energy required in the Climeworks CO_2 capture if calculated from the minimum thermal energy demand by 1000kg of captured CO_2[30]. This estimate is naturally unrealistic by assuming no heat loss by heat transfer for example, but gives an idea how significantly these two processes can benefit from each other.

As the CO_2 is produced on location with DAC, the costs of CO_2 transportation and storage can be minimized. To use the CO_2 produced in PCC, transportation is an essential part, and the most reasonable alternatives are onshore- or offshore pipelines[31] or transportation by ships[31]. It has been evaluated[31], that if for example 2.5 million tonnes of CO_2 is produced by annum, the transportation for a distance of 1500 km can cost from about 19.8€/t CO_2 up to over 50€/t CO_2. If one considers the cost of post-combustion capture of CO_2 from concentrated point sources of about 80$(ca. 60€ using exchange rate of 30.12.2010 [32])/t CO_2 as evaluated by APS[33], it can be seen, that the transportation cost can reach almost the cost of the capture process. The cheapest and most flexible way of transportation is by ship, in which the cost does not increase strongly by distance [31]. However, ship transportation demands liquefaction of the CO_2 to lower the expenses, and is not continuous, needing thus intermediate storages [31]. The CO_2 also has to be transported by onshore pipelines to the location, where the ship is loaded [31].

1.2 Scope of the thesis

DAC may be the only way to control CO_2 levels emitted from scattered sources. The economic viability at least at this point, however, arises from the integration of DAC into other processes as a CO_2 fuel source. For this purpose, DAC even has economic advantages compared to PCC. To create economically feasible PtG processes with DAC that are accepted by the public and the decision-makers, the CO_2 capture process itself needs scientific focus. This is where this thesis comes into the picture.

This thesis is divided into literature- and experimental parts. In the literature part, DAC technologies are discussed. Of these, solvent-based technologies are addressed first, because DAC was first introduced by such technologies. The focus is in solid sorbent-based processes, however. The basic concepts of a solid sorbent-based separation process are shortly described, but the main focus is in the performance of the active materials. Recent DAC studies using solid adsorbents or absorbents are reviewed and analysed to provide guidelines for the selection of these materials in DAC processes, and further, to emphasize important parameters for future studies.

In the experimental part, two sorbent materials are studied for DAC purposes. Experiments that were conducted based on the essential information gained from literature about the most important parameters of a good solid sorbent material for DAC are described in detail. The experimental results are discussed, and based on these and results gained from literature, conclusions are drawn.

I Literature part

DAC is studied in several research groups, and has inspired some start-up companies. Climeworks has been founded by Jan Wurzbacher and Christoph Gebald, who have published reports concerning DAC with a nanofibrillated cellulose sorbent [34–37]. The Climeworks process is thus probably based on this sorbent material. Other real cases of commercialized DAC include Carbon Engineering Ltd founded by David Keith and others [38], and Global Thermostat founded by Peter Eisenberger and others [39]. Carbon Engineering has a DAC pilot plant under development in Canada, and their DAC process is based on an aqueous sodium hydroxide solution [38]. Global Thermostat has operational pilot process plants for DAC and PCC purposes, also in Canada. The results by these groups and many others are presented and discussed in this literature review.

In a DAC technology assessment by American Physical Society [33], the binding steps of CO_2 in direct air capture systems are divided to four stages. Step 1 is the transport of the CO_2 containing gas mixture to the boundary of the medium, which contains the binding material. Step 2 is the transferring of CO_2 from the gas phase into the medium. Step 3 involves the transportation of the CO_2 within the medium to the binding site. Step 4 is the reaction itself at the binding site. The binding steps are followed by three steps needed to complete the cycle. In step 5, CO_2 is released from the binding material. Step 6 is the regeneration of the binding material. Step 7 is the final step, and consists of the purification and compression of the CO_2. The DAC process is shortly in these seven steps. The following is focused in steps 4-6, because mass-transfer itself is not discussed in detail, although may be mentioned in some cases.

2 DAC based on solvents and other non-sorbent technologies

In this chapter, methods of CO_2 capture based on methods less studied in the recent years are reviewed shortly. Sodium hydroxide based DAC is first reviewed, because it was the first DAC method that was considered [40] and critically analyzed [33] in full process scale. As an introduction to sodium hydroxide- and generally solvent-based CO_2 capture, the chemistry of CO_2 in water solutions is shortly reviewed. Other solvent options such as monoethanolamine (MEA), and other process options such as electrodialysis are also reviewed shortly.

2.1 Sodium hydroxide solutions

Probably the first time that capturing CO_2 directly from atmospheric air was proposed, was in 1999 by Lackner et al. [41]. In 2004, Lackner and Zeman [40] proposed a process for the removal of CO_2 from atmospheric air using NaOH. As sodium hydroxide based DAC used to be the definitive process option for DAC, it is reviewed here shortly.

2.1.1 CO_2 in water solutions

Carbon dioxide is slightly soluble in water in room temperature, and as with other gases, the solubility quickly decreases with temperature, but increases with increasing total or partial pressure [42]. In water, CO_2 produces hydrated CO_2 species, but also a small amount of carbonic acid, H_2CO_3.

$$CO_2(g) + 3H_2O \leftrightarrow CO_2(aq) + 3H_2O \leftrightarrow H_2CO_3 + 2H_2O \quad (2)$$

$$H_2CO_3 + 2H_2O \leftrightarrow HCO_3^- + H_3O^+ + H_2O \leftrightarrow CO_3^{2-} + 2H_3O^+ \quad (3)$$

The total reaction pattern of diluted CO_2 and resulting species can be seen in Equations (2) and (3). In Equation (2), the CO_2 is diluted from air into water, resulting in the formation of carbonic acid. In Equation (3), the carbonic acid is deprotonated to bicarbonate, which in turn is deprotonated to carbonate. [43]

2.1.2 Capture mechanism

The capture mechanism of CO_2 with aqueous NaOH is based on an acid-base reaction between carbonic acid and NaOH [33]. The general reaction is in equation (4).

$$2NaOH(aq) + CO_2(g) \rightarrow Na_2CO_3(aq) + H_2O \qquad (4)$$

Sodium hydroxide is a strong base, dissociating practically completely in water. Thus, 1 mole of NaOH creates 1 mole of OH^--ions that are able to react with carbon dioxide. An excess of NaOH results in a strongly basic carbonate solution, whereas the molar ratio of 1:1 for NaOH:CO_2 results in a mildly basic bicarbonate solution [33]. The hydroxide ion has a strong binding energy [40], being therefore suitable for direct air capture. Other advantages of aqueous NaOH are high load capacity and fast reaction time [40].

2.1.3 The CO_2 capture process

Treating CO_2 containing gas mixture with NaOH is an absorption process, where sodium carbonate is generated [40,41]. NaOH was selected by Lackner and Zeman [40] instead of KOH because KOH was more expensive. Calcium hydroxide has also been proposed as a solvent, but it suffers from the generation of low-soluble calcium carbonate, which scales on the surfaces of the gas-liquid contactor [44].

The wet scrubbing process proposed by Lackner and Zeman [40] generates sodium carbonate solution, which is reacted with solid calcium hydroxide. This process is causticization, and regenerates the NaOH. The resulting calcium carbonate is then decomposed by thermal regeneration or calcination, releasing solid CaO (lime) and the gaseous CO_2.

In a process design study by Baciocchi et al.[44], two process schemes were proposed based on the process steps proposed by Lackner and Zeman, although the cost of these processes could not be evaluated. In a study proposing CO_2 absorption with a spray column contactor using NaOH, the price estimate was \$100/tCO_2 on average [45]. The NaOH based DAC process was also thoroughly discussed and evaluated in an APS report [33], and dismissed with minimum total costs of \$610/tCO_2. Other cost estimates for the same or similar DAC processes were presented above in the introduction, although the APS report estimate may be closest to realism. All in all, the NaOH DAC probably was not to be applied in full scale, as the costs, especially the energy costs in the decomposition of

$CaCO_3$, are very high. Klaus Lackner, the first proposer of a NaOH based CO_2 capture process, moved on from NaOH to present a solid sorbent-based DAC process already in 2011 [46].

2.2 Other solvent-based options for DAC

Here, other methods for solvent-based CO_2 capture are shortly reviewed. The methods include for example amine based solvents, membranes and electrodialysis. The methods described here may or may not be applicable as DAC processes.

2.2.1 Amine based solvents, ionic liquids and chilled ammonia

Amine based solvents used in CO_2 capture are alkanolamines such as monoethanolamine (MEA), diethanolamine (DEA) and N-methyldiethanolamine (MDEA) [47]. The most used is MEA because of its high reactivity with CO_2 [48]. MEA is a weak base and reacts efficiently with CO_2 only in a solution with excess of MEA [33]. The capture mechanism of CO_2 with MEA is based on the formation of an intermediate zwitterion, which further reacts with another MEA molecule to produce carbamate anion and an alkyl ammonium cation [33]. The reaction thus uses 2 moles of MEA per one mole of captured CO_2. However, MEA is only efficient in capture from sources with high concentrations of CO_2, such as from flue gases [33,44].

Ionic liquids have been proposed as solvents for CO_2 capture instead of MEA. Ionic liquids are mixtures of salts liquid in room temperature. The advantage to MEA is lower energy needed in the regeneration step. However, CO_2 solubility in ionic liquids is lower than in MEA. Ionic liquids are also more selective for SO_2 and H_2S than for CO_2, causing possible problems for capture from sour gases. Ionic liquids are also more viscous and more expensive compared to MEA for example. [48] No DAC applications of ionic liquids have been reported.

Using chilled ammonia solutions for CO_2 capture was proposed by Kozak et al.[49]. In this process, the ammonia reacts with CO_2 to produce ammonium carbonate that is regenerated by heating. Lower regeneration energy compared to an amine based process was listed as an advantage, for example. This process also, however, was designed for post combustion flue gases with high concentrations of CO_2.

2.2.2 Membrane and electrodialysis

Different membrane processes such as gas separation membranes, liquid membranes or chemically reactive membranes in CO_2 capture have been studied, but the applications, if any, are usually in post combustion CO_2 capture. For example, membranes as contactor units in solvent-based CO_2 capture processes have already been implemented. [50] Some solvent-based membrane processes have potential for DAC, and are discussed here. Solid sorbent-based Ion-exchange membranes are discussed along with ion-exchange resins in chapter 3.2.4.

One example of a proposed DAC suitable membrane is ionic liquid membrane proposed in a study by Cheng et al.[51]. The membrane in question has a polymeric support that is covered with a commercial ionic liquid. Capture of CO_2 from ambient air with ionic liquid membranes was achieved with high CO_2/N_2 selectivity of 20 calculated by the ratio of permeances of CO_2 and N_2, respectively. The process was thus presented as a plausible option for DAC.

Membranes have also been proposed to be implemented in electrodialysis [52,53]. The technology is based on regenerating a CO_2-enriched capture solution from a solvent-based air capture process. Voltage is applied into an alternating stack of bicarbonate permeating anion-exchange membranes and bipolar membranes, which dissociate water into H^+ and OH^- ions. The hydroxide ions regenerate the capture solution, and the protons react with bicarbonate to yield carbonic acid. Pure CO_2 is extracted from the acidic solution, which is then recycled to the electrodialysis. This technology was reported to be more energy-efficient than other solvent-based DAC processes.

3 Sorbent-based DAC

Using solid sorbents is clearly the most widely considered option for DAC, and therefore, these solid sorbent-based technologies are reviewed in detail in this chapter. The theory behind sorption processes is first addressed by reaction mechanisms, adsorption isotherms and basic principles of a fixed-bed adsorption process. As a preface to the sorbent material review, important parameters concerning a DAC process are reviewed. Articles on DAC are then reviewed, keeping focus in the sorbent materials and their characteristics. Finally, the results gained from the literature are analysed by comparing these results and drawing relevant conclusions.

3.1 Mechanisms and models

Relevant theory considering adsorption and ion-exchange is presented in this chapter. The reaction mechanisms are presented at a general level. Also, the most relevant sorption equilibrium models, such as Langmuir and Freundlich models are presented. The theory in chapters 3.11-3.13, if not otherwise stated, is based on a textbook of separation processes by Seader et al. [54].

3.1.1 Mechanisms behind adsorption

Adsorption and ion-exchange are sorption phenomena, where components separated from fluid phase, the sorbates, are bound by physical or chemical interactions onto a sorbent material. In gases for the sorption to occur, the forces between the sorbent material and the sorbate must be higher than the forces between the gas and the sorbate. Adsorption is at least in most cases [55] exothermic, and the amount of heat released is measured by heat (enthalpy) of adsorption.

Adsorption requires a solid adsorbent material, and the interactions between the adsorbent and adsorbate can be of physical or chemical nature. The physical interactions are referred to as physisorption, and the mechanism behind them is based on weak intermolecular forces, the van der Waals forces. Physisorption is reversible as one-layered (unimolecular) sorption, but can occur in multiple layers, and can then be irreversible. The chemical interactions are referred to as chemisorption, and are based on covalent bonds, that can be irreversible. Chemisorption only occurs as one-layered, i.e. the molecules can form only

one molecular layer onto the adsorbent by chemisorption. The highest possible specific surface area is thus important for a good adsorbent material. The principle of adsorption can be seen in Figure 3.

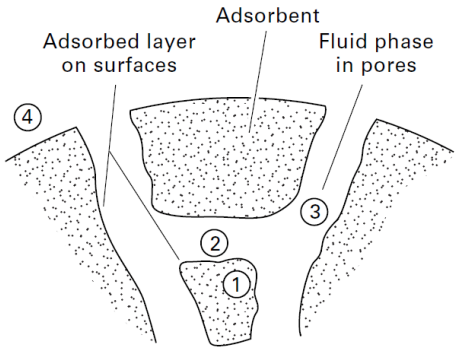

FIGURE 3 Adsorption on solid particles. [54]

Adsorption as an exothermic phenomenon releases heat, and thus, the adsorption heats (enthalpies) are negative. The greater the binding strength, the greater the absolute value of enthalpy of adsorption. However, the binding of CO_2 on the sorbent also decreases the entropy of the system. [33]

$$\Delta G = \Delta H - T\Delta S \quad (5)$$

Where
ΔG the Gibbs free energy,
ΔH the enthalpy of adsorption,
T temperature,
ΔS the entropy of the system.

In the thermodynamic Equation (5), the Gibbs free energy is composed of the enthalpy and the entropy terms. For the adsorption to be spontaneous, the Gibbs free energy must be negative.[33]

3.1.2 Adsorption isotherm models

When adsorption is conducted long enough, equilibrium is reached for the concentration of the adsorbate between the gas and the adsorbent surface. When the amount of adsorbate adsorbed in the adsorbent, q (for example in unit mmol adsorbate/g sorbent), is plotted against the concentration or partial pressure of the adsorbate in the gas to be treated, an adsorption isotherm is gained. Adsorption isotherms have been divided to five different types by Brunauer et al. [56], shown in Figure 4 below.

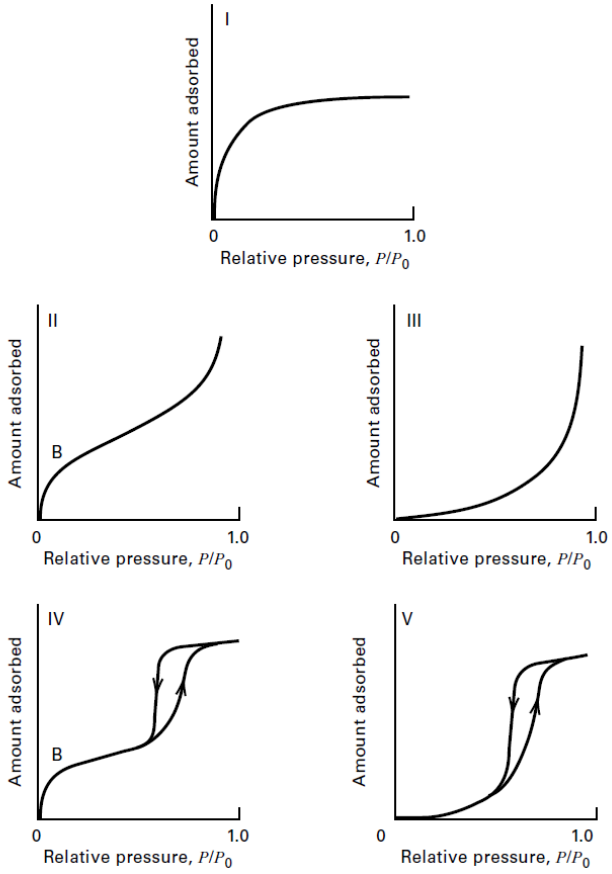

FIGURE 4 Five adsorption isotherm types by Brunauer. P/P_0= total pressure/vapour pressure. [54]

As described by Brunauer et al. [56], type I relates to unimolecular adsorption, and type II to multi-layered, so called Brunauer-, Emmet-, Teller- (BET) adsorption. Langmuir and BET isotherms associated with these types of isotherms will be described in this chapter below. Type III isotherm corresponds to multi-layered adsorption, where the heat of adsorption increases with each layer of molecules adsorbed. In this isotherm, when the partial pressure of the adsorbate is increased in the gas, the adsorption is delayed until saturation pressure is reached or near it, leading to very unfavourable adsorption. These three types assume infinite adsorption layers, and do not take into account capillary condensation, where the pores of the adsorbent become filled with the adsorbate, leading to condensation of the adsorbate as liquid. Types IV and V correspond to adsorption of types II and III with capillary condensation. In such cases hysteresis occurs, which is seen as the adsorption and desorption curves differing from each other in Figure 4. Regardless of sorbent material, whether silica [57], zeolite [58], activated carbon [59], ion-exchange resin [46], or other

materials [60,61], the adsorption or absorption of CO_2 on solid sorbents tends to follow the isotherm of type I.

The isotherm types above are described by different models. The simplest model used is the linear isotherm.

$$q = kp \tag{6}$$

Where q adsorbate loading,
k empirical temperature-dependent constant,
p partial pressure of the adsorbate.

In Equation (6), the loading of the adsorbate in the adsorbent is linearly correlated to the partial pressure of the adsorbate. This relation is only valid for low amounts of the adsorbate. This linear region can be seen from Figure 4, when examining the type I isotherm at low pressure at the beginning of the curve. Thus, other models such as the Freundlich model or the Langmuir model are usually used for type I adsorption.

$$q = kp^{1/n} \tag{7}$$

Where n empirical temperature-dependent constant.

Equation (7) is the Freundlich isotherm, in which the dependence of the loading of the adsorbate of the partial pressure is nonlinear. In comparison to the linear isotherm (Eq. 3), another empirical constant n has been added. If $n = 1$, the Freundlich isotherm is reduced to the linear isotherm.

$$q = \frac{Kq_m p}{1 + Kp} \tag{8}$$

Where K adsoption-equilibrium constant
q_m the maximum amount of adsorbate in the adsorbent.

The nonlinear Langmuir model is in Equation (8). The adsorption-equilibrium constant is the ratio of the kinetic constants of adsorption and desorption, respectively. The maximum loading of the adsorbent q_m is the amount of adsorbate on the adsorbent, when all adsorption positions are full on the surface of the adsorbent. The Langmuir isotherm is reduced to the linear isotherm at low pressures, i.e. $Kp \ll 1$.

Although the sorption of CO_2 on solid sorbents usually follows unimolecular type I isotherm, the surface area of the sorbents is usually studied by nitrogen adsorption, which is modelled with the BET equation.

$$\frac{p}{v(p_0 - p)} = \frac{1}{v_m c} + \frac{c-1}{v_m c}\frac{p}{p_0} \quad (9)$$

Where
p partial pressure of the adsorbate,
v volume adsorbed at 0°C and 760mmHg,
p_0 vapor pressure of the of the adsorbate at temperature T,
v_m maximum volume of the adsorbate as a unimolecular layer,
c constant related to the heat of adsorption.

The BET equation in Eq. (9), like already stated, is used to model types II and III adsorption. Constants v_m and c can be determined, when experimental data is gained for p and v, and $\frac{p}{v(p_0-p)}$ is plotted against $\frac{p}{p_0}$. When the vapour pressure of the adsorbate is very small, i.e. $p_0/p \ll 1$, the BET equation is reduced to Langmuir equation.

An isotherm worth to mention is also the Dual-Site Langmuir isotherm [62]:

$$q = \frac{K_A\, q_{m,A}\, p}{1 + K_A p} + \frac{K_B\, q_{m,B}\, p}{1 + K_B p} \quad (10)$$

Where
K_A adsorption-equilibrium constant for A sites,
$q_{m,A}$ the maximum amount of adsorbate in the adsorbent for A sites,
K_B adsorption-equilibrium constant for B sites
$q_{m,B}$ the maximum amount of adsorbate in the adsorbent for B sites.

In the Dual-Site Langmuir isotherm in Equation (10), the adsorbate is assumed to adsorb on two sites A and B. The adsorbate is distributed on these sites based on the constants K_A and K_B. The dual-site model was also used to model a mixture of two gases, and was recommended for cases in which the saturation capacities of the two gases are similar [62].

3.1.3 Basic principles of a Fixed-bed sorption process

Fixed-bed sorption, or packed-bed sorption, is a common process setup for CO_2 capture studies [34,58,63–69]. The sorbent material is packed in a column, into which the fluid is introduced. The fluid passes through the interstices between the particles, while the sorbates are diffused from the fluid phase into the pores of the sorbent. The sorption then follows on the surfaces of the pores, and the sorbate-poor fluid comes out of the column as outlet, or effluent.

In an ideal fixed-bed operation, the flowing fluid and the sorbent bed are assumed to reach a local equilibrium instantaneously. This zone of equilibrium moves through the bed as so-called stoichiometric front. The fixed-bed column is divided into two sections, consisting of the sorbate-saturated equilibrium zone (ES) upstream of the stoichiometric front and the unused bed (UB) downstream the stoichiometric front. The corresponding lengths and widths for these sections are called LES, WES, LUB and WUB. The adsorption takes place in the mass transfer zone (MTZ), which is divided by the sections of equilibrium zone and the unused bed in Figure 5.

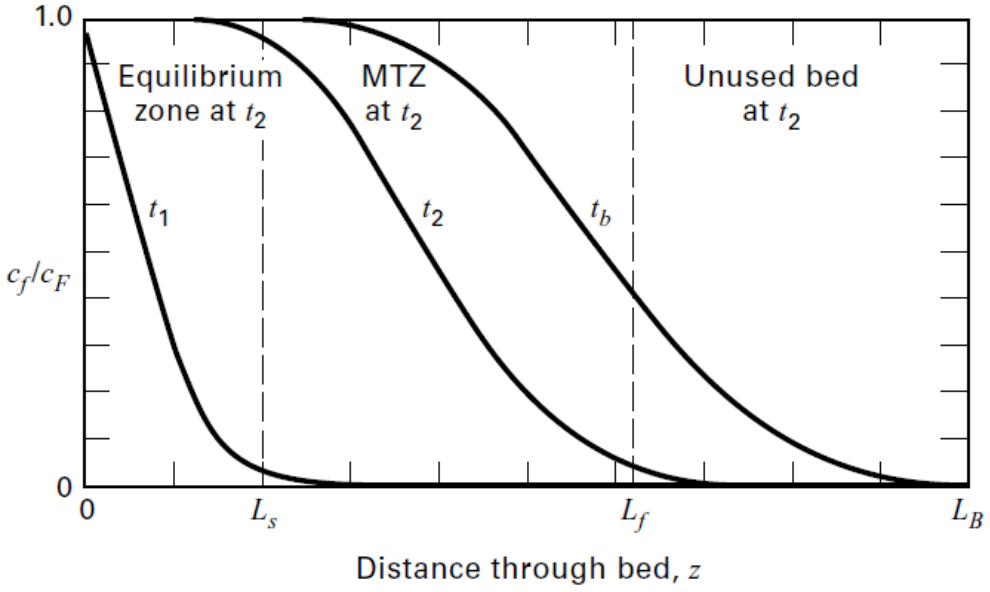

FIGURE 5 The concentration wave-fronts and the sections of the equilibrium zone, the mass-transfer zone and the unused bed in a nonideal fixed-bed adsorption process. c_f and c_F refer to concentrations of the fluid and the feed, respectively. L_s is the point in the column at which the sorbent bed is almost saturated, and L_f is the point at which the bed is almost clean of sorbate. L_B is the column outlet. [54]

In Figure 5, a nonideal case of fixed-bed sorption is depicted, where the concentration profiles of the concentration of the fluid c_f, the concentration wave fronts, are broadened by transport-rate resistances. The broadening effect is typical for linear isotherms or type III isotherms (see Figure 4). The broadening occurs when the wave-front at high c_f moves slower than the wave-front at low c_f. On the other hand, "self-sharpening", which is typical for type I isotherms, means that the wave-front at high c_f moves faster than the wave-front with lower c_f. The transport-rate resistances limit self-sharpening, however, and a constant-pattern front is developed. In constant-pattern behaviour, the MTZ becomes constant. The transfer of the stoichiometric front and the formation of the breakthrough curve from the wave front are depicted in Figure 6.

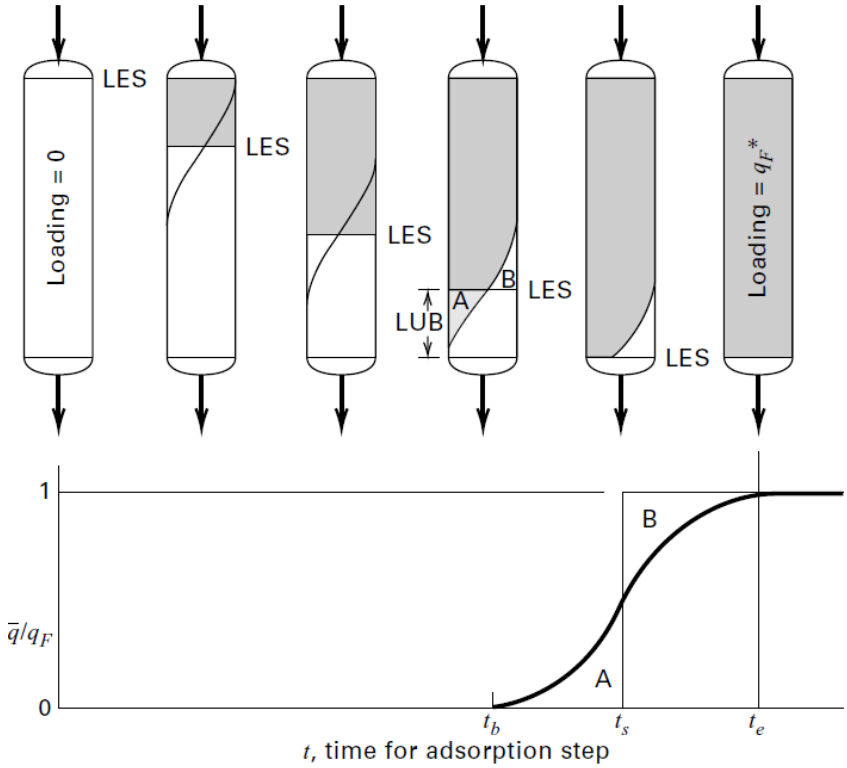

FIGURE 6 In the upper figure, the transfer of mass-transfer zone through the fixed-bed, and the loading of the sorbent bed from 0 to q_F are depicted. In the lower figure, a breaktrough curve related to the fixed-bed behaviour above is depicted. t_b refers to breaktrough time, t_s refers to the stoichiometric time, and t_e is the time at which the sorbent bed is fully loaded. [54]

In Figure 6, at time t_b, the highest point of the stoichiometric wave reaches the end of the column, and the breakthrough is reached. At this point, the feed into the column is stopped to prevent the loss of sorbate to the outlet. Time t_s is referred to as the stoichiometric time,

at which point the stoichiometric front reaches the end of the bed. At time t_e, the sorbent column becomes fully saturated with the sorbate. At breakthrough time, the sorbent bed, if not discarded, must be regenerated.

The regeneration of the sorbent bed is conducted by desorption of the sorbate by increasing temperature, introducing vacuum or increasing humidity level. The regeneration is based on lowering the bed-capacity towards the sorbate by altering conditions. Temperature-swing-adsorption (TSA) is based on the difference in sorption- and desorption temperatures. Sorption is carried out in lower temperature, and temperature is increased for desorption. Pressure-swing-adsorption (PSA) conducted by lowering the pressure to initiate desorption. If the pressure is lowered to near vacuum-pressure, the swing is called vacuum-swing-adsorption (VSA). Inert-purge-swing can be introduced in the same conditions as the sorption, by purging the sorbent bed with an inert gas, such as pure nitrogen[70] or argon[34]. The desorption step can also be conducted by humidity- or moisture-swing[46,71], in which the sorption is conducted with dry sorbent, and the desorption is conducted by introducing moisture. These different swings can also be used in combination, such as in temperature-vacuum-swing (TVS)[34,37], or temperature-concentration swing (TCS)[34] using heated inert-gas purge.

3.1.4 Critical parameters in CO_2 adsorption processes

The most relevant parameters related to sorption of CO_2 on solid materials are introduced here. The purpose is to make it easier for the reader to understand the experiments and results that are reviewed. Some examples[7,8,54,57,58,68,71–80] are given to the definitions of each parameter, but the reader is advised to examine the literature to learn how these parameters have been described in each case. Although cost of the materials is an important factor when considering process feasibility, it is rarely available, often because the studied materials have no marketing name, or are not reported properly. The cost factor is thus not addressed here.

The binding energy of a sorbent is usually discussed by determining enthalpy of sorption [57,68,72–74], presented in the unit kJ/mol. The isosteric heat of adsorption is the negative of the difference in the total enthalpy of a closed system [81]. The binding strength of a sorbent is one of the most important parameters in CO_2 sorption: Low concentration of CO_2 in the atmospheric air means that the binding strength of the sorbent material has to be

higher than when capturing CO_2 from flue gases [82]. On the other hand, a very strongly bonding material usually needs high temperature or pressure swings for desorption, raising the energy cost [7,8,68]. A comparison of heats of sorption and the regeneration temperatures of different sorbent materials by Wang et al. (2013) [75] can be seen in Figure 7.

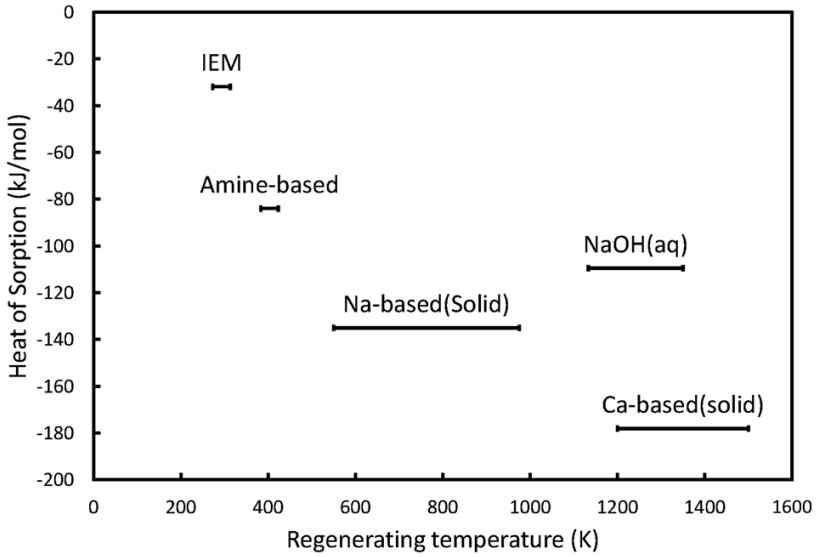

FIGURE 7 A thermodynamic comparison of different materials for air capture by Wang et al. (2013) [75]. IEM stands for ion-exchange membranes.

Capacity for CO_2 capture is probably the most critical characteristic of a sorbent material. A high capacity is important for acquiring the most out of the least amount of sorbent material. However, the ability of the sorbent material to lose its capacity under certain circumstances is as important as a high capacity. The difference in sorption capacities at different temperatures for a certain sorbent[34] can be seen from Figure 8.

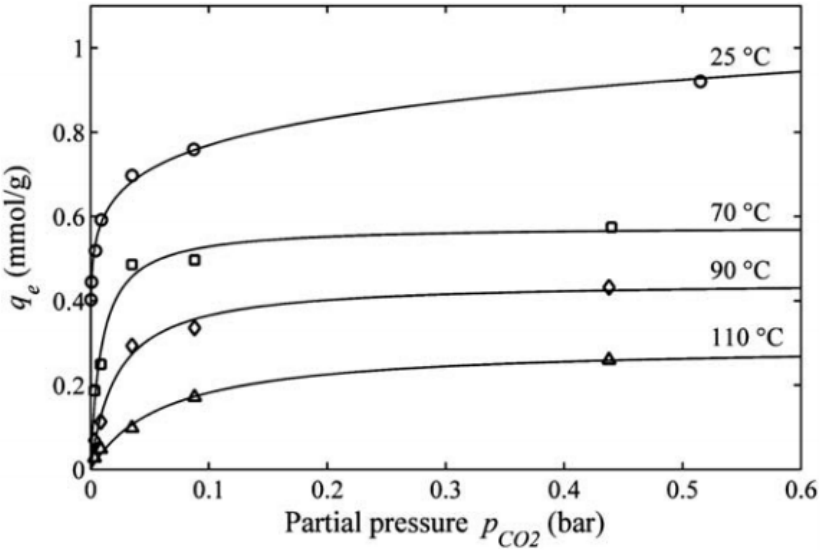

FIGURE 8 Adsorption isotherms of CO_2 on a silica gel sorbent [34].

CO_2 capture capacity is usually reported as mmol CO_2/g sorbent or mg CO_2/ g sorbent. The equilibrium capacity is most often reported[80,83–85]. In the case of regeneration cycle experiments, lower CO_2 sorption capacities are gained, because the cycles are shorter than what needed for reaching equilibrium. The reason for this can be seen from Figure 9.

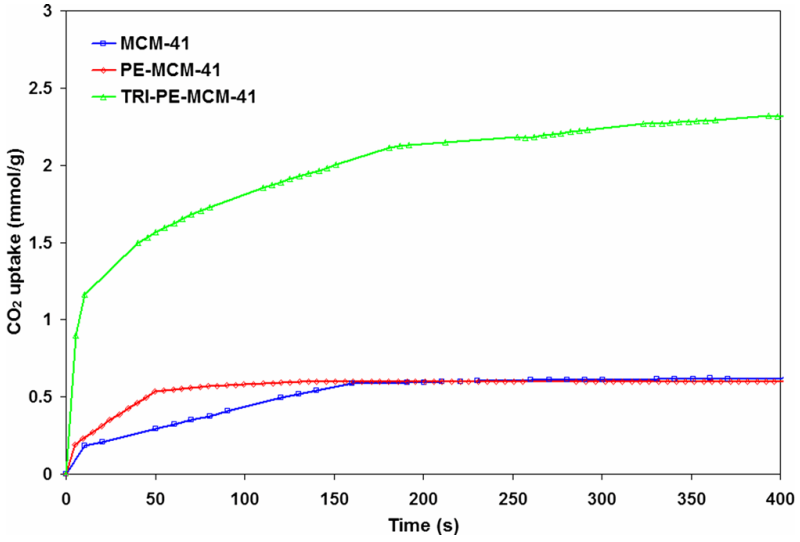

FIGURE 9 The kinetics of CO_2 adsorption at 25°C and 1bar from pure CO_2 gas on different mesoporous silicas [72].

In Figure 9, the adsorption of CO_2 is very fast at first, but is followed by a long gently sloping curve. Thus, lower sorption capacities are more reasonable to be settled for in regeneration cycles. Also, sorption and desorption capacities may be reported separately,

such as in the case of Wurzbacher et al. (2011)[34]. Sorption capacity may also be referred to as swing size, such as in the studies of He [71,76,77]. Similar concept is the working capacity[73], which is shortly the adsorption capacity at initial conditions subtracted by the adsorption capacity at the regeneration conditions.

Selectivity of the sorbent towards CO_2 in DAC is important due to the minor concentration of CO_2 in atmospheric air compared to nitrogen, oxygen and water vapour. Selectivity is often determined from gas mixtures of CO_2 and N_2, by comparing the uptake of these gases, i.e. the sorption capacities. Selectivity of adsorption is traditionally defined by the following equation [54], and was used for selectivity calculations for example in the study by McDonald et al.[74]:

$$\alpha_{i,j} = \frac{q_i/q_j}{p_i/p_j} \quad (11)$$

Where
$\alpha_{i,j}$ the selectivity of component i over j,
q_i the loading of component i in the sorbent,
q_j the loading of component j in the sorbent,
p_i the partial pressure of component i,
p_j the partial pressure of component j.

In Equation (11), component i is CO_2, and component j is usually N_2. Selectivity has also been reported as simply the ratio of CO_2 and N_2 uptake on the sorbent [58]. Ideal adsorption solution theory (IAST) is used to predict adsorption behaviour of gas mixtures, and gives more precise results for selectivity compared to ones calculated using Equation (11) [78]. For example, Shekhah et al.[79] used IAST and determined selectivity by the following equation:

$$S_{\frac{CO_2}{N_2}} = \frac{(Uptake\ CO_2/Uptake\ CO_2\ and\ N_2)/(Uptake\ N_2/Uptake\ CO_2\ and\ N_2)}{Composition\ CO_2/Composition\ N_2} \quad (12)$$

Purity of CO_2 in the outlet gas is closely related to selectivity, and can be a more describing parameter when comparing sorbents, such as in the case of a study by Lu[73]. As stated above (Ch. 1.1.2), the purity of the CO_2 stream is important for its utilization in the methanation process. The purity of the CO_2 can be calculated using the following equation [74]:

$$Purity = \frac{q_{CO_2}}{q_{CO_2} + q_2} \cdot 100\% \quad (13)$$

Where q_{CO_2} the loading of CO_2 in the sorbent,
q_2 the loading of component 2 in the sorbent.

Sorption kinetics can be evaluated in several ways. In a sorption process driven in a fixed-bed manner, the breakthrough time is reached, when the concentration of the sorbate in the effluent, which is in this case the treated gas, starts to increase (see 3.1.3). Adsorption half time is a term used in adsorption experiments, and means the time when half of the pseudo-equilibrium adsorption capacity is reached [80]. The pseudo-equilibrium adsorption capacity is reached at the point, at which no significant weight gain of the sorbent from adsorption of CO_2 in TGA is observed [80]. Kinetics in the sorption/desorption cycle experiments can be evaluated by determining sorption/desorption rates from the corresponding capacities and times [71,76,77]. Adsorption- or desorption rate is gained by dividing the sorption capacity by the time taken to reach it. The unit of sorption/desorption rate is thus mmol CO_2 /(min×g sorbent).

The stability of the sorbent material is related to stability towards conditions such as temperature, pressure and moisture or oxidation. The stability of the sorbent relates to the ability to retain its sorption characteristics, most importantly the capacity to capture CO_2. The sorbent materials discussed in the following are usually chemically functionalized, and thus the instability of the sorbent is usually related to the decomposition of these functional groups.

Regenerability of the sorbent material is closely related to the stability. To create a cost-effective CO_2 adsorption process, the sorbent material must be regenerable, i.e. retain its sorption performance through recurring adsorption/desorption cycles. The sorbent material may undergo critical structural changes during these cycles, and regenerability is thus often studied in detail. Although usually unacceptable for solid sorbents, the mechanism behind CO_2 capture can be based on an irreversible reaction, which renders the material unregenerable.

Porosity is closely related to the capacity, as larger the specific surface area, the more surface for the sorption to take place. Pores in sorbent materials can be classified as micropores which are larger than 2nm, mesopores which are in the range of 2-50nm and macropores which are larger than 50nm. In the case of functionalized materials, larger

specific surface area means more theoretical loading of the material with functional groups. Amine efficiency is the ratio of the moles of CO_2 captured versus the moles of nitrogen of the amines in the sorbent material [86].

3.2 Sorbent materials

The sorbent materials and the corresponding results in CO_2 capture from air discussed here have been divided into subchapters based on the type of the support material (matrix). The material properties and the mechanisms of the CO_2 capture are presented. Articles are reviewed from the perspective of the most important characteristics, such as CO_2 adsorption capacity, regenerability of the sorbent and kinetics of the sorption.

3.2.1 Zeolites

Zeolites are porous aluminosilicates consisting of a crystalline structure composed of negatively charged tetrahedrons of SiO_4 or AlO_4 [54,86]. The sorption of CO_2 by zeolites is based mainly on physisorption, but a small portion of the CO_2 is chemisorbed as carbonate or carboxylate [86]. Zeolites have certain sized apertures in their crystalline structure, acting thus as molecular sieves for different sized molecules, while separating similar sized molecules according to their charges [54]. Zeolites have been reported to have reasonable CO_2 adsorption capacities in room temperature at least from flue gases [58]. Zeolites have also good regeneration properties at high temperatures (over 600K) and high adsorption kinetics at least in high concentrations of CO_2 [86]. Zeolites have also been functionalized with amine groups for CO_2 capture [87].

Although the studies and possible applications of zeolites in CO_2 capture usually relate to capture from flue gases or other sources with high concentration of CO_2 [67,86–88], CO_2 capture from low concentration sources with zeolites is not completely unheard of [58,85]. In a study by Stuckert et al. [58], different zeolites were compared with mesoporous silica SBA-15 for the capture of CO_2 from atmospheric 395ppm air. Na-zeolites were ion-exchanged with hydroxides of Li, K and Ca to gain corresponding ion-exchanged zeolites. Li-LSX zeolite powder had the highest adsorption capacity of 1.34 mmol CO_2/g adsorbent. Selectivity ratio of CO_2/N_2 calculated from the adsorption capacities was circa 1.6 for the zeolite in question, whereas the corresponding value for K-LSX zeolite was circa 3.0. Breakthrough curves were determined for the two zeolites in pellet form in a fixed-bed

setup, and saturation was achieved in less than 2 hours. The curves were also much sharper for the zeolites than for amine-grafted samples used in comparison. At a relative humidity of 80%, however, most of the adsorption capacity was lost for the zeolites. With only temperature swing adsorption, the CO_2 purity of the desorption gas was highest for Li-LSX zeolite with about 60% purity. With a combined vacuum swing adsorption and temperature swing adsorption, over 90% purity was achieved for zeolites Li-LSX and K-LSX and for the amine-grafted silica SBA-15.

In a study of Cho et al. [85], ground zeolites mixed with LiOH were studied for the capture of CO_2 from 1000-7000ppm gas streams simulating indoor CO_2 concentration. The samples showed high adsorption capacities for CO_2 (3-5 mmol/g adsorbent), although, due to higher concentrations of CO_2, the results are not fully comparable to the results of Stuckert et al. [58], for example. In contrast to the zeolites in the study by Stuckert et al. [58], relative humidity enhanced the adsorption capacities of LiOH loaded zeolites. This could be explained by the formation of a reactive lithium hydroxide monohydrate ($LiOH{\cdot}H_2O$), which reacts with CO_2 to produce Li_2CO_3. However, this reaction is irreversible, and thus, the LiOH loaded zeolites could not be regenerated, but were only divided into smaller particles to provide more reactive surface. In the same study, it was also found that the zeolites ground into particles smaller than 250μm did not adsorb any CO_2.

3.2.2 Silica- based materials

Silica materials used in CO_2 capture are ordered SiO_2 frameworks with specifically customized pore sizes, shapes and other properties [86]. Mesoporous silicas often act as support materials, and are functionalized with different amines. The resulting aminosilicas are divided into three classes, which are presented in Figure 10. The CO_2 capture on these materials is based on chemisorption, i.e. different reactions with the amines.

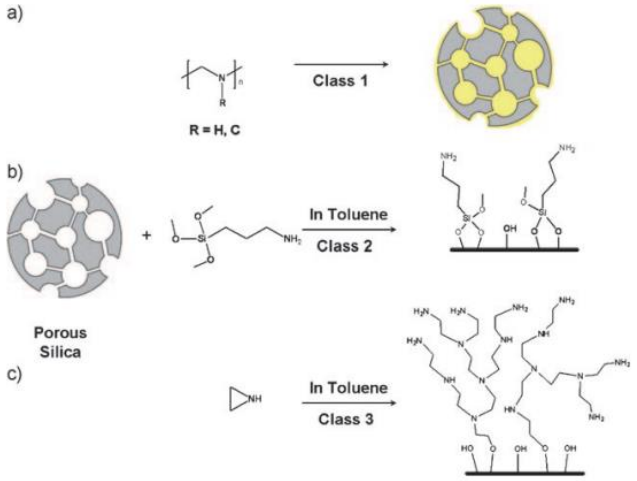

FIGURE 10 Three different classes of porous silica grafted with amines. Class 1 silica sorbents are impregnated with monomeric or polymeric amines by physisorption. Class 2 silica sorbents have covalently bound amine groups. Class 3 silica sorbents are prepared by polymerization of amines with the solid support by amine-containing monomers. [65]

Such as in the case of MEA solutions described above, primary and secondary amines react with CO_2 in a zwitterion reaction to produce carbamate (Fig. 11). The reaction between CO_2 and tertiary amines, however, is different (Fig. 12).

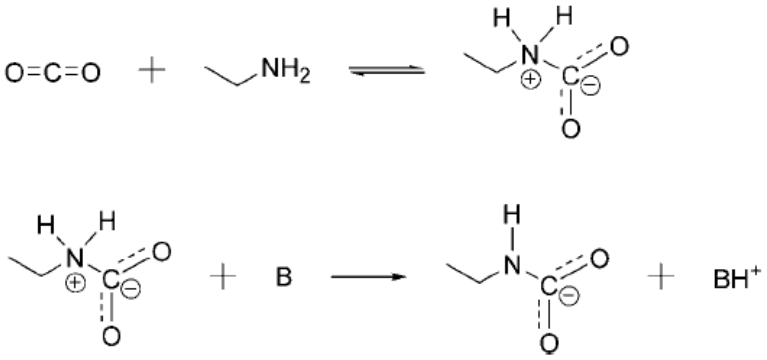

FIGURE 11 The reaction of CO_2 with primary, secondary or hindered amines. Amine reacts first with the carbon atom of CO_2, and a zwitterion is formed. The zwitterion then reacts with a free base to form carbamate. The free base can be another amine, H_2O or OH^-. [86]

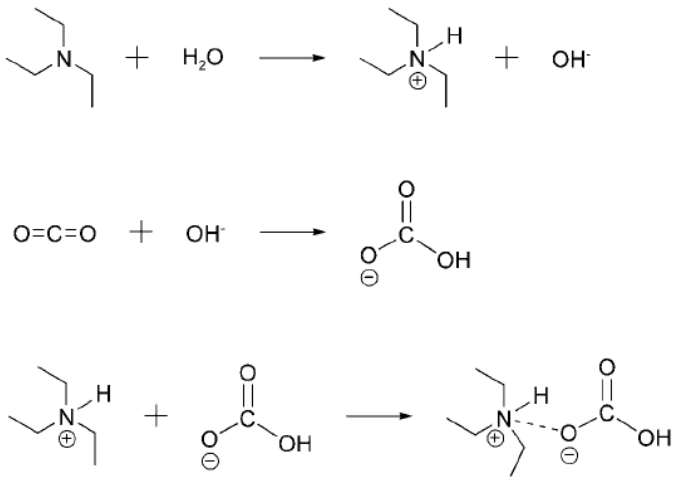

FIGURE 12 The reaction of CO_2 with tertiary amines. The tertiary amine reacts with a water molecule to produce a cationic quaternary amine and a hydroxide ion. Hydroxide ion then reacts with the carbon of CO_2 to produce a bicarbonate anion. In the last step, the bicarbonate and the quaternary amine ions react with each other. [86]

For primary and secondary amines, the maximum amine efficiency of an amine functionalized sorbent in dry conditions is 0.5 mmol CO_2/mmol N, because another amine group acts as a free base needed for the zwitterion to deprotonate to carbamate. In humid conditions, the corresponding value can be 1 mmol CO_2/mmol N, because the free base can be produced by H_2O. Also, it has been presented that in humid conditions, primary and secondary amines react similarly as tertiary amines, producing first carbamate, and then bicarbonate and carbonate. [86]

The doubling of the amine efficiency and the formation of bicarbonate or carbonate species in humid conditions was questioned by Bacsik et al.[89]. However, Didas et al. (2014)[90] proved the formation of bicarbonate species in CO_2 capture under humid conditions on silica with a low loading of amine, in which case the CO_2 reacts with the amine with a molar ratio of 1:1. Apparently, with high loading, the “free base” is provided by the adjacent amine group, leading to lower amine efficiency.

The most commonly used amine for the functionalization of porous silicas is polyethyleneimine (PEI), which can be branched or linear [86]. The branched structure of PEI contains a mixture of primary, secondary and tertiary amines, whereas linear PEI has only primary and secondary amine groups [86]. PEI-functionalized silica adsorbents belong

to class 1 aminosilica sorbents (see Figure 10) [80]. PEI-functionalized sorbents have been reported to suffer from low stability in repeated adsorption/desorption cycles [80].

PEI-functionalized silica were stabilized with silane- and titanium-based additives in a study by Choi et al. (2011a)[80] to provide class-1 aminosilicas with for example enhanced thermal stability. The additive-treated silicas were thermally more stable, as the decomposition temperatures of PEI were 185°C, 225°C and 235°C for the untreated sorbent, the silane treated sorbent and for the titanium treated sorbent, respectively. The CO_2 adsorption experiments were conducted with simulated air consisting of argon and 400 ppm CO_2. The amine loadings and adsorption capacities were in the ranges of 10.5-10.7 mmol N/g sorbent and 2.19-2.36 mmol CO_2/g sorbent, respectively. The treated aminosilicas had adsorption half times around 200 minutes, while the untreated aminosilica had an adsorption half time of over 300 minutes. In TSA cycles, adsorption was conducted at 25°C, desorption at 110°C. In 4 temperature swing cycles in dry conditions, the capacity decrease of the untreated aminosilica was 2.36-1.65 mmol CO_2/g sorbent, while the corresponding values for silane-treated and titanium-treated aminosilicas were 2.26-2.05 mmol CO_2/g sorbent and 2.19-2.16 mmol CO_2/g sorbent, respectively.

Kuwahara et al. (2012)[91] incorporated zirconium into a PEI-funcionalized mesoporous silica (SBA-15). Under gas with argon and 400 ppm CO_2, the resulting sorbents had higher CO_2 adsorption capacities, stability and regenerability compared to PEI-silica without Zr atoms. The silica-PEI sorbent with no Zr had an adsorption capacity of 0.19 mmol CO_2/g sorbent. A sorbent with the molar ratio of Zr/Si of 0.070 had the highest adsorption capacity, which was 0.85 mmol CO_2/g sorbent with amine loading of 8.33 mmol N/g sorbent. The decomposition temperatures of PEI were 30°C higher for the Zr-incorporated silicas. Bare Zr-silica sorbent had a negligible adsorption capacity towards CO_2. In 4 TSA cycles with regeneration under Ar flow and temperature swing from 25°C to 110°C, a PEI-silica with Zr atoms suffered a 2% drop in adsorption capacity. In similar cycles, the adsorption capacity of the PEI-silica with no Zr atoms was decreased 34%.

Potential materials for DAC are also class 3 aminosilicas (Fig. 4), so called hyperbranched aminosilicas (HAS). They are prepared by reacting aziridine with the porous silica surface [66]. Choi et al. (2011b)[64] investigated the CO_2 adsorption capacities, kinetics and regenerability of class 3 silica sorbents under humid air with 400 ppm CO_2. Choi et al. (2011b) argued that the reduction in adsorption capacities, when lowering the

concentration of inlet CO_2 from 10% to 400ppm, for class 3 sorbents was less significant than for class 2 aminosilicas. For the class 3 sorbents studied, the reductions in adsorption capacities were in the range of circa 1.1-2.0mmol CO_2/g sorbent, while the amine loading of the materials was in the range of circa 2.3-10.0 mmol N/g sorbent. The amine loading and thus adsorbent capacity, which was in the range of 0.15-1.72 mmol CO_2/g sorbent, was increased with the cost of adsorption half time from about 90 minutes to 167 minutes. For a certain tested HAS type sorbent, in four temperature swing cycles, no significant loss of adsorption capacity was noticed.

Different propyl-silane group functionalized, class 2 aminosilicas, were examined in a study by Didas et al. (2012)[57] to compare the efficiency of primary, secondary and tertiary amines in CO_2 capture from gas with helium and different concentrations of CO_2. At temperatures 25°C, 45°C and 65°C, silica materials functionalized with primary amines had significantly higher adsorption capacities for CO_2 than silica materials functionalized with secondary or tertiary amines. For example, at 25°C with amine loadings of 3.75 mmol N/g adsorbent and 2.41 mmol N/g adsorbent, the adsorption capacities in 400 ppm CO_2 were circa 1.1 mmol CO_2/g adsorbent and 0.2 CO_2/g adsorbent for silicas with primary and secondary amines, respectively. The adsorption of CO_2 for tertiary amines was negligible. Circa 47% higher heats of adsorption were gained for primary amines than for secondary amines, indicating to stronger bonding, and probably explaining the results. It was also found, that primary amine functionalized silica adsorbed more water than other samples, and further, that higher loading of amine resulted in increased water uptake.

Heats of adsorption of CO_2 on amine grafted silica materials were also studied by Alkhabbaz et al. (2014)[92]. Heats of adsorption were found to increase with higher loadings of 3-aminopropylsilyl groups, with loadings varying from 0.87 to 1.87 mmol N/g sorbent. The material with the lowest loading of amine gave heats of adsorption of similar scale to that of bare silica. The values of these heats of adsorption were about 50% of value of the heats of adsorption for the material with the highest amine loading. The effect of the amine structure on the heats of adsorption was also studied, and amines containing syclohexyl- or a benzyl group gave especially low heats of adsorption. The heats of adsorption of the 3-aminopropylsilyl functionalized silica and of secondary amine functionalized silicas were of similar magnitude, but the primary amine still had significantly higher CO_2 uptakes from concentrations of CO_2 similar to ambient air. The

higher uptake of the primary amine compared to the secondary amines could therefore not be contributed to higher heat of adsorption, i.e. enthalpic factor. The difference in CO_2 uptakes was explained by entropic factors related to methyl chain bound to the amine.

Polyallylamine (PAA) instead of PEI was proposed for the preparation of class 1 adsorbents in a patent by Khunsupat et al.[93]. The PAA-functionalized silica sorbents were found to have almost as high or slightly higher adsorption capacities, but were more stable than the PEI-functionalized silicas. The PAA-functionalized materials had greater resistance to oxidative degradation, as these materials lost no more than 12% of the CO_2 adsorption capacity, while the capacity loss for the PEI-materials was in the range of 7.5-70.1%. Other proposed possibilities for support materials than mesoporous silica foam were mesoporous alumina-based materials.

Wagner et al.[94] used amine-grafted mesoporous silica to adsorb CO_2 from atmospheric air in outdoor conditions. To compare the results, experiments in pure CO_2 and synthetic air conditions were also conducted. Although the results were not fully comparable due to for example different temperatures, it is remarkable how poorly the sorbent material was found to perform in outdoor conditions: the adsorption capacities were reduced to almost zero after just 3 temperature swing cycles. The adsorptions were conducted overnight, with air temperature varying from -2^{o}C to +5^{o}C, and in relative humidity of 60-100%. The desorption was conducted at 75-100^{o}C. This was evidently caused by degradation of the amines at the cost of the formation of urea groups. Such degradation had been shown to occur in amine adsorbents in dry conditions before [95].

Mesoporous silica materials such as SBA-15 have often been chosen as the silica support [57,64,80,91]. However, other silica materials, such as silica gel[34], fumed silica[96,97] and macroporous silica[98] have also been proposed for direct air capture.

Diaminosilane-functionalized silica gel sorbent in the form of beads of a few millimetres in diameter were used in TCS and TVS for DAC in a study by Wurzbacher et al. (2011)[34]. Adsorption was conducted at 25^{o}C from gas with argon and 400-440ppm CO_2. The desorption, or the regeneration, was performed under vacuum and by heating in the TVS process, and in the TCS process by argon purge and heating. The amount of amine in the sorbent material was 2.48 mmol N/g adsorbent. The desorption temperature strongly affected the capacity of CO_2, which was 0.30 mmol CO_2/g adsorbent at 90^{o}C and 0.16

mmol CO_2/g adsorbent at 74°C in the TVS in dry air. The TCS process gave higher capacities of 0.40 mmol CO_2/g adsorbent and 0.32 mmol CO_2/g adsorbent correspondingly in dry air. In humid air, the corresponding values were 0.44 and 0.38 mmol CO_2/g adsorbent in TCS. Also, in the TVS cycles, higher desorption pressures gave lower desorption capacities of CO_2. In 40 TVS cycles, desorption capacity was in the range of 0.17-0.19 mmol CO_2/g, with no observable decrease in capacity.

Fumed silica has been proposed [96,97] as an easily prepared support material for DAC purposes. Goeppert et al. (2014)[97] compared different PEI-functionalized fumed silicas for the capture of CO_2 from air with 400-420 ppm CO_2. The effect of particle size on adsorption was first studied, and it was found, that using middle-sized particles (0.5-1.7 mm) resulted in the fastest saturation of the sorbent bed. However, desorption was faster for even smaller particles, and on the other hand, adsorption capacity from air increased slightly with increasing particle size. Further experiments were thus conducted with particles with the size of 0.25-0.50 mm. At 25°C, PEI-loading of 50 w-% was found to give the highest adsorption capacity of 73.7 mg (1.67 mmol) CO_2/g sorbent, but also resulted in the highest sorbent bed saturation time. For the PEI-loading of 50 w-%, maximum adsorption capacity was gained at 35°C, probably due to increasing diffusion in the sorbent. For a sorbent with 33 w-% of PEI, the corresponding maximum capacity was gained at 25°C. For both sorbents, the desorption temperature of 85°C was enough to decrease sorption capacity in the bed near to zero. Increasing air flow rate from 335 to 945 ml/min decreased the equilibrium capacity by 6% for sorbent with 33 w-% PEI, and by about 17% for the sorbent with 50 w-% PEI. Desorption in the cycling experiments was conducted by nitrogen purge and elevated temperature. Purities were 10% and 4% in desorption temperatures of 100°C and 85°C, and the desorption took 20 and 40 minutes, correspondingly. Over 4 cycles, no decrease in adsorption capacity was observed.

Macroporous silica (pore size >50 nm) was used as the solid support for CO_2 capture in a study by Liu et al. (2014)[98]. The macroporous silicas were functionalized with 3-aminopropyltrimethoxysilane (APTMS). When a gas with argon and 400 ppm CO_2 was used for adsorption, a capacity of 2.65 mmol CO_2/g sorbent was gained with amine loading of 10.98 N/g sorbent at 50°C. Although TSA cycling experiments were conducted with 10% CO_2 containing gas, it is notable, that the capacity decreased only 2% in 120 cycles.

3.2.3 Mesoporous carbon and -alumina

In addition to mesoporous silica, mesoporous carbon has been proposed for DAC, such as in a fairly recent study by Wang et al. (2015)[99]. The used gas in the study was a mixture of CO_2 and N_2, and was humid or dry gas, with 400 ppm and 5000 ppm of CO_2. The mesoporous carbon was functionalized by impregnation with PEI, and the samples with 55 weight-% of PEI were used in the adsorption experiments. Interestingly, the maximum CO_2 adsorption capacity of the sorbent was increased in all experiments, when temperature was increased from 25°C to 75°C, and only in higher temperatures started to decrease quickly. For example, for a certain mesoporous carbon sample under 400 ppm CO_2, the adsorption capacity was about 1.5 mmol CO_2/g adsorbent at 25°C, and about 2.0 mmol CO_2/g adsorbent at 75°C. For samples treated with a CO_2 diffusion enhancing additive, the corresponding values were 2.25 mmol CO_2/g adsorbent and circa 2.4 mmol CO_2/g adsorbent. Adding humidity to the CO_2 containing gas improved adsorption capacity slightly. TSA cycling was performed, after saturation of the sorbent with 400 ppm CO_2, by conducting desorption for 45 minutes, reaching 110°C. After 10 cycles, the adsorption capacity was decreased by 2-3%.

PEI-functionalized mesoporous alumina was used for CO_2 adsorption from simulated air in a study by Chaikittisilp et al.[84]. From 400 ppm air, the adsorption capacity for the bare alumina was 0.17 mmol CO_2/g adsorbent. With amine loadings of 8.66 and 11.20 mmol N/g sorbent, the corresponding sorption capacities were 1.73 and 1.95 mmol CO_2/g sorbent. Over three argon-purge cycles, the adsorbent didn't lose its capacity. For another PEI-functionalized mesoporous alumina [100], a capacity of 1.7 mmol CO_2/g adsorbent was gained from simulated air with N_2 and 400 ppm CO_2. The previous material's durability under steam stripping was also tested, because using industrial waste steam was proposed as a viable regeneration method. The material retained its capacity for 12 hours, but then dropped to 0.66 mmol CO_2/g adsorbent after 24 hours of steam exposure.

3.2.4 Porous polymer networks and colloidal crystals

Lu et al.[73] studied amine functionalized porous polymer networks (PPN) for DAC. The used amines were ethylenediamine (EDA) and diethylenetriamine (DETA). In synthetic air, DETA-functionalized PPN performed much better than the EDA-PPN, and was found to have a CO_2 loading of about 1.04 mmol CO_2/g adsorbent, and a high selectivity for CO_2

over N_2 and O_2. The resulting CO_2 output gas reached a purity of over 99.99% with the DETA-PPN. The working capacity reached zero at 98^oC, and almost 1.0 mmol CO_2/g adsorbent at 170^oC.

He has been involved in many studies[71,76,77] concerning various different polymer-based materials for DAC. Humidity swing is the used regeneration method in these studies, and the cycle times are shorter compared to the temperature swing cycles with aminosilicas, for example. The focus in these studies was not in the maximum CO_2 sorption capacities for these materials, but rather in the sorption kinetics.

Colloidal crystals, materials consisting of crystalline lattices formed of uniformly sized spheres, were studied for DAC by He et al. (2013a)[76]. The swing sizes, i.e. the working capacities, for these materials were in the range of 0.19-0.57 mmol CO_2/g sorbent. In the humidity swing cycling for a 20% crosslinked colloidal crystal material, the cycles lasted about 100 minutes, and the maximum load of CO_2 in a cycle was about 0.25 mmol CO_2/g sorbent, on average. In 15 cycles, there was no observed decrease in performance.

Another material class studied by He are polyHIPEs [77], in which the polymerization of monomers has been carried out in the continuous phase of a high internal phase emulsion (HIPE). The resulting polymer structure is highly porous and interconnected. The polyHIPEs in the study were functionalized with quaternary ammonium hydroxide groups. The swing sizes ranged from 0.16 mmol CO_2/g sorbent to 0.72 mmol CO_2/g sorbent. Humidity swing cycles were performed for the polyHIPEs with the lowest and highest swing size. The material with the lowest swing size was only run for one 35 minute lasting cycle, in which the maximum CO_2 load was ca 0.16 mmol CO_2/g sorbent. The material with the highest swing size had cycle times of about 60 minutes on average, with maximum CO_2 load decreasing from ca 0.7 mmol CO_2/g sorbent to ca 0.6 mmol CO_2/g sorbent after 5 cycles. The performance of the polyHIPE with the highest swing size was evidently caused by larger pore size, enhancing CO_2 diffusivity, and also by higher density of OH^- groups.

The results described above in the studies of He[76,77] were compared to Excellion membrane or -resin, which were significantly outperformed by the colloidal crystals and polyHIPEs. These materials, and carbon black functionalized by introducing quaternary ammonium groups, were compared with each other in another study by He et al.

(2013b)[71]. The HIPE based materials had the highest maximum CO_2 load of about 0.5 mmol CO_2/g sorbent, and the shortest cycle of about 35 minutes. The colloidal crystal material had a maximum CO_2 load of about 0.37 mmol CO_2/g sorbent in a 65 minute lasting cycle. The maximum CO_2 loads of the Excellion membrane and the carbon black based material were both only about 0.1 mmol CO_2/g sorbent, with the cycles lasting over 120 minutes.

3.2.5 Nanofibrillated cellulose

Nanofibrillated cellulose (NFC) was proposed for CO_2 capture from pressurized air with CO_2 concentration of 506ppm by Gebald et al. (2011)[35]. The NFC was grafted with aminosilanes, resulting in amine content of 4.9 mmol N/g adsorbent. Desorption was performed by argon purge. In a 12-hour adsorption experiment in 40% humidity, the CO_2 loading was found to be 1.39 mmol CO_2/g sorbent, and the adsorption half time was under 100 minutes. After 20 2-hour adsorption- and 1-hour desorption cycles (TSA), no significant decrease in CO_2 adsorption capacity was noticed. The average CO_2 adsorption capacity in the 3-hour cycles was 0.695 mmol CO_2/g sorbent.

Wurzbacher et al. (2012)[36] proposed a TVS cycling process for another amine-functionalized NFC material. Air used for the adsorption was dried and compressed ambient air with CO_2 concentration of 400-510 ppm. The amine content of the material was 3.86 mmol N/g adsorbent. 5-hour adsorptions were conducted in different adsorption temperatures of 10-30 ^{o}C and relative humidities of 20-80%. The capacities were in the range of 0.32-0.65 mmol CO_2/g sorbent, depending on the conditions. The adsorption capacity was found to increase with increasing humidity level, but decrease with increasing temperature. Cycling was performed in 20^{o}C and 40% relative humidity, and after 10 cycles, no significant reduction in the adsorption/desorption of CO_2 (0.415/0.421 mmol CO_2/g sorbent on average) was noticed. Heat requirements for the regeneration in different conditions were also measured, and the lowest and highest requirements were 205 kJ/mol CO_2 and 434 kJ/mol CO_2 for 10^{o}C (or 20 ^{o}C) cycle with relative humidity of 20% (or 20%) and for 20 ^{o}C cycle with relative humidity of 80%.

The stability of the NFC material in the TVS cycling for the CO_2 capture from air was later further studied [37]. In the cycles, adsorption was carried out for 150 minutes at 30^{o}C in relative humidity of 60%, and desorption was carried out for 45 minutes at 90^{o}C and 30

mbar pressure. The CO_2 adsorption capacity was around 0.90 mmol CO_2/g sorbent, and the equilibrium capacity of 1.28 mmol CO_2/g sorbent was lowered only about 5% after a hundred TVS cycles. The slight performance decrease was caused by O_2 during desorption, leading to loss of amine groups and formation of amide/imide species. A stronger degradation of over 30% in capacity occurred, when the sorbent was exposed for 15 hours to humid gas containing only nitrogen and 20% O_2, but no CO_2.

In a more recent study [101], PEI-containing NFC sorbent was studied for DAC under moist air with 400 ppm CO_2. Increasing relative humidity from 20% to 80% was found to affect increasingly on the CO_2 adsorption. The CO_2 adsorption capacity was 2.2 mmol CO_2/g sorbent at its highest, and was found to decrease after PEI content was increased above 44% of the total weight of the sorbent. The adsorption half times of the PEI-NFC sorbents were compared and found to be lower than with previously reported half times of aminosilane-NFC or PEI-silica sorbents. For example, the NFC sorbent with 44 w-% PEI had adsorption half times around 10-15 min. Cycling experiments were conducted by increasing the adsorption temperature of 25^{o}C to 85^{o}C at 5^{o}C/min. After five cycles, the CO_2 adsorption capacity was not significantly lowered for the NFC samples with amine content 44% or below, but the samples with more amine content were clearly more unstable.

3.2.6 Metal-organic frameworks

Metal-organic frameworks (MOF) are crystalline solids, which are formed of ligands of organic groups that are coordinated to metal-ions, creating a network that can be either rigid or flexible. In rigid MOFs, the selectivity of adsorption is based on molecular sieving and/or adsorbate-surface interactions. Flexible MOFs respond to external conditions such as temperature, pressure or molecules entering the network, allowing condition-dependent molecular sieving along with the mechanisms of rigid MOFs. The pore sizes of MOFs are most often in the range of 3-20Å. [61] Probably the most important disadvantage in MOFs is the hydrolysis of metal-ligand bonds by water [68]. An example of a MOF structure is presented in Figure 13.

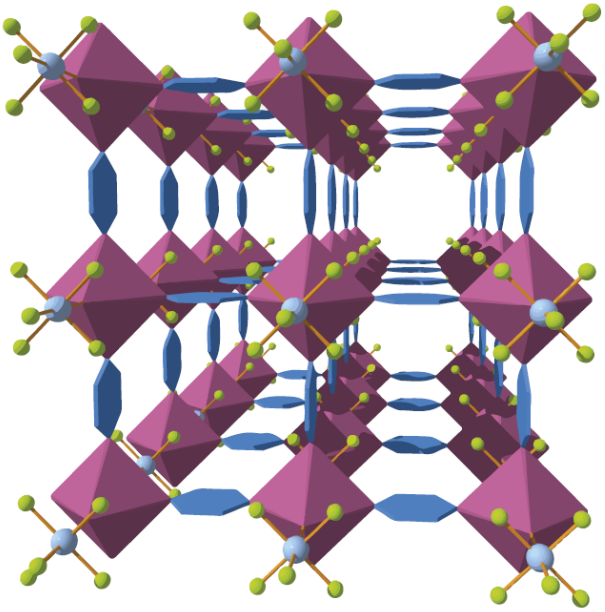

FIGURE 13 SIFSIX-3-Cu/Zn, an example of a metal organic framework material. SIFSIX-3-Cu/Zn consists of $CuSiF_6$ or $ZnSiF_6$ and pyrazine rings. The metal-ions are depicted as purple polygons, Si as blue spheres, F as green spheres and the pyrazine as blue polygons. [79]

Mcdonald et al.[74] studied the adsorption of CO_2 from dry air on N,N'-dimethylethylenediamine (mmen) functionalized MOFs. From air containing 390 ppm of CO_2 at 25°C, the adsorption capacity was about 2.0 mmol CO_2/g sorbent. In adsorption experiments from synthetic gases containing only 400 ppm CO_2 and N_2 or O_2, the estimated purities of desorption gas were 96% and 98%, respectively. In cycling experiments, adsorption was performed under simulated air with 390 ppm CO_2 at 25°C for 60 min, and the desorption was carried out by a N_2 flow at 150°C for 30 min. A capacity of 1.05 mmol CO_2/g was achieved, and no decrease was observed after 10 cycles.

Higher adsorption capacity was gained with a diethylenediamine functionalized MOF in a study by Lee et al.[70]. The effect of moisture in cycling experiments was also studied. Adsorption onto the MOF under air with 390 ppm of CO_2 at 25°C resulted in a capacity of 2.83 mmol CO_2/g sorbent. TSA cycling was performed by first saturating the sorbent for 15 hours under simulated moist ambient air with a CO_2 concentration of 390 ppm, and then desorbing the CO_2 by N_2 purge at 150°C for 2 hours. After 5 of these cycles, capacity decreased 6%.

The above MOF examples are based on amine functionalization, but Shekhah et al.[79] proposed a MOF for DAC with no amine- or other post-synthesis functionalization, but a small average pore size of 3.5Å. From synthetic air composed of N_2 and 400 ppm CO_2, the studied MOF adsorbed 1.24 mmol CO_2/g sorbent at 25°C. The MOF in question could be fully regenerated by vacuum at as low temperature as 50°C. The material was also reported to be stable after at least 4 such cycles under dry or humid air.

3.2.7 Ion-exchange resins and -membranes

With ion-exchange resins, the CO_2 is absorbed within the resin, and reacts with the anion-groups attached to the polymer structure. Resins containing quaternary-ammonium ions, and also resins functionalized with primary amines or PEI are discussed here. The most defining common factor for the sorbent materials in this chapter is, that the matrix is crosslinked polystyrene. In Figure 14, the principle of the CO_2 capture mechanism a certain resin containing quaternary-ammonium groups is presented.

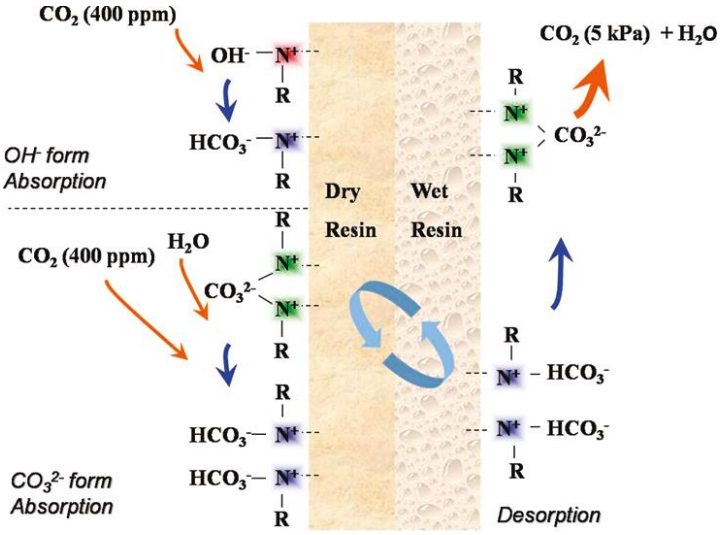

FIGURE 14 The principle of CO_2 capture mechanism of an anion-exchange resin proposed by Wang et al. (2011) [46]. The alkaline OH^- groups react with CO_2 in the dry state to produce bicarbonate (HCO_3^-). CO_3^{2-} groups need water from the resin or from air to produce bicarbonate. When the resin is wetted, the reaction equilibriums are shifted so that CO_2 is released.

An anion-exchange resin in the form of flat sheets, i.e. an anion-exchange membrane, containing polypropylene (PP) as the matrix and a resin powder with quaternary ammonium groups, was proposed for DAC by Wang et al. in 2011 [46]. The original sorbent material contained Cl^--ions for the ion-exchange, but was washed in dilute NaOH and

$NaCO_3$ to introduce OH^- and CO_3^{2-} ions into the resin instead. The resin was saturated up to 99% of the CO_2 from a gas with 400 ppm CO_2 and 0.5% moisture. At around 23^oC, the resin was desorbed to 55% saturation level of the CO_2, when humidity level was increased to 18 parts per thousand (volume H_2O/volume air). Either humidity swing or water swing were proposed, with both having their own advantages and disadvantages. For example, water swing would probably provide higher kinetics, but would require purified water. At 25 ^oC, the resin absorbed 0.86 mmol CO_2/g sorbent from dry air with 440 ppm of CO_2 [75]. Evidently, this was the same resin that was outperformed by colloidal crystal materials and polyHIPEs (see 3.2.4). Although the sorption capacity of this resin for CO_2 was comparable to other materials such as colloidal crystals, it suffered from much lower absorption and desorption rates when humidity swing was used [71]. For example, the adsorption rate of the colloidal crystal sorbent was 5 times faster than of the resin.

A primary amine functionalized resin was used for CO_2 capture in a study by Alesi and Kitchin [69]. The As the sorption experiments were conducted under 10% CO_2 stream at 50^oC, the sorption capacities gained in the study are not comparable to results obtained from CO_2 capture under near ambient conditions. However, it is worth mentioning, that the resin retained its adsorption capacity after 18 TSA cycles, with temperature swing from 50^oC to 120^oC. Also, the resin was claimed to adsorb circa 1 mmol CO_2/g sorbent when exposed to air at ambient conditions.

PEI-impregnated resins have also been proposed for capture of CO_2 from CO_2/N_2 gas, with 400 ppm CO_2 [102]. Loading of 50% of PEI on the resins, and adsorption temperature of 25^oC was found to give the highest CO_2 adsorption capacities. Cycling experiments were conducted by adsorption for 12 hours and desorption for 3 hours by heating at 100^oC under N_2 flow. In the first cycle, the adsorption capacity was 99.3 mg (2.26 mmol) CO_2/g sorbent, and 97.8 mg (2.22 mmol) CO_2/g sorbent after the fifth cycle.

3.3 Discussion

What is needed to describe the suitability of a CO_2 sorbent material is not necessarily evident or universal. As could be seen from literature, the quality of reported information about the CO_2 sorbents varies. Naturally, scientists often report parameters best suited for their own experiments or conclusions. It is evident, that not every aspect of the suitability of a CO_2 sorbent can be reported by universally valid and fully comparable parameters. The great differences of the sorbent materials and the experimental procedures contribute to this variability of different parameters. In this chapter, the results of the literature are discussed. The perspective here is focused on the most significant factors contributing to the suitability of the materials. The discussion involves both material characteristics and external conditions affecting the performance of the sorbents. Most important results have been summarized in Appendix I.

3.3.1 Amine functionalization

The majority of the sorbent-based CO_2 capture processes are based on chemisorption of CO_2 on an amine group on the sorbent material. One example of a promising material[79] based on physisorption for DAC was a MOF structure with a very small average pore size. However, the binding energy in physisorbents is usually not enough for DAC, because the capacities were found to be low or negligible. In the case of ion-exchange resins, the CO_2 capture mechanism is not based on ion-exchange, but on the formation of bicarbonate with resins containing quaternary ammonium groups. In resin materials the mechanism of CO_2 capture is also different such that the CO_2 is also soluble in the resin structure, and is not perhaps limited to chemisorption [69]. Using materials that capture CO_2 by unregenerable chemisorption[85] is hardly practical or cost-effective for DAC purposes. Amine functionalized sorbents seem to lead the technological development of solid CO_2 sorbents.

The options of amine functionalization seem to be almost limitless, but are often different aminosilanes or alcohol-amines. Evidently, the production of primary amine groups is most desirable, because primary amines provided the highest CO_2 adsorption capacities in the study by Didas et al. (2012). Although Didas et al. (2012) found higher heats of adsorption for primary amines, in the study of Alkhabbaz et al. (2014) the heats of adsorption were similar for primary and secondary amines. The entropic factor related to steric limitations can therefore be as important as a strong binding strength. Therefore, heat

of adsorption alone is not adequate in predicting whether a sorbent is a strong CO_2 sorbent. Primary amines have a higher binding strength and also less crowded conformation compared to secondary and especially tertiary amines.

Amine loading is one of the most important design parameters in amine functionalized CO_2 sorbents. Materials with higher amine loadings usually had higher adsorption capacities also. The effect of amine loading on the equilibrium CO_2 adsorption capacity can be seen in Figure 15.

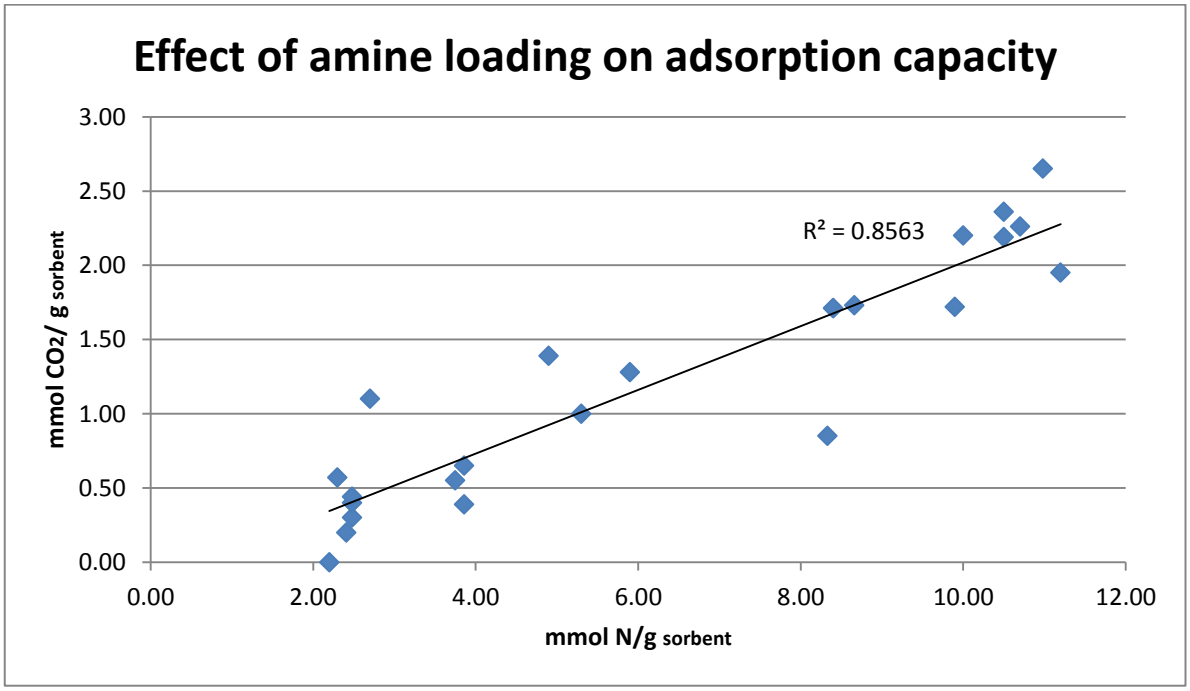

FIGURE 15 The effect of amine loading on the adsorption capacities of different amine functionalized CO_2 sorbents gained from literature in variable conditions. The concentration of the inlet gas was in the range of 390-510ppm. Adsorption temperatures were 20-50^{o}C.

From Figure 15 it can be seen, that the adsorption capacity is dependent on the amine loading, and a linear correlation is found. Linear correlation was tested by regression analysis t-test (see App. II). Significant deviations can be seen from linearity, however. The deviations are naturally caused by the type of amine and different physical conditions, but also significantly by the amine loading. Indeed, the maximum loading was not the optimum. Here, amine efficiency became the most important parameter.

The amine loading was found to often give the highest amine efficiency at about 50 w-% at least in the case of PEI (see App. I).This optimum amine loading was explained by better

diffusion of CO_2 [84,97,99,102]. However, the reaction mechanism of CO_2 adsorption was also argued to be dependent on the amine loading in addition to the effect of moisture [90]. Moisture and lower amine loading would provide higher amine efficiency. Because the theoretical amine efficiency may be either 0.5 or 1.0 depending on these conditions, it is important to attempt to identify the mechanism behind the CO_2 capture. Even though it is not clear to what extent the amine efficiency can and is reasonable to be enhanced by decreasing the amine loading, it is a matter worth investigating. Whether the reaction mechanism or diffusive factors are dominating in amine efficiency, the optimization of the amine loading is clearly an important parameter when designing new CO_2 sorbents in any case.

3.3.2 Equilibrium capacity

The adsorption capacity of a CO_2 sorbent is clearly the most compared parameter, and is usually at the centre of focus in the literature. However, as was stated in chapter 3.1.4, the sorbent material needs to lose its capacity in reasonable conditions. The equilibrium capacity alone is not a descriptive parameter about the material's feasibility for a CO_2 capture process. For example, the approach of He[71,76,77] was more process oriented and less about reaching maximum equilibrium capacity. Equilibrium CO_2 capacity is however a good parameter in comparing the effect of different conditions and parameters to the performance of the sorbent material. The capacities referred here to as equilibrium capacities are the maximum capacities reported in each case, but are not necessarily equal to the maximum capacity. Mostly physical factors affecting the equilibrium capacities are discussed below.

Different mesoporous and microporous materials were well represented in the literature. The reported equilibrium capacities of sorbent materials gained from 390-510ppm CO_2 were plotted against the corresponding surface areas of these materials in Figure 16.

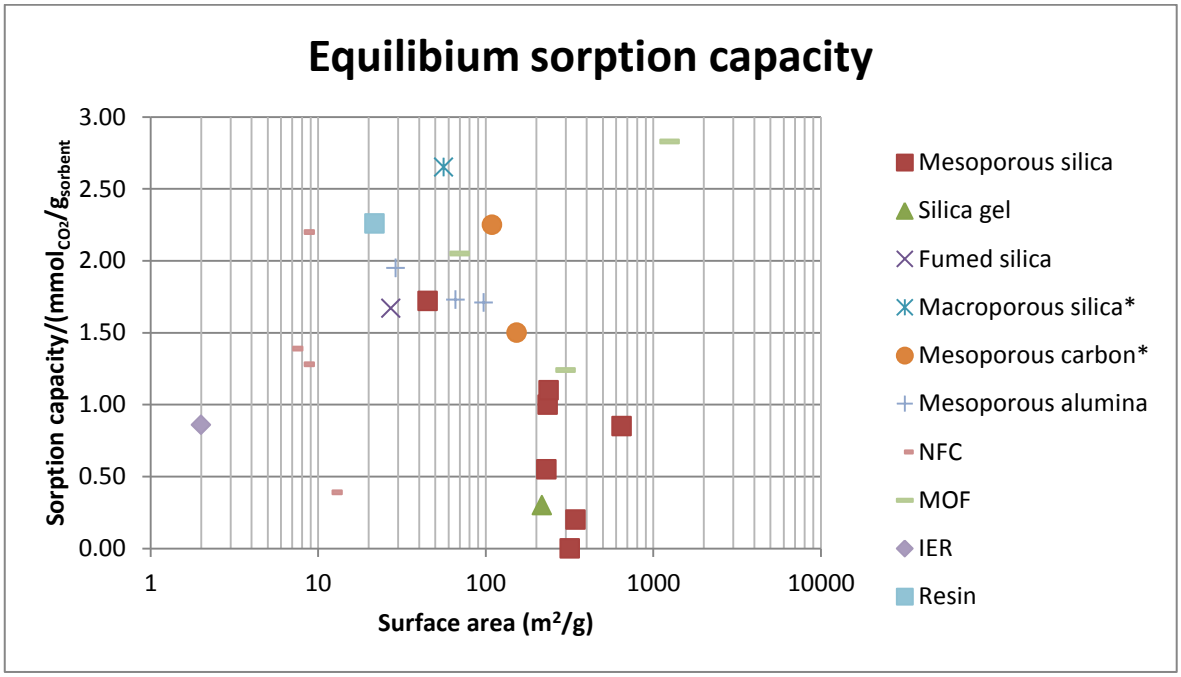

FIGURE 16 The effect of surface area on the adsorption capacities of different CO_2 sorbents gained from literature in variable conditions. The concentration of the inlet gas was in the range of 390-510ppm. Adsorption temperatures were 20-30°C. *Adsorption temperature was 50°C.

For the sorbents reviewed, no direct correlation is established between equilibrium capacity and surface area (see Figure 16). A MOF adsorbent with high surface area had also high capacity, but NFC materials with low surface areas still have reasonable capacity. Amine functionalized mesoporous silica have high surface area but relatively low adsorption capacity.

While larger surface area provides more space for functionalization, it does not equate to high adsorption capacity, and cannot be considered as an important DAC parameter. As argued by Liu et al., high surface area from very small pore size can cause crowding and deteriorate diffusion of CO_2 in the matrix. He et al. found that larger pore sizes, leading to higher surface area, enhanced the diffusion of CO_2.

The equilibrium capacity is also a good parameter for studying how a sorbent functions in different conditions. It was known, that the CO_2 concentration of the inlet gas affects the sorption capacity. For example, in the case of Liu et al. with a macroporous silica sorbent, the equilibrium capacity from 400ppm versus 10% CO_2 was approximately 31% lower. This kind of a change is significant, but not necessarily in the sense of process feasibility.

Air flow rate and the size of sorbent particles are examples of parameters that must also be taken into account. These parameters were not studied usually, except in the case of Goeppert et al., and were found to affect the kinetics and equilibrium capacities. However, these parameters could be classified as secondary parameters, because they are easily modified, although important in sorbent material design.

The positive effect of humidity was found in many of the results, excluding MOFs. The effect of humidity was probably due to the advantageous reaction mechanism for amines (see 3.3.1). The best adsorption temperature was usually 25^{o}C, although for some sorbents, 50^{o}C provided the highest capacities. The operation conditions are discussed from a process point of view in 3.3.4.

3.3.3 Kinetics

The kinetics of adsorption has been reported in many different ways, such as adsorption half time or sorption rates. It must be taken into account, that for example the kinetics in a TGA experiment is usually not comparable with fixed-bed adsorption due to different experimental setups. Also, the amount of different options in TGA experiments such as crucible type or the way in which the gas flows on the sample may have crucial effect on the kinetics of the experiment. For example, Sehaqui et al. compared the adsorption half times from experiments determined in a fixed-bed experiment to adsorption half times determined by TGA by Choi et al. (2011). Without accurate knowledge of the setup in the TGA in question, it is hard to evaluate to which extent the shorter half times by Sehaqui et al. were simply due to a well optimized fixed-bed adsorption setup. In a Netzsch STA[104] for example, the gas flows past the sample in TGA, whereas in a fixed-bed the gas flows through the sample. In general, it may be hard to compare the kinetics, if the experimental setups are not exactly the same.

As stated, especially TGA experiment setups can differ significantly, but kinetics in similar conditions can be descriptive. In TGA experiments, the adsorption half times were in the range of 90-300 min, while the time to reach pseudo-equilibrium took up to 24 hours. This strengthens the claim, that it may not be reasonable to reach the full equilibrium capacity because of deceleration of the increase in adsorption capacity (see 3.1.4). Here, adsorption half time as a parameter describes the kinetics well. It is an useful parameter also in comparing the effect of different conditions or even different materials in the same

experimental setup. For example, it was found that lower amine loading as well as the use of some additives decreased adsorption half-times.

Adsorption rate can also be a descriptive parameter, and could be used for comparison. However, it is questionable whether using equilibrium capacities and times as long as 24 hours really impart about the process feasibility of a material. Breakthrough time also describes kinetics, but from a different angle. Although one can observe how fast the sorbent bed is saturated, it does not tell how much CO_2 has been adsorbed and released for use. To evaluate kinetics better, the whole adsorption-desorption cycle should be studied in several cycles, with the CO_2 capacity reported, such as in Figure 17.

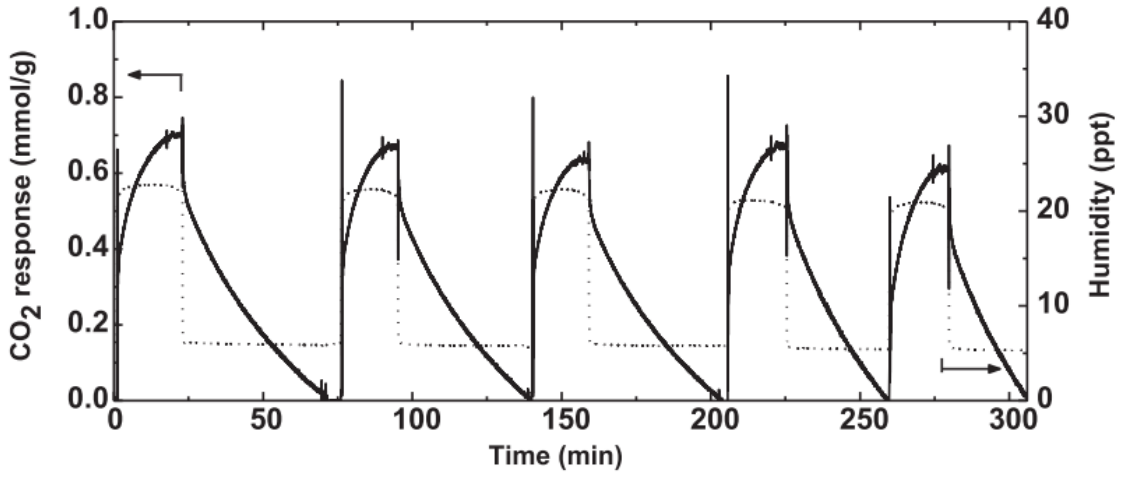

FIGURE 17 Adsorption and desorption profiles of a porous polymer CO_2 sorbent containing quaternary ammonium groups. The adsorption was conducted from 400ppm CO_2.[77]

From Figure 17, it can clearly be seen how the cycle times are different with each run. It can be seen that the adsorption step is significantly shorter than the desorption step. The overall rate, reported by He[76], consisting of adsorption and desorption rates is probably one of the best ways to report kinetics of a CO_2 sorption process. It is especially important in a process in which the desorption step is significantly slow compared to the adsorption step. However, overall rates were not reported as frequently as needed to make comprehensive comparison.

3.3.4 Regeneration and stability

Optimal DAC process conditions are governed by the sorbent material type. The regeneration conditions in the case of different sorbent types are discussed here. Thermal and cyclic stability are also discussed.

To find a balance between high CO_2 uptake and a low regeneration cost, different process options have been proposed. It was found that TSA was the most common regeneration process used. Vacuum swing was often used along with temperature swing to bring down the required temperature for desorption. An inert gas purge was also often used with TSA. Due to the different reaction mechanism (see 3.2.7), humidity swing was used for resins, colloidal crystals and polyHIPEs containing quaternary ammonium groups. The humidity swing was conducted by wetting the resin with liquid water in the case of Wang et al.[46], and by changing the humidity of the experimental atmosphere in the case of He et al.[71]. However, the way in which He et al. performed the humidity swing was not reported.

Working capacity (see 3.1.4) is one of the most concrete parameters describing a CO_2 sorbent in process conditions, because it is dependent on the regeneration conditions. The actual released CO_2 in reasonable conditions may be much lower than the equilibrium capacity. Such as in the case of Lu et al., the working capacity was still negative under 98^{o}C, which means that the sorbent doesn't release any CO_2 under this temperature. If a reasonable working capacity is not gained in lower temperatures, the energy cost may increase too high. The working temperatures, i.e. the differences of adsorption and desorption temperatures, of sorbent groups based on TSA or TVA are presented in Figure 18.

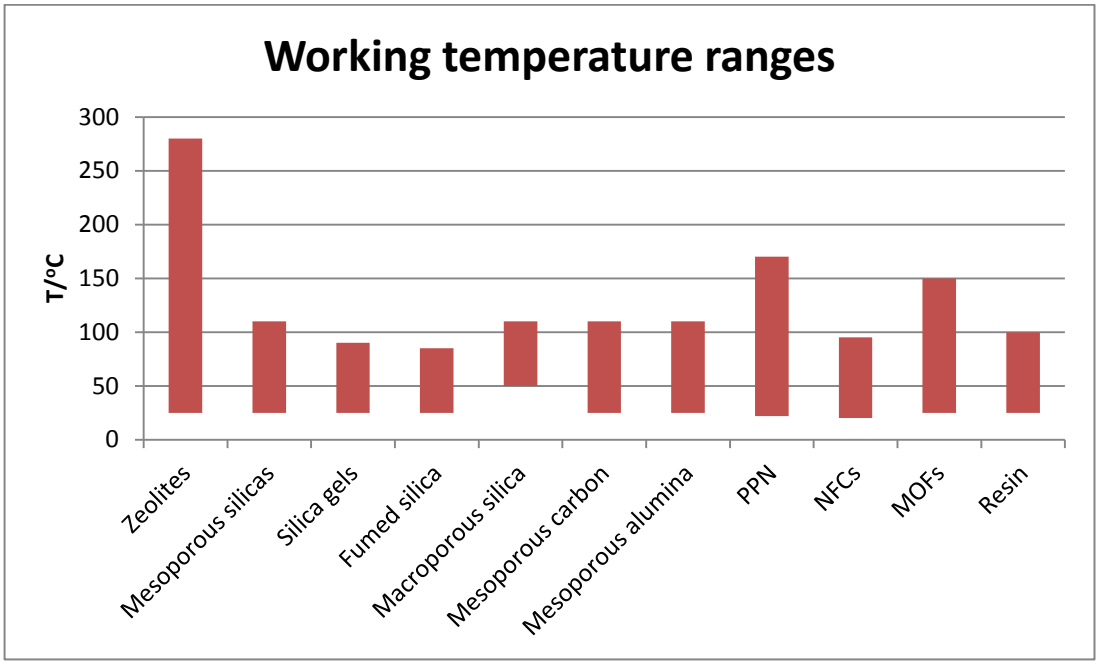

FIGURE 18 Working temperatures of different CO_2 sorbents by group.

The differences between adsorption and desorption temperatures were highest for zeolites, MOFs and PPN materials. The lowest corresponding temperatures were for different NFC materials and the MOF based on physisorption. For the macroporous silicas and –carbons, the best results were gained at adsorption temperature of 50°C. For such materials, and ones that require especially high desorption temperatures such as zeolites, DAC is probably not the best process application. Even though these materials were tested in DAC conditions, they would probably be more suited for flue gas conditions.

The regeneration energy cost is also affected by other factors than the desorption temperature. It must be taken into account, that vacuum was often used to decrease the desorption temperature (see App. I). Also, humidity was found to strongly increase the regeneration heats (see 3.2.5). The heating of water during desorption is part of the so called parasitic heat losses [105].

The stability of the sorbent materials was rarely tested comprehensively. Thermal stability by thermal degradation tests is not as relevant in DAC conditions as in PCC conditions. However, especially for sorbent materials requiring high desorption temperatures, the decomposition of the amines is a risk. The thermal stability of PEI-functionalized silicas was enhanced by Ti and Zr additives, but overall, other amines were preferred, evidently because of the stability issue. The degrading effect of water vapour apparently is the

biggest problem for promising physisorbent materials[103], of which amine-loaded MOFs were also found to suffer. This MOF stability issue was clearly under examination[70,74], but not yet solved.

Cyclic stability is a very descriptive parameter for evaluating process feasibility. However, often the amount of cycles conducted, if any, was less than 5, and most often less than 10. A sorbent surviving less than 10 cycles is not acceptable. Extensive cycling with 100 or more cycles was conducted to NFC and macroporous silica sorbents, and the adsorption capacities were retained by 95-98%. Both were functionalized with similar types of silanes, imparting of this material's superiority against PEI in terms of stability. The amine degradation products were imides or amides in the NFC case, which was conducted in humid conditions. Therefore, the humidity affects the degradation species, because in dry conditions, the result of oxidative degradation of similar type of amines was urea (see 3.2.2). Whether the degradation species has any effect on possible reuse of a spent sorbent material was not discussed in literature. Repeated functionalization of spent sorbents was not discussed either. Functionalization of a spent sorbent is not probably seen as a viable option, and therefore extended cyclic stability is of outmost importance.

3.3.5 Selectivity and purity

The selectivity of the sorbent material towards CO_2 was rarely reported. Comparison is also difficult because of different ways to report selectivity (see 3.1.4). Selectivity was only reported for zeolites, PPNs and MOFs. The reason to this lies in high confidence in the selectivity of the amine-CO_2 reaction mechanism. N_2 and O_2 are not necessarily seen as a problem, if the outlet gas is not intended for utilization. Also, in DAC purposes, the air used as the inlet can be assumed to be free of for example catalyst poisons. However, it is important for the outlet gas to be as pure CO_2 as possible because of the quality limitations in a methanation process (see Table I) and the CO_2 transportation costs (see 1.1.3).

The selectivity of CO_2 vs N_2 gained by Shekhah et al. with a physisorbent MOF was 5-7 times lower than the corresponding values gained by Mcdonald et al. and Lee et al. with amine functionalized MOFs. The amine functionalized material was therefore more selective.

Purity of the desorption gas was more often reported than selectivity, and is also a more descriptive parameter. It must be taken into account, however, that the way in which the

desorption is performed and other process conditions can affect the purity. Sorbents with low purities reported are not necessarily hopeless cases, but the processes may require development. The purity of the outlet CO_2 gained was plotted against the reported equilibrium capacities in Figure 19.

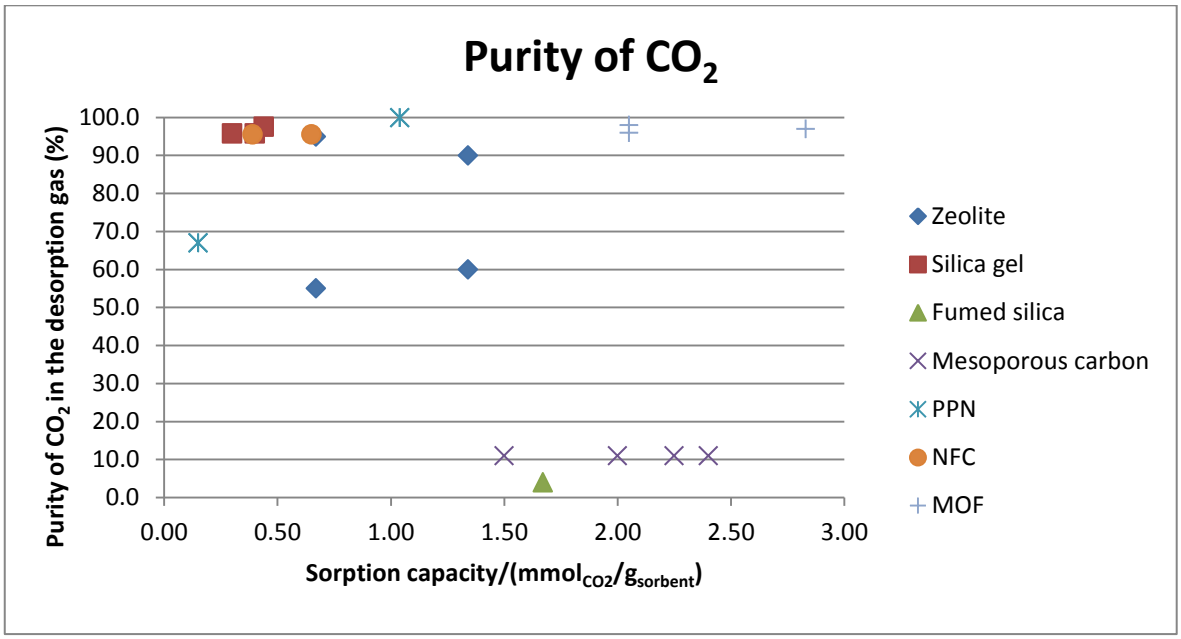

FIGURE 19 The purities of outlet CO_2 and the adsorption capacities for different CO_2 sorbents gained from literature in variable conditions. The concentration of the inlet gas was in the range of 390-510ppm. Adsorption temperatures were 20-50°C.

Among the sorbents compared in Figure 19, MOFs have the highest sorption capacity and purity. An especially high purity was also reported for a PPN material along with a reasonable CO_2 capacity. NFCs and silica gels also had high purities, although sorption capacities were low compared to many other materials. Mesoporous carbons and fumed silica had high sorption capacities but low purities.

3.3.6 Material comparison

Although many sorbents showed potential and innovative solutions were presented, few showed feasibility for full-scale application. The advantages and disadvantages of different materials discussed above are summarized here. Comparisons are also made.

Zeolites had reasonable sorption capacities, but had either very high regeneration temperatures, or were completely unregenerable. Many mesoporous sorbents performed

well, but a higher porosity itself was not an advantage. In silica sorbents, certain macroporous silica had superior overall performance, but the purity of outlet CO_2 was not reported.

An exceptionally important quality for a DAC sorbent is adaptability to different humidity conditions. The equilibrium capacities of a mesoporous carbon sorbent were almost as high in both dry and humid conditions. Mesoporous carbons also had high sorption capacities, but as with fumed silica, reported CO_2 purity was low. The application of industrial waste steam for regeneration of a mesoporous alumina sorbent was proposed to lower energy costs, but the material wasn't able to retain its capacity in excessive steam exposure.

Humidity swing sorbents were also promising especially from kinetic and energetic points of view. The overall process feasibility was yet hard to evaluate, because for example the purity of the outlet CO_2, and process procedures were not reported. Also, they may not be the best choice for use in humid conditions [105].

PPNs had reasonable sorption capacities and high CO_2 purity, but stability was not reported. Amine functionalized MOFs are promising especially because of the high selectivity towards CO_2 and high CO_2 adsorption capacity, but their stability under humid conditions has not been ascertained as of current knowledge. Also, for both amine functionalized MOFs and PPNs, desorption temperatures were higher than for mesoporous materials.

When examining all of the parameters discussed in the literature and comparing the sorbent materials, it seems that the most promising overall performance was gained with NFC material functionalized with aminosilane by Gebald et al. (2013). It had a good stability, reasonable CO_2 adsorption capacity, reasonable desorption temperature and it performed well in humid conditions. For a similar material reported by Wurzbacher in 2012, CO_2 purities were also high. Although the material is not superior compared to others, it was characterized and tested by the most important parameters in DAC, and was found to perform well.

II Experimental part

The determination of the process feasibility of a CO_2 sorbent is a task requiring comprehensive examination of the material from many different angles, as was seen in the literature part. The first task when testing a sorbent for CO_2 sorption process should be conducting characterization experiments that provide fundamental knowledge of the sorbent character, parameters for comparison purposes, as well as parameters to benefit further experiments. This was the purpose of the experiments presented in this thesis.

The experimental part has been divided into chapters 4 and 5. In chapter 4, the objectives of the experiments are discussed in more detail, and the experimental equipment and procedures are explained. In chapter 5, the results of the experiments are presented. Most of the experiments described below were conducted in the Chemtech laboratories of Lappeenranta University of Technology.

4 Experimental

Extensive tests were conducted to study the properties of CO_2 adsorbing amine functionalized resins. The goals of these experiments are first presented here to explain, why these experiments were conducted. The equipment, materials and the experimental procedures needed to conduct the experiments are then discussed.

4.1 Experimental aims

In short, the purpose of these experiments was to provide important information about two CO_2 adsorbing resins, one proprietary and another commercially available. The first goal was to characterize a resin sample known to be used for CO_2 adsorption purposes, and to provide important physical and chemical parameters for modelling of larger scale CO_2 adsorption. The second goal was to compare the characteristics of this resin to another one, and attempt to find out whether the two resins were similar. The third important goal was to compare the properties evaluated to those of other materials reported in literature, and to find out, at least to a preliminary level, whether these resins are reasonable sorbents to be used in CO_2 adsorption from thin air. The aims in each experimental procedure are provided in more detail below, divided into physical and chemical characterization tests.

4.1.1 Physical characterization aims

The purpose in the physical characterization tests was to determine the density, and size and shape properties of outer and inner structure of the resin beads. In addition to general observations, the aim was to determine parameters for modelling and comparative purposes.

To provide general insight about the surface properties and the quality of porosity of the resins, scanning electron microscopy was used. Size of the resins could best be described by determining particle size distributions using laser diffraction. As an important modelling parameter, the bulk density of the resins was determined by a simple measurement. The internal porosity of the resin beads is also an important modelling parameter, and thus, the skeletal density was determined by a pycnometric measurement. The cumulative pore volumes needed for the determination of the internal porosity were also to be determined. A combined BET and BJH analysis was used to gain surface areas, cumulative pore volumes and average pore sizes.

4.1.1 Chemical characterization aims

The purposes of the chemical characterization tests were to examine the resin's chemical structure and the CO_2 adsorption properties. The chemical structure and the species participating in the adsorption process were studied by FTIR experiments. Chemical structure was also studied by conducting elemental analyses. One of the most important goals of this study was to examine CO_2 adsorption capacity of resin samples in different conditions.

The aims of the FTIR experiments were to first of all provide information about the structure of the resin. The matrix material and the CO_2-capturing group were to be identified. Secondly, the species of the product of CO_2 sorption was to be identified, whether it was carbamate, carbamic acid or bicarbonate, such as in the study of Bacsik et al.[89]. Thirdly, the two different resins were compared to each other in respect of the matrix, the CO_2 capturing group and the species of captured CO_2. Finally, an attempt was made to examine peaks quantitatively to determine the effect of different conditions to the amine groups and the species of captured CO_2.

The elemental analyses were conducted by x-ray methods. These analyses were conducted to bring qualitative insight into the elemental structure, and not to try to predict the quantity of different species. Energy-dispersive x-ray spectroscopy (EDS) was used to study and compare different areas revealed in the SEM images. X-ray fluorescence (XRF) was then used as a supportive method for the determination of the elemental composition.

The aim in studying the CO_2 adsorption capacity was first to provide concrete evidence about the capability of the resin for the adsorption process. Secondly, the effect of pre-treatment of the resin and different adsorption temperatures were to be examined. Thirdly, the adsorption capacity is an important modelling parameter.

4.2 Equipment and materials

In this chapter, the materials and devices used for the experiments are described. Also, the experimental procedures are described in some cases. The experiments have been divided to physical and chemical characterization here, for the sake of clarity.

4.2.1 Physical characterization

Two resins of different origin were studied. Below, the resins are referred to as “resin 1” and “resin 2”. The resins were studied “as received” with no pre-treatment, and after pre-treatment. In the experimental section below, pre-treatment refers to drying the resin sample in a vacuum oven, at 90^{o}C or at 120^{o}C for 2 hours. Vacuum was applied in a vacuum-swing manner so that the pressure was lowered to approximately 60mbar, after which it was increased to approximately 100mbar, and this was repeated several times during the treatment. This swing-type process was applied to remove evolving moisture in the oven. The samples were transferred using petri dishes covered with watch glasses, and stored in a desiccator.

Scanning electron microscope (SEM) images were taken from the resins using SU3500 SEM (Hitachi). As received samples, and samples that were dried at 90^{o}C in the vacuum oven were imaged. Images were also gained from a gold-sputtered as received resin 1 sample. The voltage used was 10kV, and 15kV in the case of the images gained from the gold-sputtered sample.

Particle size distributions were determined with Malvern Mastersizer 3000 Aero laser diffractometer. A sample was taken from each resin and pre-treated in the vacuum oven at 120^{o}C. A few millilitres of the sample were dosed into the device, and two repeats were conducted for each sample.

Bulk densities were measured by simply weighing the sample on a graduated cylinder upon an analysis scale. Bulk density was determined for resin 1 pre-treated at 90^{o}C and 120^{o}C, and for resin 2 pre-treated at 90^{o}C. The skeletal density for resin 1 was measured by Geological Survey of Finland (GTK) by a pycnometric method.

BET and BJH analyses were conducted using Micromeritics Gemini V surface area and pore size analyser. FlowPrep 060 sample degas system was used for the degasification of the samples. The analysis was conducted for 4 different samples: for both resins dried in the vacuum oven at 120^{o}C or 90^{o}C for 2 hours. The samples were degasified by first introducing N_2 into the sample tube in a cool bath for approximately 10 minutes, then moving the sample to a heated bath for a certain time, and again putting the sample into the cool bath for 10 minutes. The resin 2 samples were deliberately longer in the degasification step, because the water content was known to be higher than with resin 1. The samples were weighed before and after the degasification, of which the latter was used to calculate the results. The pre-treatment and degasification conditions and the masses are provided in the Appendix III.

4.2.2 Chemical characterization

To study the chemical composition of the resins and the reaction species of CO_2 and the amine, Perkinelmer Frontier FTIR device was used with Attenuated Total Reflectance (ATR) sampling. No pre-treatment was needed to analyse the samples. A sample plate suitable for solids was used, and a small amount of sample was poured on the notch in the plate. The sample was then pressed against the ATR diamond with the pressure arm using similar force each time. Isopropanol was used to clean the diamond after each sample analysis. The device was set to conduct 4 scans to provide each spectrum. Absorbance was used as the unit instead of transmittance.

FTIR analysis was performed after many different treatments and experiments to the resins. In addition to pre-treatments described above, in the thermal stability group the resin samples were subjected to 150 ^{o}C, 180 ^{o}C and 200 ^{o}C for 1 hour. Also, a sample that

was subjected to hot nitrogen purge in STA is included in this group. The experiment was begun by introducing 25 ^{o}C N_2, and increasing the temperature by 5 ^{o}C/min up to 250 ^{o}C.

The used SEM was coupled with EDS. Because the EDS elemental analysis only covers very small sections of one bead, the sample heterogeneity is dismissed. Therefore, to gain a more reliable qualitative analysis of the elemental composition on the resin, x-ray fluorescence was used. The device in question was a portable Niton XL3t 900s -XRF-analyser by Thermo Scientific.

Netzsch STA 449 C Jupiter simultaneous thermal analyser was used to gain CO_2 adsorption capacities for resin 1. Sample crucibles were of Al_2O_3, into which 10-20mg of sample was placed. To prevent the samples from being blown away, the crucibles were closed with lids that had a small gap in the middle for the gas to contact the sample. In the sample furnace, one crucible was always as a reference, and the other contained the sample. The gases used were grade 5.0 N_2, grade 4.0 gas mixture consisting of 1% CO_2 balanced with N_2, and grade 4.6 He. Helium was used as a protective gas for the scale and was used at all times at 50ml/min. He was not in direct contact with the sample. The samples were pre-treated by drying them in a vacuum oven for 2 hours at 60-100mbar at 120^{o}C or 90^{o}C. An experiment was also conducted with an "as received" sample. Environics series 2000 computerized multi-component gas mixer was used to produce the 400ppm CO_2 from 1% CO_2 and N_2. The outlet from the gas mixer was connected to the STA. The total flow rate of N_2 and the CO_2 mixture to the sample was 50ml/min at all times.

The first step in each adsorption experiment was a drying step to remove excess water and to desorb any pre-adsorbed CO_2 from the sample. In this step the sample was heated from room temperature to 120^{o}C or 90^{o}C in 50ml/min flowing N_2, and then keeping the hot N_2 flow steady for 2 hours. In the cooling step, cool N_2 flow was introduced to cool the sample down to the wanted adsorption temperature in the range of 25-50^{o}C at 5^{o}C/min. Except in the case of the sample dried at 120^{o}C, the cool N_2 flow was continued for 1 hour after the cooling step to bring down the temperature of the sample, because the cooling step wasn't enough to completely cool down the sample. The adsorption was then started by introducing the 400ppm CO_2 into the sample furnace. Because of the shorter cooling step, for the sample dried at 120^{o}C, the adsorption started approximately 48 minutes earlier. The adsorption times were 20 or 24 hours.

An experiment with adsorption from 1% CO_2 was also conducted. A sample with pre-treatment in vacuum oven at 90^oC at 60-100mbar was used. Here the crucible was left open without a lid. The drying step in the STA was also at 90^oC, and similarly to other experiments, the sample was cooled down to 25^oC before the adsorption step. The adsorption was continued for 2 hours, after which desorption step was initiated. In the desorption step, the temperature of the sample was increased to 80^oC and kept at this temperature for 2 hours with hot N_2.

A control experiment was conducted using the same steps as in the CO_2 adsorption experiments, but with only N_2 flowing on the sample. The sample was resin 1 as received. The run consisted of the same steps as in the adsorption experiments, the heating, the cooling and the 20-hour adsorption. An experiment with no sample was also run in a similar way as the control experiment.

5 Results and discussion

In this chapter, all relevant experimental results are presented and discussed. Physical characterization results consist of all the determined physical parameters. For the sake of clarity, chemical characterization has been divided into FTIR results, the elemental analyses and the adsorption capacity results.

5.1 Physical characterization

All the relevant physical or physicochemical results are presented and discussed here. They have been divided into subchapters based on the experimental device used or the parameters determined. They include, in order, SEM, size distributions, bulk and skeletal density and porosity.

5.1.1 SEM

As described in section 4.2.1, both as received resins and pre-treated samples were imaged. No significant differences were noticed, however, and thus only images from the as received resins are presented here. Only the most relevant images have been selected. General views on the resin beads can be seen in Figure 20.

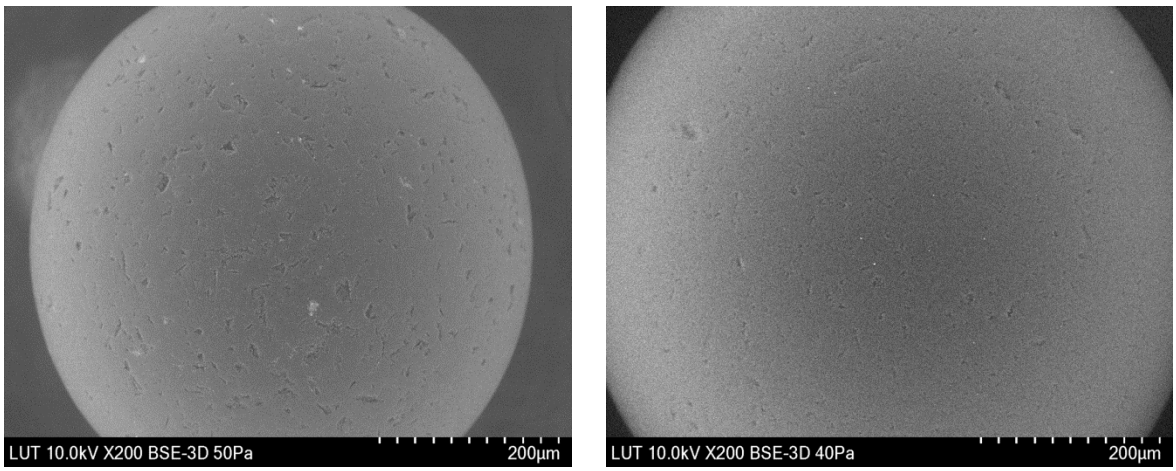

FIGURE 20 SEM images from two different resins as received. The image on the left is from resin 1, the image on the right from resin 2. A backscatter electron detector was used in this case. Voltage was 10kV, and pressures were 50Pa and 40Pa for resin 1 and resin 2 samples, respectively.

Almost whole beads can be seen in Figure 20 for both resins. Small white spots can be seen on the surface of both resins. Resin 1 has more of these white spots and they are

larger. Different sized macropores can be seen on the surface of both of these resins. The pores can be seen more accurately from Figure 21

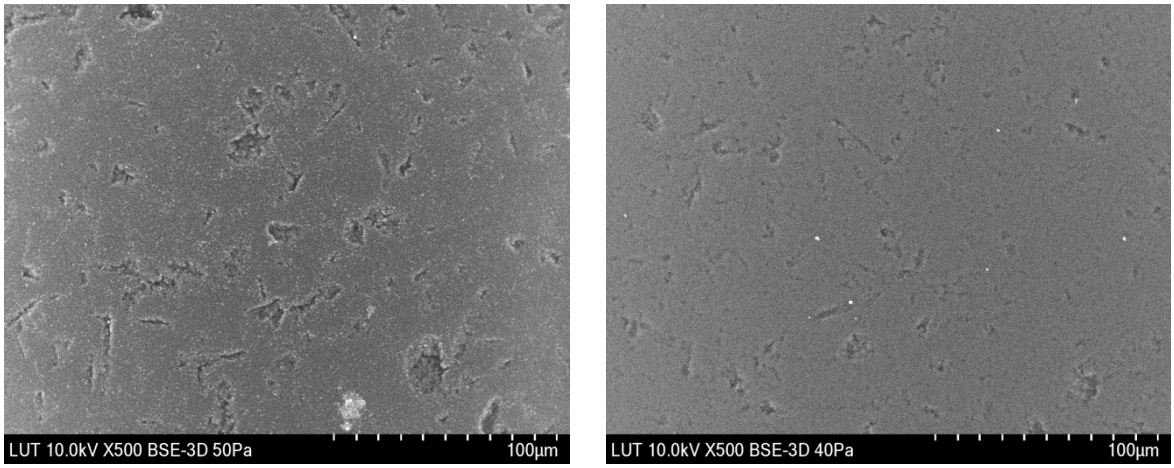

FIGURE 21 SEM images from two different resins as received. The image on the left is from resin 1, the image on the right from resin 2. A backscatter electron detector was used in this case. Voltage was 10kV, and pressures were 50Pa and 40Pa for resin 1 and resin 2 samples, respectively.

From Figure 21 the surface of the resin beads can be seen more closely. The white spots mentioned above are distinguished better. The white spots seem to be more small crystal-like shapes for resin 2, while on resin 1 the spots are relatively large, over 10µm in diameter. The high level of macroporosity can be observed for both resins, with the largest pores being circa 20µm wide. Mesoporosity could be studied from Figure 22.

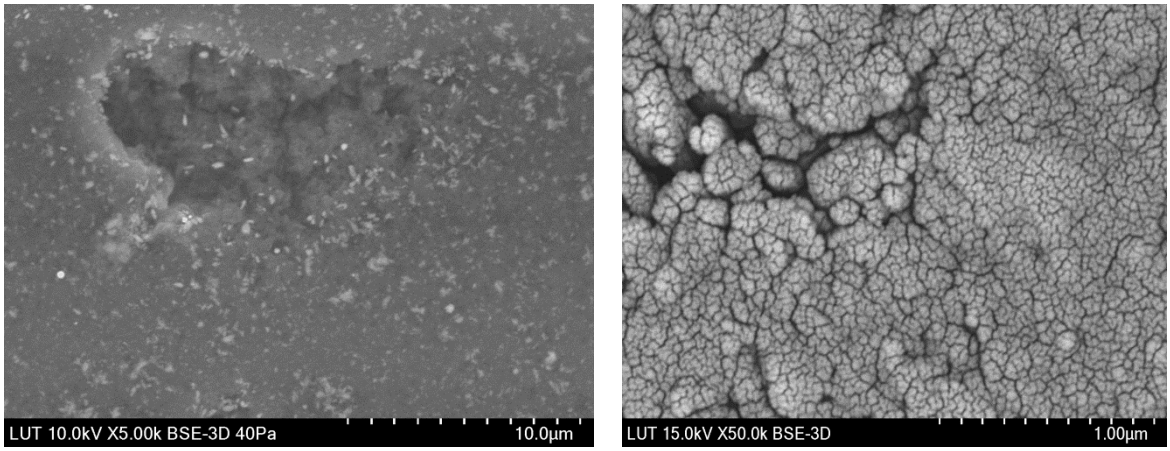

FIGURE 22 SEM images from as received resin sample on the left, and one with gold sputtering on the right. A backscatter electron detector was used in this case. Voltage was 10-15kV.

Figure 22 represents close-ups of an as received resin sample, and the same sample with gold sputtering. It can be clearly seen, that the resolution is higher for the gold-sputtered

sample, even with 10 times larger magnification. However, the gold-sputtering naturally covers any details on the surface. Mesoporosity can however be identified on the surface of the resin sample, with gaps smaller than 50nm.

5.1.2 Particle size distributions

The particle size distribution is described by three values, D10, D50 and D90. Each of these values represents the particle size below which 10%, 50% or 90% of the distribution lies, respectively.

TABLE II Particle size distributions of two CO_2 adsorbing resins determined with laser diffraction. The results are averages from two runs. The samples were dried in vacuum oven for 2 hours at 120^{o}C at 60-100mbar.

Sample	D10/µm	D50/µm	D90/µm
Resin 1	434	584	790
Resin 2	504	626	781

In Table II, the particle sizes of the resins are somewhat similar. The water content of resin 2 was higher, and could to some extent explain their larger particle sizes. The D90 value is however slightly bigger for resin 1. However, the most describing value is probably the median value D50, which is bigger for resin 2.

5.1.3 Bulk- and skeletal densities

Bulk densities for different samples are found in Table III.

TABLE III Bulk densities of two CO_2 adsorbing resins. The uppermost result is a mean value from two measurements. The samples were dried in vacuum oven for 2 hours at 120^{o}C or 90^{o}C at 60-100mbar.

Resin	Pre-treatment T/^{o}C	ρ/(g/cm^3)
Resin 1	120	0.4544
Resin 1	90	0.4625
Resin 2	90	0.4088

The skeletal density, i.e. the density of the solid material, was determined for resin 1. Specific gravity gained from pycnometer was multiplied with the density of water at 20°C to gain the skeletal density (see App. IV) of approximately 1.225g/cm^3.

5.1.4 BET-BJH analysis

The results of BET and BJH analysis from nitrogen isotherms are presented in Table IV. The pre-treatment and degasification conditions for each sample can be found in the Appendix III.

TABLE IV BET and BJH desorption results of two different resins with different pre-treatment conditions. Surface areas with errors, cumulative pore volumes and average pore diameters are reported. * refers to results from BET adsorption. ** refers to results from BJH adsorption.

Sample	S_A/(m^2/g)	±	Δ/(m^2/g)	V_p/(cm^3/g)	d_p/Å
1	32.03	±	0.39	0.0896	145.1
2	40.65	±	0.48	*0.2144	*256.4
3	26.17	±	0.85	**0.1001	**287.3
4	40.08	±	0.46	0.2736	389.9

In Table IV, some results have been taken from the adsorption and not from the desorption results. The reason was that BJH desorption was unsuccessful for sample 2, and both desorption curves were unsuccessful for sample 3. The reason for the difficulties to produce reasonable desorption curves is not evident, but imparts about the limitations in the experimental procedure for the samples in question. The nature of the sample itself may explain some difficulties, for example that the beads are prone to static electricity, and thus tend to stick for example on the surfaces of the sample tube. Examples of the N_2 BET isotherms and BJH pore volume plots can be found in Appendix III.

In Table IV, the surface areas differ somewhat between resins, but are still comparable. The surface areas, along with the cumulative pore volumes and average pore volumes are larger for resin 2. The surface areas between samples 1 and 4 differ only about 20%, whereas the cumulative pore volume is 3 times larger for sample 4. This refers to resin 2 having a significantly higher porosity.

The porosity of these materials is naturally much lower than with MOFs. If one compares the average pore sizes of these resins and the one reported for a physisorbent MOF (see

3.2.6), they could even be classified as nonporous sorbents in the group of solid DAC sorbent materials. The surface areas are generally on an average level when compared to other amine functionalized sorbents reported in the literature (see 3.3.2). The surface areas were higher than with other resin materials reported, and even comparable to some mesoporous materials.

The cumulative pore volume was then used to determine the internal porosity of the resin material. Porosity of resin 1 was determined by the following equation.

$$\varepsilon_p = V_p \cdot \rho_s \qquad (14)$$

Where ε_p internal porosity,
V_p cumulative pore volume,
ρ_s skeletal density.

The result was circa 0.110, which is fairly low compared to other porous adsorbents, of which porosities have been listed by Seader et al.[54]. However, it has to be taken into account, that the BJH desorption cumulative pore volume included only pores with diameter smaller than approximately 200nm, or 0.2µm. A significant amount of macroporosity is thus dismissed in this figure, and it is therefore only directional.

5.2 FTIR results

Due to the large amount of data obtained from the FTIR analyses, only the most relevant results are presented here. Comparable spectra were gathered under different groups that were plotted using Matlab and then analysed. All of the resin spectra presented here have been ATR-, and baseline corrected using the software package of the FTIR device. Also, the spectra were normalized using Matlab, by setting the spectrum baseline to zero, and a known polystyrene peak to 1 at 2920 cm^{-1}.

Different peaks were analysed using wavenumbers found in literature[69,89,92,106–108]. The peaks may sometimes refer to different species, and rarely have exact positions, but rather wavenumber range where they can be found. Thus, in some cases, only suggestions can be presented of the origin of the peaks. The peak wavenumber assignments and the sources can be found in Appendix IV. Only the most matching wavenumber annotations were added to the spectra below. Thus, the reader is advised to examine the table in the Appendix IV. In the following figures, carbamate is referred to as three different terms. "Ionic carbamate" and "bound carbamate" are terms used by Danon et al.[106], and refer to an alkylammonium carbamate stabilized by nearby amines, and to a carbamate bound to the surface of the sorbent material, correspondingly. Peaks of "carbamate" may refer to any of these two species or other forms of carbamate.

In sections 5.2.1-5.2.3, the resins were compared with each other by comparing the spectra of the as received resins and resins that were pre-treated at 90^{o}C. The spectra in these chapters were gained from 3 repeats for each different sample, by calculating the mean spectra. Three different sections of the spectra were analysed, which are discussed in the following. In section 5.2.4, the effect of high temperature thermal treatment on resin 1 is presented. The thermal treatments are described in section 4.2.2.

5.2.1 Identification of the amine group

The amine group accountable for the CO_2 adsorption could be characterized by examining the wavenumber range of 3700-2800cm^{-1}. This region can be seen in Figure 23.

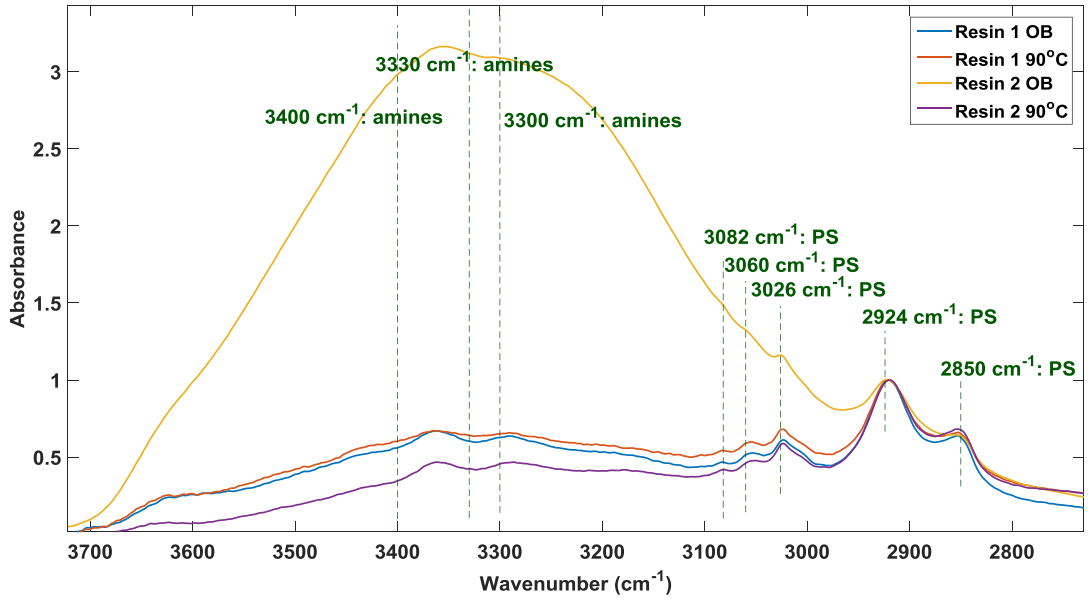

FIGURE 23 Normalized mean spectra from two different resins. "OB" means a resin with no thermal treatment. Resin samples "90°C" underwent a thermal treatment in a vacuum oven at this temperature at 60-100mbar vacuum for 2 hours. Normalization was performed by setting the baseline at a wavenumber of 3900 cm^{-1} to zero, and a known strong polystyrene peak at 2920 cm^{-1} to 1.

Similar peaks referring to polystyrene and amines can be found for each spectrum in Figure 23. The difference in peak amplitudes is significant, however. Thermal treatment at 90°C lowered the amplitudes in the spectrum of resin 2 to similar level as in the spectra of resin 1. A faint increase in the spectra can be seen in the range of 3440-3450cm^{-1} referring to carbamate. Two broad peaks between circa 3400-3250 cm^{-1} are clearly seen, referring to amines. Especially the presence of two peaks in this section refers strongly to a primary amine [109]. Both resins are thus functionalized with primary amine groups.

5.2.2 Identification of the adsorption reaction species

The focus in this section is in identifying the CO_2 chemisorption species formed on the resins. The adsorption mechanism in amine functionalized solid sorbents can be found in section 3.2.2. In Figure 24 is a wavenumber section in which significant carbamate activity can be found due to the strongly IR-absorptive species consisting carbon, oxygen and nitrogen.

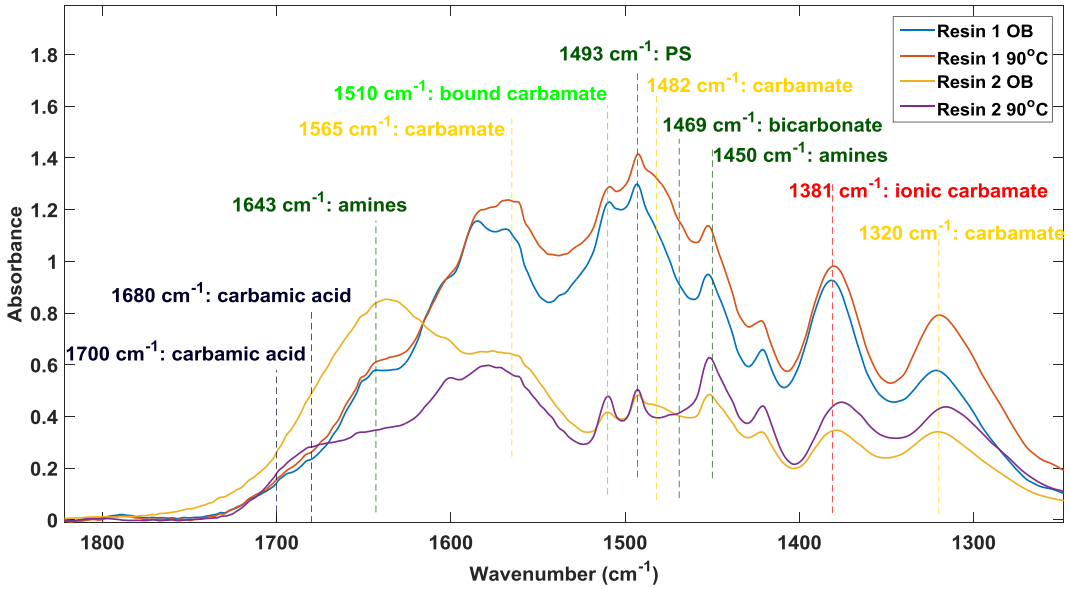

FIGURE 24 Normalized mean spectra from two different resins. "OB" means a resin with no thermal treatment. Resins with "90 °C" underwent a thermal treatment in a vacuum oven at this temperature at 60-100mbar vacuum for 2 hours. Normalization was performed by setting the baseline at a wavenumber of 3900 cm^{-1} to zero, and a known strong polystyrene peak at 2920 cm^{-1} to 1.

In this region peaks at 1482cm^{-1} and 1320cm^{-1} are assigned to $NCOO^-$ skeletal vibration, peaks at 1381cm^{-1} and 1565cm^{-1} are assigned to COO^- stretching, and peak at 1510cm^{-1} is assigned to CHN-group. All of these peaks refer to carbamates. In Figure 24, peaks at 1565cm^{-1}, 1510cm^{-1}, 1381cm^{-1} and 1320cm^{-1} are clearly found in each spectrum. A peak shoulder is also found at 1482 cm^{-1}, which occurs clearly for all samples except dried resin 2. Also, a faint shoulder is found at 1469 cm^{-1} for both samples in resin 1, which could refer to bicarbonate. For resin 2, no such peak can be found. For the dried resin 2, a broad shoulderlike peak can be found in the wavenumber range of 1700-1680^{-1}, which should refer to carbamic acid. In other spectra this peak is not found. A very broad peak maximum for the as received resin 2 is found in the range of 1643-1633 cm^{-1}, which could refer to amines. Also, a strong peak shoulder exists for resin 1 in this section. However, the same region is quite flat for the same resin that was dried at 90°C, except for a small peak at circa 1652 cm^{-1}, which can be found in each spectrum. It is unlikely, that the thermal treatment caused the amine to disappear, but that the amplitude is caused by excess water. Another peak at 1453cm^{-1} is closest to an amine found at 1450cm^{-1} in the literature[106]. Based on these findings, it can be concluded that in both resins the CO_2 capture mechanism is based on a similar reaction, where carbamates are the main reaction product.

5.2.3 Comparing the polystyrene region of the resins

The wavenumber region of 500-1200cm^{-1} was a known fingerprint region for polystyrene peaks. This region is depicted in Figure 25.

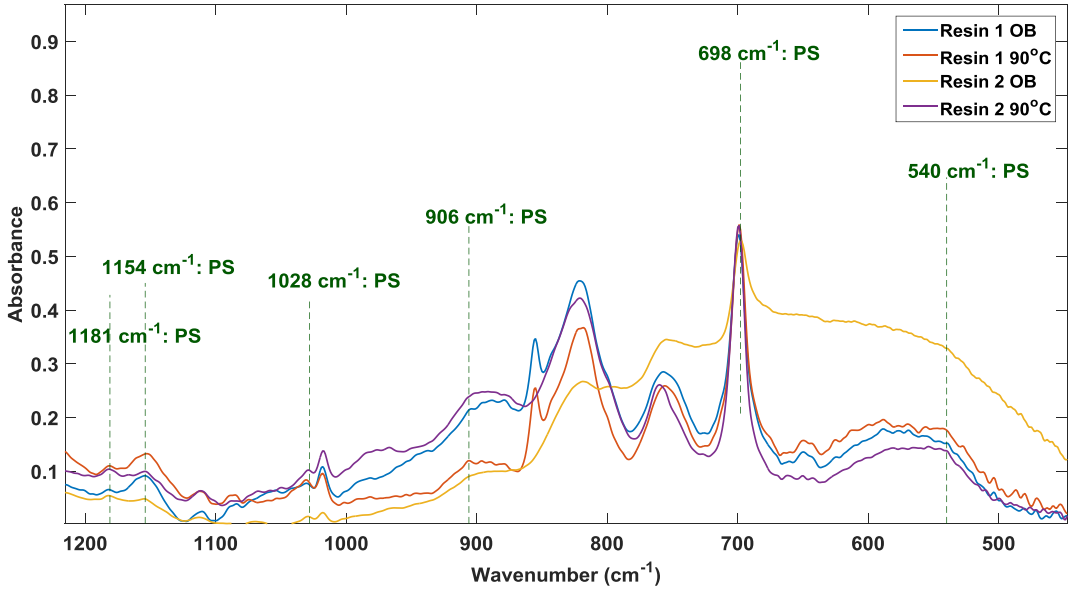

FIGURE 25 Normalized mean spectra from two different resins. "OB" means a resin with no thermal treatment. Resins with "90 °C" underwent a thermal treatment in a vacuum oven at this temperature at 60-100mbar vacuum for 2 hours. Normalization was performed by setting the baseline at a wavenumber of 3900 cm^{-1} to zero, and a known strong polystyrene peak at 2920 cm^{-1} to 1.

In Figure 25, not all of the peaks in this region can be identified as polystyrene peaks used for calibration in various standards[107]. However, this wavenumber region is important in the identification of the resin matrix, because the IR-fingerprints representing different substitutions of the aromatic ring can be found here[108]. Wavenumber regions 770-730cm^{-1} and 710-690 cm^{-1} refer to monosubstitution in the aromatic ring, and strong peaks can be found in these regions for all samples. However, the first of these may also refer to o-disubstituted aromatic ring. Wavenumber regions 810-750 cm^{-1} and 900-860 cm^{-1} refer to m-disubstituted aromatic ring, and peaks can be found also in these regions. However, a peak between 810-780 cm^{-1} is only a shoulder for other samples than the as received resin 2, and the other in the region of 810-750 cm^{-1} is the same as the one referring to monosubstitution. In the region of 860-800 cm^{-1}, which refers to p-disubstitution, occurs 2 peaks for resin 1, but only one peak for resin 2. Also, at approximately 650 cm^{-1} a peak can be found for the samples of resin 1, but not for the samples of resin 2. However, it cannot

be confirmed whether these smaller peaks refer to different substitution in the polystyrene structure, or some other compound. Undeniably the matrix of each resin is consisted of polystyrene.

5.2.4 Thermal stability

For each sample in this group, 3 repeats were conducted in the FTIR, and mean spectra were calculated to minimize the effect of sample heterogeneity. The effect of thermal treatment on amine peaks can be seen from Figure 26.

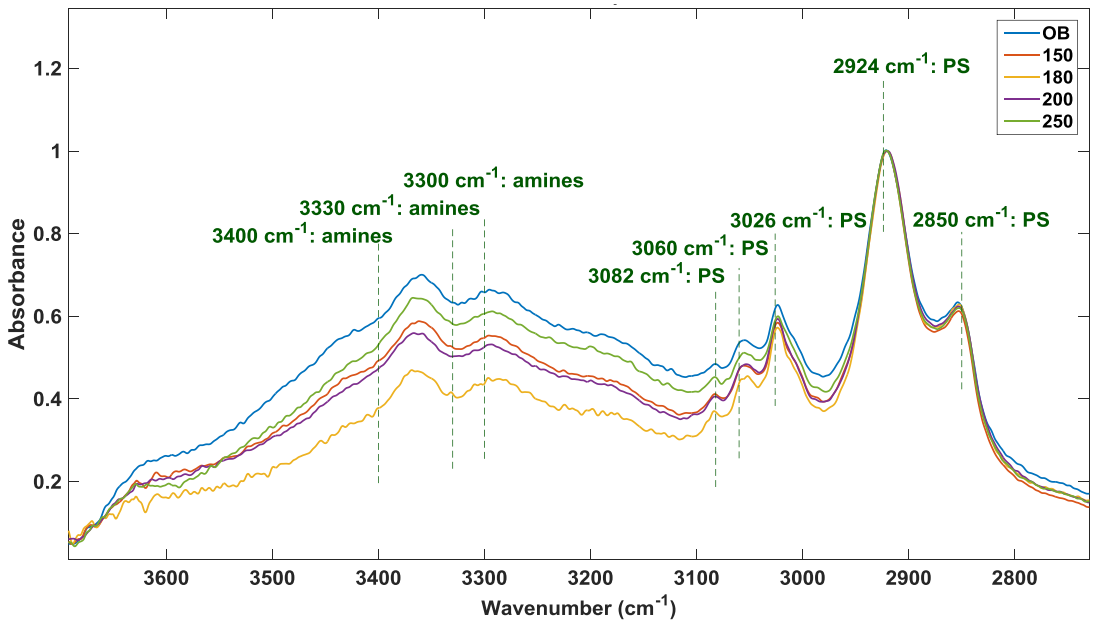

FIGURE 26 Normalized mean spectra from samples with different thermal treatments. "OB" means a resin with no thermal treatment. Samples "150", "180" and "200" were heated at these temperatures in ^{o}C for 1 hour. "250" was heated from 25 ^{o}C to 250 ^{o}C 5 ^{o}C/min in N_2 purge in STA. Normalization was performed by setting the baseline at a wavenumber of 3900 cm^{-1} to zero, and a known strong polystyrene peak at 2920 cm^{-1} to 1.

From Figure 26, the reduction of amplitude in sections referring to amines can be seen after thermal treatments. However, one would expect that a clear pattern could be found, such that the amplitude decreases with increasing thermal treatment. By examining the amine region peaks, it could be found that the peak amplitudes first decrease with higher temperature, but then increase again with samples treated at 200^{o}C and 250^{o}C. Therefore, quantitative analysis would not have provided relevant information. However, it is evident, that the amine groups were not completely decomposed even after treatment at 250^{o}C.

Differences were sought from the region 1800-1300 cm^{-1} in Figure 27 to see, if thermal treatment affected the amplitudes of known carbamate peaks.

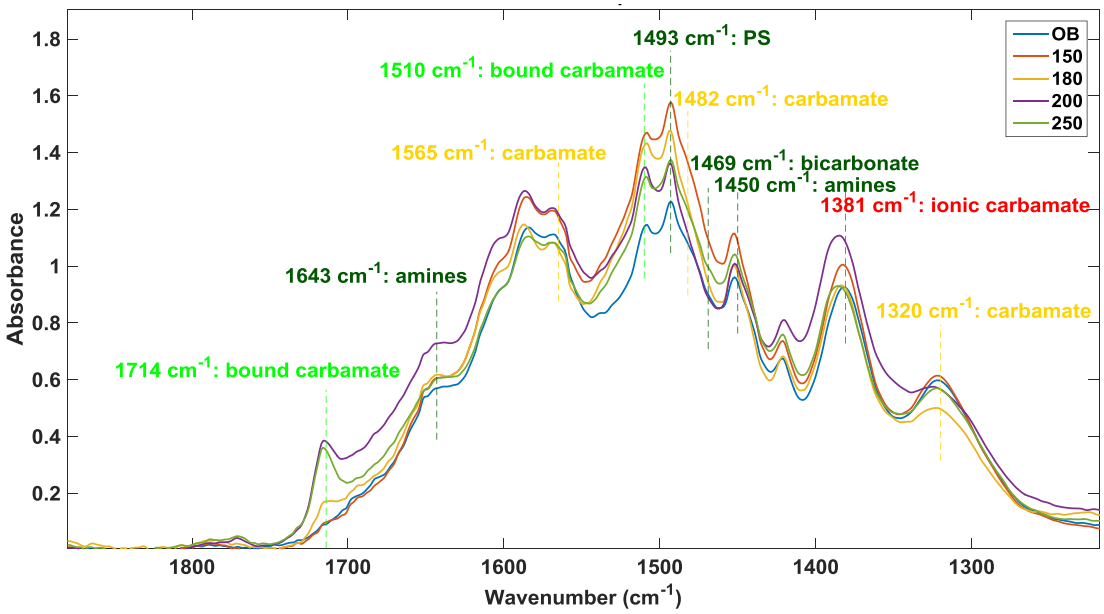

FIGURE 27 Normalized mean spectra from samples with different thermal treatments. "OB" means a resin with no thermal treatment. Samples "150", "180" and "200" were heated at these temperatures in ^{o}C for 1 hour. "250" was heated from 25^{o}C to 250^{o}C 5^{o}C/min in N_2 purge in STA. Normalization was performed by setting the baseline at a wavenumber of 3900 cm^{-1} to zero, and a known strong polystyrene peak at 2920 cm^{-1} to 1.

In Figure 27, quantitative analysis was not relevant. However, a new peak appeared at 180^{o}C at about 1715 cm^{-1}, which could refer to bound carbamate. The peak also grows stronger for samples "200" and "250".

When the resin was heated in STA, one significant mass decrease of circa 2.8 m-% was detected in the range of 45-150^{o}C, which probably was at least partly caused by drying (see App. V). From 150^{o}C to approximately 225^{o}C, a small mass increase of circa 0.2 m-% was detected, after which the mass started decreasing slowly. This mass increase supports the finding of a new species in the FTIR spectrum in the high temperature range. This finding could refer to sintering, perhaps from the deactivation of the amine group forming unregenerable carbamate species. However, apart from the one between 45^{o}C and 150^{o}C, no significant mass decreases were detected in the range of 25-250^{o}C. The matrix structure was thus still mostly intact after this treatment, although the colour was found to have

changed from the normal light brown to darker brown. Because the primary amine peaks didn't disappear, the amine was not at least completely decomposed. The results are in line with literature[86], where decomposition temperatures for amines in solid sorbents were determined to be as high as 250-300^{o}C. Because the CO_2 adsorption capacity was not tested after these higher temperature treatments, the degradation of the amine species could not be satisfactorily confirmed. In-situ FTIR would be required to quantitatively detect the decomposition.

Quantitative analysis was also attempted so that samples that underwent thermal treatments at 90^{o}C and 120^{o}C under vacuum were analysed in FTIR after different time intervals in open laboratory air. No clear pattern was found for the amplitude of carbamate peak sections versus time under laboratory air. This was confirmed by both PCA (Principal Component Analysis) and by observing the peaks. This and the experiments described above impart that quantitative analysis is not reasonable in such experimental setup. Whether this is due to sample heterogeneity or the time between analyses enough to cause changes, it seems that proper quantitative analysis would require in-situ FTIR.

5.3 Elemental analyses

The elemental analyses were conducted as supportive methods for the characterization of the chemical structure of the resin. The results of SEM-EDS and XRF elemental analyses are presented here.

5.3.1 EDS

The white spots in the SEM images originate from heavier elements. Thus, energy dispersive X-ray spectroscopy was also conducted on resin 1 as received sample to gain an elemental analysis. The results are in Table V, and the images of the areas of which the EDS was taken can be found in the Appendix VI.

TABLE V EDS elemental analysis of a CO_2 adsorbing resin from two different locations. Area 1 was a section with white spots in SEM images, whereas area 2 was taken from the darker background.

	The first measurement		The second measurement	
	area #1	area #2	area #1	area #2
Element	**Wt.%**	**Wt.%**	**Wt.%**	**Wt.%**
C	62.8	75.6	51.2	74.8
N	3.4	8.9	2.4	8.3
O	22.6	11.6	34.5	13.2
Na	3.7	4	2.6	3.8
Mg	1.4	-	6.4	-
Al	0.9	-	-	-
Si	1.5	-	0.3	-
Ca	3.8	-	2.6	-

In Table V, the amount of metals is significant in the areas with white spots. The occurrence of sodium, magnesium and calcium could simply be explained by common water hardness, which in turn could come from the manufacturing process, for example. The origin of silica and aluminium, however, is not evident, but could be the result of dust in factory conditions, for example. The nitrogen content could be used as a comparison value for determining amine loading by titration for example, but is not dependable enough to be used as an absolute value.

5.3.2 XRF

Here, all results that were not below limit of detection (LOD), or over 100 ppm are presented. Elements below Mg in atomic number were not detected due to instrumental limitations. Mg also contained large amount of uncertainty, because although the amount of Mg was below LOD, the amount of error was in the scale of 2500-3500ppm.

TABLE VI XRF elemental analysis of CO_2 adsorbing resins.

Sample	Balance/m-%	Cl/m-%	Ca/m-%	P/m-%	S/m-%
Resin 1	99.318	0.179 ± 0.004	0.161 ± 0.004	0.145 ± 0.006	0.173 ± 0.006
Resin 2	99.817	0.024 ± 0.002	0.025 ± 0.002	0.110 ± 0.005	0.017 ± 0.004

XRF detected significant quantities of elements not detected in the EDS analysis in Table VI. On the other hand, no aluminium was found by the XRF as was by the EDS. Major differences between the resins are in the amounts of Cl, Ca and S. The results confirm that resin 1 contains more impurities, as was observed from the SEM-images (see 5.1.1).

Chlorine could be the result of water chlorine content, originating from the manufacturing process, for example. The occurrence of phosphorus and sulphur are harder to explain. One explanation is that the precursor PS of the amine functionalized resin contains these elements to provide wanted properties such as higher thermal stability[110,111]. The PS resin used to manufacture the amine-containing resin could also be in the form of polystyrene sulfonate such as an ion-exchange resin by Dow Chemical [112]. One explanation to these impurities could also be, that the resins have affinity towards them, and capture them easily from air or by being in contact with different surfaces.

5.4 The adsorption capacity

In the STA results it was found, that the mass did not stabilize in 20 hours, and that the mass increased during the hot N_2 flow in some experiments. A control experiment was thus conducted as described above (see 4.2.2). In the control experiment, the mass-% against time curve was found to be similar to the other experiments, although the mass change of the sample after the 20-hour adsorption was significantly smaller (see App. VII). An anomaly in the otherwise constantly increasing mass curve was found at approximately between 8-11 hours after the start of the experiment. This was assumed to be some occasional instrumental error, and was thus first removed from the curve, and replaced with interpolated values (see App. VII). The mass-% changes were then subtracted from the other results. Thus, the effect of other factors such as nitrogen on the mass increase could be minimized. In the experiment with an empty crucible, the mass-% curve followed similar pattern as in the other experiments, with mass increasing after the start of adsorption step. This mainly confirmed that the mass increases due to instrumental limitations. The mass-% results from the STA experiments were used to calculate adsorption capacities (see App. VII), and the results are in Figure 28.

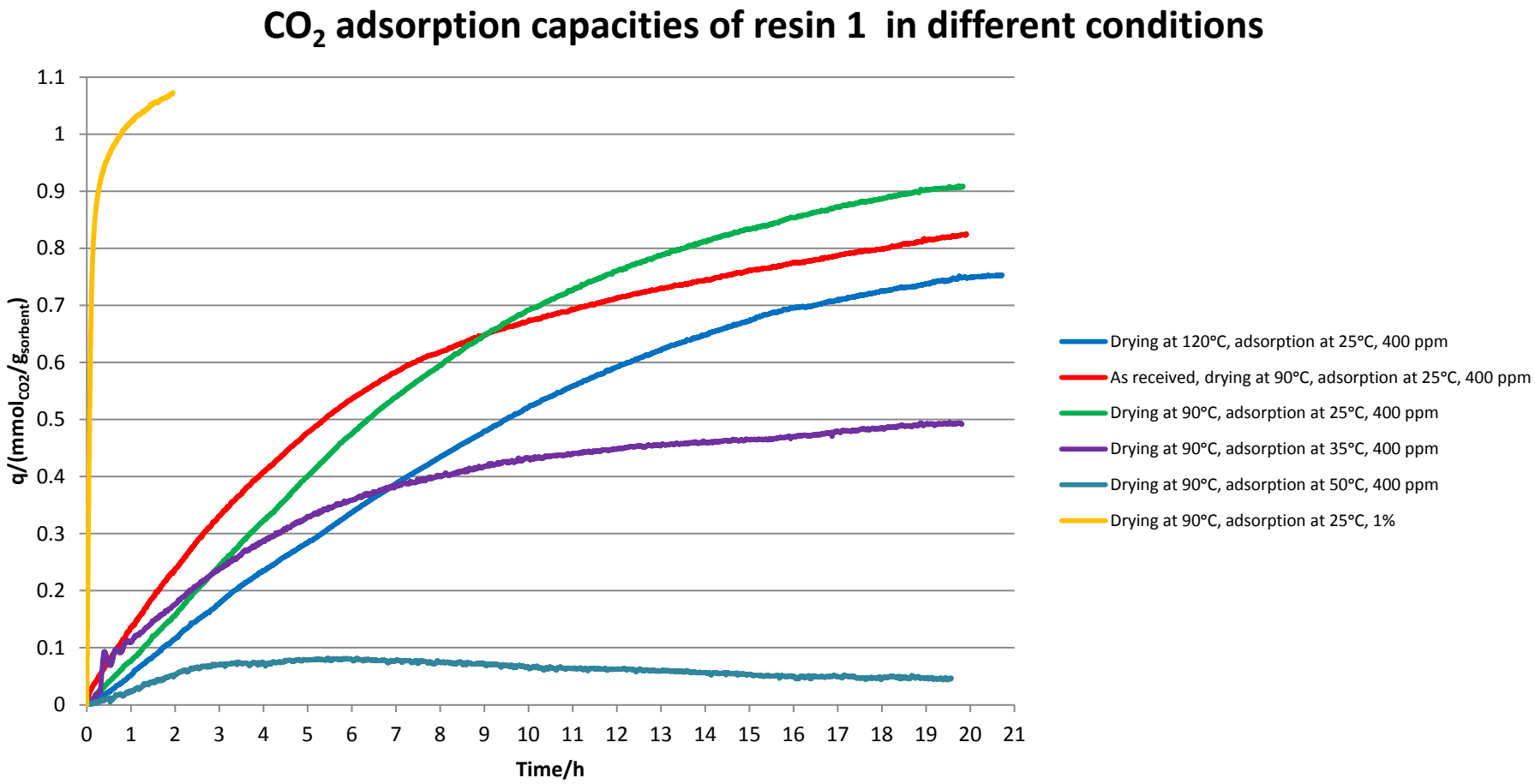

FIGURE 28 The adsorption capacities of a CO_2 adsorbing resin gained from simultaneous thermal analysis data. The mass-% changes of a sample in a control experiment with only N_2 flow were subtracted from the results. The samples were pre-treated in vacuum oven at the same temperatures as they were dried in STA at 60-100mbar, except for the as received sample.

In Figure 28, 20 hours was not enough in most experiments to reach equilibrium, i.e. to saturate the sorbent material and to cease the increase of mass. The mass seemed to stabilize best for the sample that was dried at 120°C and for the samples with adsorptions at 35°C and 50°C. The final adsorption capacities as well as the experimental conditions can be found from the Appendix VII.

When comparing the adsorptions at different temperatures, it can clearly be seen that adsorption at 25°C gave the highest adsorption capacity. The adsorption capacity at 35°C is only about half of that of the best result gained at 25°C. However, at the beginning of the adsorption less than 3 hours from the start, the capacity is higher for the higher temperature adsorption. This could be explained by higher thermal kinetics. At 50°C, the adsorption capacity is already very low. Interestingly for this experiment, it seems that the capacity is at its highest after 5-6 hours from the start of the adsorption, and then starts to decrease.

The sample with pre-treatment and drying at 120°C gave the lowest adsorption capacity of the three experiments conducted at 25°C and with 400ppm CO_2. The kinetics are also slower for this sample, but this, as well as the lower adsorption capacity, could be explained with around 50% larger amount of sample, and thus with limited diffusion of CO_2 to the whole sample material.

Using 1% CO_2 for 2 hours resulted in a significantly higher adsorption capacity compared to the 400ppm CO_2 adsorptions. After 2 hours, the adsorption capacity was approximately 18% higher than the highest result in 400 ppm CO_2 adsorption after 20 hours. Also, the sample was not yet saturated after 2 hours, so the adsorption capacity after 20 hours is probably even higher. It must be taken into account, however, that the sample crucible was open in this case, probably contributing partly to faster kinetics.

The equilibrium adsorption capacities gained from the 400ppm adsorption are reasonable, when compared to those in literature (see 3.3.2). Similar values were gained with mesoporous silicas, an ion-exchange resin[75] and a PPN, for example.

6 Conclusions

Solid amine-functionalized sorbent materials are the most proposed solution for DAC. Solid sorbents are more energy-efficient than solvent-based solutions in DAC. Primary amine functionalization provides high binding strength and selectivity towards CO_2 contributing to higher purity of the outlet CO_2. The optimization of amine loading is more important than a high surface area in amine-based CO_2 adsorbents.

The matrix type of the sorbent material greatly affects the performance towards DAC. Many potential solid sorbent materials exist, but few have been studied exhaustively to prove their process feasibility. Studies differ significantly in perspective and in the studied parameters. For DAC purposes, the most important parameters are low adsorption and desorption temperatures, good regenerability and stability in both humid and dry conditions, high outlet CO_2 purity and a reasonable working capacity. Regenerability over multiple cycles is an exceptionally important parameter in addition to working capacity in process scale, but was rarely studied satisfactorily. NFC materials by Gebald and Wurzbacher were found to have good performance overall, although they were not necessarily superior compared to other sorbent materials. Full characterization and study of process feasibility is thus extremely important for process utilization of a DAC sorbent.

An amine functionalized resin CO_2 sorbent material sample gained from industry was studied experimentally to determine its physical and chemical characteristics and evaluate its suitability for CO_2 capture in DAC conditions at a preliminary level. For modelling of a fixed-bed adsorption process using the same sorbent, important parameters were gained. Particle size distribution, of which most importantly the median size, was determined. Sphericity could be determined from SEM-images to be approximately 1. Porosity was evaluated by BET- and BJH analyses, and internal porosity could be calculated. The adsorption capacity was studied by STA experiments in different conditions. When using 400ppm dry CO_2, the resin was found to yield the highest capacity at 25^{o}C. These parameters can be used for modelling of a fixed-bed adsorption as well as starting values for fixed-bed experiments.

The resin gained from industry, resin 1, was also compared to another amine-functionalized resin CO_2 sorbent, resin 2, in this thesis. By physicochemical

characterization experiments, it was found that their structure was very similar. SEM-images revealed the existence of macro- and mesopores, but also impurities that were confirmed by EDS and XRF elemental analyses. The particle size distributions and the densities of the two resins were comparable. Porosity determined by BET- and BJH analyses showed comparable surface areas, but porosity was significantly higher for resin 2. Resin 2 also had a larger pore size. By using FTIR, the amine species were identified as primary amines for both resins. Also, the main species of captured CO_2 was identified as carbamate. The matrix of both sorbents was identified as polystyrene. The spectra were mostly similar in sections representing PS, but small differences were detected, probably referring to different substitutions in the aromatic ring. Thus, the resin materials are both based on a crosslinked polystyrene structure that has been functionalized with a primary amine for CO_2 capture applications. The differences in the physical and chemical properties impart that the resins are manufactured by different processes.

When comparing the experimental results to literature, the resins were found to have surface areas comparable to many mesoporous sorbents, but higher than with other resins reported. The CO_2 adsorption capacities from 400ppm CO_2 for resin 1 were reasonable if compared to literature values. The optimal adsorption temperature of 25^{o}C was the same as for most of the sorbents. Also, it was found that the amines endured thermal treatment reasonably well. These results give confidence in the sorbent material being suitable for DAC conditions. Data about the process performance of this resin in DAC is needed, however.

The porosity determined in this thesis mostly omits the macroporosity. Therefore, a mercury porosimetry should be conducted to fully determine the porosity for modelling purposes. To further study the material structure, in-situ FTIR would be required. Thus, the effect of for example operation temperature and humidity on the CO_2 species could be monitored, and the reaction mechanism would be better revealed. This would be important in finding the optimal conditions, where the amine efficiency of the material is highest. Also, this would allow for better determination of a decomposition temperature of the amines, and other stability examination.

An important modelling parameter that couldn’t be determined reliably was specific heat capacity. This should be determined by well calibrated and reliable differential scanning calorimetry (DSC). Regeneration energy was also not determined reliably, and can be

estimated with the same device. Reliable determination of regeneration energy may require multiple adsorption/desorption cycles.

Cyclic performance of the CO_2 sorbent, as stated, is extremely important to be determined for evaluation of process feasibility. The working capacity, stability and kinetics can be determined from cyclic fixed-bed adsorption experiments. This would require comprehensive examination, with each experiment consisting of at least 20 cycles, but preferably closer to a 100 cycles. The consistency of the inlet gas should be varied from only dry CO_2 and humid CO_2 to synthetic air consisting also oxygen, to study the effect of these conditions on the cyclic capacity as well as stability. FTIR could also be used here as a supportive tool. Finally, if DAC and PCC conditions are compared, different concentrations of CO_2 and higher temperatures should be used. Also, the effect of different impurities in the inlet gas should be studied.

Literature

[1] Mauna Loa Observatory, Atmospheric CO2, NOAA Dataset Summary, (2015). http://co2now.org/images/stories/data/co2-mlo-monthly-noaa-esrl.pdf (accessed November 12, 2015).

[2] International Energy Agency, CO2 emissions from fuel combustion highlights, (2014).

[3] M.E. Boot-Handford, J.C. Abanades, E.J. Anthony, M.J. Blunt, S. Brandani, N. Mac Dowell, et al., Carbon capture and storage update, Energy Environ. Sci. 7 (2014) 130–189.

[4] D.W. Keith, M. Ha-Duong, J.K. Stolaroff, Climate strategy with CO2 capture from the air, Clim. Change. 74 (2006) 17–45.

[5] C. Chen, M. Tavoni, Direct air capture of CO2 and climate stabilization: A model based assessment, Clim. Change. 118 (2013) 59–72.

[6] M. Ranjan, Feasibility of air capture, (2010) Master's Thesis, MIT, 89 pp.

[7] K.S. Lackner, Capture of carbon dioxide from ambient air, Eur. Phys. J. Spec. Top. 176 (2009) 93–106.

[8] K.Z. House, a. C. Baclig, M. Ranjan, E. a. van Nierop, J. Wilcox, H.J. Herzog, Economic and energetic analysis of capturing CO2 from ambient air, Proc. Natl. Acad. Sci. 108 (2011) 20428–20433.

[9] Eric Mack, Audi just created diesel fuel from air and water, Gizmag. (2015). http://www.gizmag.com/audi-creates-e-diesel-from-co2/37130/ (accessed November 12, 2015).

[10] Wendy Koch, Cars that run on air and water? Audi rolls out E-diesel, Natl. Geogr. Mag. (2015). http://news.nationalgeographic.com/energy/2015/04/150428-audi-ediesel-made-from-water-air/?utm_source=Facebook&utm_medium=Social&utm_content=link_fb20150428news-energycars&utm_campaign=Content&sf8861216=1 (accessed November 12, 2015).

[11] Kevin McSpadden, Audi just invented fuel made from CO2 and water, Time Mag. (2015). http://time.com/3837814/audi-environmental-protection-green-energy-climate-change-cars/ (accessed November 12, 2015).

[12] Communication From the Commission To the Council and the European Parliament, Renewable energy road map - Renewable energies in the 21st century: building a more sustainable future, COM. (2006) 848.

[13] F. Steinke, P. Wolfrum, C. Hoffmann, Grid vs. storage in a 100% renewable Europe, Renew. Energy. 50 (2013) 826–832.

[14] M. Lehner, R. Tichler, M. Koppe, Power-to-gas : Technology and business models, Springer, 2014.

[15] S. Becker, S. Lübbehüsen, Bilfinger Industrial Technologies, Power-To-Liquids, Fact Sheet. (2015). http://www.sunfire.de/wp-content/uploads/BILit_FactSheet_POWER-TO-LIQUIDS_EMS_en.pdf (accessed July 30, 2015).

[16] K. Zeng, D. Zhang, Recent progress in alkaline water electrolysis for hydrogen production and applications, Prog. Energy Combust. Sci. 36 (2010) 307–326.

[17] M. Carmo, D.L. Fritz, J. Mergel, D. Stolten, A comprehensive review on PEM water electrolysis, Int. J. Hydrogen Energy. 38 (2013) 4901–4934.

[18] J. Gao, Y. Wang, Y. Ping, D. Hu, G. Xu, F. Gu, et al., A thermodynamic analysis of methanation reactions of carbon oxides for the production of synthetic natural gas, RSC Adv. 2 (2012) 2358–2368.

[19] W. Wang, J. Gong, Methanation of carbon dioxide: An overview, Front. Chem. Eng. China. 5 (2011) 2–10.

[20] D. Peebles, D. Goodman, Methanation of carbon dioxide on nickel (100) and the effects of surface modifiers, J. Phys. Chem. 87 (1983) 4378–4387.

[21] K. Müller, M. Fleige, F. Rachow, D. Schmeißer, Sabatier based CO2-methanation of flue gas emitted by conventional power plants, Energy Procedia. 40 (2013) 240–248.

[22] B. Liu, S. Ji, Comparative study of fluidized-bed and fixed-bed reactor for syngas methanation over Ni-W/TiO2-SiO2 catalyst, J. Energy Chem. 22 (2013) 740–746.

[23] L. Grond, P. Schulze, J. Holstein, Systems analyses power to gas: A technology review, Final report, DNV KEMA Energy & Sustainability, (2013) Report No. GCS 13.R.23579.

[24] O. Ehret, K. Bonhoff, Hydrogen as a fuel and energy storage: Success factors for the German Energiewende, Int. J. Hydrogen Energy. 40 (2015) 5526–5533.

[25] H. Dagdougui, Models, methods and approaches for the planning and design of the future hydrogen supply chain, Int. J. Hydrogen Energy. 37 (2012) 5318–5327.

[26] W.J. Buttner, M.B. Post, R. Burgess, C. Rivkin, An overview of hydrogen safety sensors and requirements, Int. J. Hydrogen Energy. 36 (2011) 2462–2470.

[27] M. Gullberg, J. Gahnström, E. Lindfeldt, B. Forsman, L. Styhre, H. Paradis, et al., A feasibility study for an LNG filling station infrastructure and test of recommendations, Draft Feasibility Report, North European LNG Infrastructure Project, (2011).

[28] A. Caballero, P.J. Pérez, Methane as raw material in synthetic chemistry: the final frontier., Chem. Soc. Rev. 42 (2013) 8809–8820.

[29] S. Kumar, H.T. Kwon, K.H. Choi, W. Lim, J.H. Cho, K. Tak, et al., LNG: An eco-friendly cryogenic fuel for sustainable development, Appl. Energy. 88 (2011) 4264–4273.

[30] Climeworks, subsites: “Climeworks CO2 Capture Plant”, “Climeworks CO2 Kollektor”, “The Climeworks Team,” (2015). http://www.climeworks.com (accessed July 28, 2015).

[31] P.A. Nilsson, S. Apeland, H.M. Dale, S. Decarre, N.H. Eldrup, H.-R. Hansen, et al., The costs of CO2 transport - Post-demonstration CCS in the EU, European Technology Platform for Zero Emission Fossil Fuel Power Plants, 2010.

[32] Bank of Canada, 10-Year Currency Converter, (2015). http://www.bankofcanada.ca/rates/exchange/10-year-converter/ (accessed July 29, 2015).

[33] R. Socolow, M. Desmond, R. Aines, J. Blackstock, O. Bolland, T. Kaarsberg, et al., Direct air capture of CO2 with chemicals - A technology assessment for the APS Panel on Public Affairs, APS Physics, 2011.

[34] J.A. Wurzbacher, C. Gebald, A. Steinfeld, Separation of CO2 from air by temperature-vacuum swing adsorption using diamine-functionalized silica gel, Energy Environ. Sci. 4 (2011) 3584–3592.

[35] C. Gebald, J.A. Wurzbacher, P. Tingaut, T. Zimmermann, A. Steinfeld, Amine-based nanofibrillated cellulose as adsorbent for CO2 capture from air, Environ. Sci. Technol. 45 (2011) 9101–9108.

[36] J.A. Wurzbacher, C. Gebald, N. Piatkowski, A. Steinfeld, Concurrent separation of CO2 and H2O from air by a temperature-vacuum swing adsorption/desorption cycle, Environ. Sci. Technol. 46 (2012) 9191–9198.

[37] C. Gebald, J. a. Wurzbacher, P. Tingaut, A. Steinfeld, Stability of amine-functionalized cellulose during temperature-vacuum-swing cycling for CO2 capture from air, Environ. Sci. Technol. 47 (2013) 10063–10070.

[38] Carbon Engineering, subsites: “Our Technology”, “People,” (2015). http://carbonengineering.com/ (accessed July 28, 2015).

[39] The Global Thermostat, subsites: “Who We Are”, “The GT Solution,” (2015). http://globalthermostat.com/ (accessed July 28, 2015).

[40] F.S. Zeman, K.S. Lackner, Capturing carbon dioxide directly from the atmosphere, World Resour. Rev. 16 (2004) 157–172.

[41] K.S. Lackner, P. Grimes, H.J. Ziock, Carbon dioxide extraction from air: Is it an option?, Proc. 24th Annu. Tech. Conf. Coal Util. Fuel Syst. (1999) 885–896.

[42] J.J. Carroll, J.D. Slupsky, A.E. Mather, The solubility of carbon dioxide in water at low pressure, J. Phys. Chem. Ref. Data. 20 (1991) 1201–1209.

[43] K. Adamczyk, M. Premont-Schwarz, D. Pines, E. Pines, E.T.J. Nibbering, Real-time observation of carbonic acid formation in aqueous solution, Science (80-.). 326 (2009) 1690–1694.

[44] R. Baciocchi, G. Storti, M. Mazzotti, Process design and energy requirements for the capture of carbon dioxide from air, Chem. Eng. Process. 45 (2006) 1047–1058.

[45] J.K. Stolaroff, D.W. Keith, G. V. Lowry, Carbon dioxide capture from atmospheric air using sodium hydroxide spray, Environ. Sci. Technol. 42 (2008) 2728–2735.

[46] T. Wang, K.S. Lackner, A. Wright, Moisture swing sorbent for carbon dioxide capture from ambient air, Environ. Sci. Technol. 45 (2011) 6670–6675.

[47] C.H. Yu, C.H. Huang, C.S. Tan, A review of CO2 capture by absorption and adsorption, Aerosol Air Qual. Res. 12 (2012) 745–769.

[48] M. Ramdin, T.W. de Loos, T.J.H. Vlugt, State-of-the-Art of CO2 capture with ionic liquids, Ind. Eng. Chem. Res. 51 (2012) 8149–8177.

[49] F. Kozak, A. Petig, E. Morris, R. Rhudy, D. Thimsen, Chilled ammonia process for CO2 capture, Energy Procedia. 1 (2009) 1419–1426.

[50] E. Favre, Membrane processes and postcombustion carbon dioxide capture: Challenges and prospects, Chem. Eng. J. 171 (2011) 782–793.

[51] L.-H. Cheng, M.S.A. Rahaman, R. Yao, L. Zhang, X.-H. Xu, H.-L. Chen, et al., Study on microporous supported ionic liquid membranes for carbon dioxide capture, Int. J. Greenh. Gas Control. 21 (2014) 82–90.

[52] M. Eisaman, D. Schwartz, S. Amic, D. Larner, J. Zesch, F. Torres, et al., Energy-efficient electrochemical CO2 capture from the atmosphere, In: Technical Proceedings of the 2009 Clean Technology Conference and Trade Show, (2009) May 3–7; Houston, USA, 2009.

[53] M.D. Eisaman, L. Alvarado, D. Larner, P. Wang, B. Garg, K. a. Littau, CO2 separation using bipolar membrane electrodialysis, Energy Environ. Sci. 4 (2011) 1319–1328.

[54] J.D. Seader, E.J. Henley, D.K. Roper, Adsorption, ion exchange, chromatography and electrophoresis, In: Separation Process Principles - Chemical and Biochemical Operations, 3rd Edition, Wiley, 2010.

[55] J.M. Thomas, The existence of endothermic adsorption, J. Chem. Educ. 38 (1961) 138–139.

[56] S. Brunauer, L.S. Deming, W.E. Deming, E. Teller, On a theory of the van der Waals adsorption of gases, J. Am. Chem. Soc. 62 (1940) 1723–1732.

[57] S. a. Didas, A.R. Kulkarni, D.S. Sholl, C.W. Jones, Role of amine structure on carbon dioxide adsorption from ultradilute gas streams such as ambient air,

ChemSusChem. 5 (2012) 2058–2064.

[58] N.R. Stuckert, R.T. Yang, CO2 capture from the atmosphere and simultaneous concentration using zeolites and amine-grafted SBA-15, Environ. Sci. Technol. 45 (2011) 10257–10264.

[59] B. Guo, L. Chang, K. Xie, Adsorption of carbon dioxide on activated carbon, J. Nat. Gas Chem. 15 (2006) 223–229.

[60] M. Zhang, Z. Perry, J. Park, H.-C. Zhou, Stable benzimidazole-incorporated porous polymer network for carbon capture with high efficiency and low cost, Polymer (Guildf). 55 (2014) 335–339.

[61] J.-R. Li, R.J. Kuppler, H.-C. Zhou, Selective gas adsorption and separation in metal-organic frameworks, Chem. Soc. Rev. 38 (2009) 1477–1504.

[62] P.M. Mathias, R. Kumar, J.D. Moyer, J.M. Schork, S.R. Srinivasan, S.R. Auvil, et al., Correlation of multicomponent gas adsorption by the dual-site Langmuir model. Application to nitrogen/oxygen adsorption on 5A-zeolite, Ind. Eng. Chem. Res. 5885 (1996) 2477–2483.

[63] T.L.P. Dantas, F.M.T. Luna, I.J. Silva Jr, a. E.B. Torres, D.C.S. de Azevedo, a. E. Rodrigues, et al., Modeling of the fixed-bed adsorption of carbon dioxide and a carbon dioxide - nitrogen mixture on zeolite 13X, Brazilian J. Chem. Eng. 28 (2011) 533–544.

[64] S. Choi, J.H. Drese, P.M. Eisenberger, C.W. Jones, Application of amine-tethered solid sorbents for direct CO2 capture from the ambient air, Environ. Sci. Technol. 45 (2011) 2420–2427.

[65] W. Li, S. Choi, J.H. Drese, M. Hornbostel, G. Krishnan, P.M. Eisenberger, et al., Steam-stripping for regeneration of supported amine-based CO2 adsorbents, ChemSusChem. 3 (2010) 899–903.

[66] J.C. Hicks, J.H. Drese, D.J. Fauth, M.L. Gray, G. Qi, C.W. Jones, Designing adsorbents for CO2 capture from flue gas-hyperbranched aminosilicas capable of capturing CO2 reversibly, J. Am. Chem. Soc. 130 (2008) 2902–2903.

[67] R. V. Siriwardane, M.S. Shen, E.P. Fisher, J. Losch, Adsorption of CO2 on zeolites at moderate temperatures, Energy and Fuels. 19 (2005) 1153–1159.

[68] K. Sumida, D.L. Rogow, J. a. Mason, T.M. McDonald, E.D. Bloch, Z.R. Herm, et al., Carbon dioxide capture in metal-organic frameworks, Chem. Rev. 112 (2012) 724–781.

[69] W.R. Alesi, J.R. Kitchin, Evaluation of a primary amine-functionalized ion-exchange resin for CO2 capture, Ind. Eng. Chem. Res. 51 (2012) 6907–6915.

[70] W.R. Lee, S.Y. Hwang, D.W. Ryu, K.S. Lim, S.S. Han, D. Moon, et al., Diamine-functionalized metal–organic framework: exceptionally high CO2 capacities from ambient air and flue gas, ultrafast CO2 uptake rate, and adsorption mechanism, Energy Environ. Sci. 7 (2014) 744–751.

[71] H. He, W. Li, M. Zhong, D. Konkolewicz, D. Wu, K. Yaccato, et al., Reversible CO2 capture with porous polymers using the humidity swing, Energy Environ. Sci. 6 (2013) 488–493.

[72] Y. Belmabkhout, A. Sayari, Effect of pore expansion and amine functionalization of mesoporous silica on CO2 adsorption over a wide range of conditions, Adsorption. 15 (2009) 318–328.

[73] W. Lu, J.P. Sculley, D. Yuan, R. Krishna, H.-C. Zhou, Carbon dioxide capture from air using amine-grafted porous polymer networks, J. Phys. Chem. 117 (2013) 4057–4061.

[74] T.M. McDonald, W.R. Lee, J. a. Mason, B.M. Wiers, C.S. Hong, J.R. Long, Capture of carbon dioxide from air and flue gas in the alkylamine-appended metal-organic framework mmen-Mg2(dobpdc), J. Am. Chem. Soc. 134 (2012) 7056–7065.

[75] T. Wang, J. Liu, M. Fang, Z. Luo, A moisture swing sorbent for direct air capture of carbon dioxide: Thermodynamic and kinetic analysis, Energy Procedia. 37 (2013) 6096–6104.

[76] H. He, M. Zhong, D. Konkolewicz, K. Yacatto, T. Rappold, G. Sugar, et al., Three-dimensionally ordered macroporous polymeric materials by colloidal crystal templating for reversible CO2 capture, Adv. Funct. Mater. 23 (2013) 4720–4728.

[77] H. He, W. Li, M. Lamson, M. Zhong, D. Konkolewicz, C.M. Hui, et al., Porous polymers prepared via high internal phase emulsion polymerization for reversible CO2 capture, Polym. (United Kingdom). 55 (2014) 385–394.

[78] W. Lu, W.M. Verdegaal, J. Yu, P.B. Balbuena, H.-K. Jeong, H.-C. Zhou, Building multiple adsorption sites in porous polymer networks for carbon capture

applications, Energy Environ. Sci. 6 (2013) 3559–3564.

[79] O. Shekhah, Y. Belmabkhout, Z. Chen, V. Guillerm, A. Cairns, K. Adil, et al., Made-to-order metal-organic frameworks for trace carbon dioxide removal and air capture, Nat. Commun. 5 (2014) 4228–4234.

[80] S. Choi, M.L. Gray, C.W. Jones, Amine-tethered solid adsorbents coupling high adsorption capacity and regenerability for CO2 capture from ambient air, ChemSusChem. 4 (2011) 628–635.

[81] S. Sircar, R. Mohr, C. Ristic, M.B. Rao, Isosteric heat of adsorption: theory and experiment, J. Phys. Chem. B. 103 (1999) 6539–6546.

[82] K.S. Lackner, S. Brennan, J.M. Matter, a.-H. a. Park, a. Wright, B. van der Zwaan, The urgency of the development of CO2 capture from ambient air, Proc. Natl. Acad. Sci. 109 (2012) 13156–13162.

[83] Y. Belmabkhout, R. Serna-Guerrero, A. Sayari, Amine-bearing mesoporous silica for CO2 removal from dry and humid air, Chem. Eng. Sci. 65 (2010) 3695–3698.

[84] W. Chaikittisilp, H.J. Kim, C.W. Jones, Mesoporous alumina-supported amines as potential steam-stable adsorbents for capturing CO2 from simulated flue gas and ambient air, Energy and Fuels. 25 (2011) 5528–5537.

[85] Y. Cho, J.Y. Lee, A.D. Bokare, S.B. Kwon, D.S. Park, W.S. Jung, et al., LiOH-embedded zeolite for carbon dioxide capture under ambient conditions, J. Ind. Eng. Chem. 22 (2014) 350–356.

[86] S. Choi, J.H. Drese, C.W. Jones, Adsorbent materials for carbon dioxide capture from large anthropogenic point sources, ChemSusChem. 2 (2009) 796–854.

[87] F. Su, C. Lu, S.C. Kuo, W. Zeng, Adsorption of CO2 on amine-functionalized y-type zeolites, Energy and Fuels. 24 (2010) 1441–1448.

[88] D.M. D'Alessandro, B. Smit, J.R. Long, Carbon dioxide capture: Prospects for new materials, Angew. Chemie - Int. Ed. 49 (2010) 6058–6082.

[89] Z. Bacsik, N. Ahlsten, A. Ziadi, G. Zhao, A.E. Garcia-bennett, B. Martin-Matute, et al., Mechanisms and kinetics for sorption of CO2 on bicontinuous mesoporous silica modified with n-propylamine, Langmuir. 27 (2011) 11118–11128.

[90] S.A. Didas, M.A. Sakwa-novak, G.S. Foo, C. Sievers, C.W. Jones, Effect of amine surface coverage on the co-adsorption of CO2 and water: spectral deconvolution of adsorbed species, J. Phys. Chem. Lett. 5 (2014) 4194–4200.

[91] Y. Kuwahara, D.Y. Kang, J.R. Copeland, N. a. Brunelli, S. a. Didas, P. Bollini, et al., Dramatic enhancement of CO2 uptake by poly(ethyleneimine) using zirconosilicate supports, J. Am. Chem. Soc. 134 (2012) 10757–10760.

[92] M.A. Alkhabbaz, P. Bollini, G.S. Foo, C. Sievers, C.W. Jones, Important roles of enthalpic and entropic contributions to CO2 capture from simulated flue gas and ambient air using mesoporous silica grafted amines, J. Am. Chem. Soc. 136 (2014) 13170–13173.

[93] R. Khunsupat, C.W. Jones, S. Ball, Supported poly(allyl)amine and derivatives for CO2 capture from flue gas or ultra-dilute gas streams such as ambient air or admixtures thereof, US patent 0241966 A1, 2014.

[94] A. Wagner, B. Steen, G. Johansson, E. Zanghellini, P. Jacobsson, P. Johansson, Carbon dioxide capture from ambient air using amine-grafted mesoporous adsorbents, Int. J. Spectrosc. (2013).

[95] A. Sayari, Y. Belmabkhout, Stabilization of amine-containing CO2 adsorbents : Dramatic effect of water vapor, J. Am. Chem. Soc. 132 (2010) 6312–6314.

[96] A. Goeppert, M. Czaun, R.B. May, G.K.S. Prakash, G. a. Olah, S.R. Narayanan, Carbon dioxide capture from the air using a polyamine based regenerable solid adsorbent, J. Am. Chem. Soc. 133 (2011) 20164–20167.

[97] A. Goeppert, H. Zhang, M. Czaun, R.B. May, G.K.S. Prakash, G. a. Olah, et al., Easily regenerable solid adsorbents based on polyamines for carbon dioxide capture from the air, ChemSusChem. 7 (2014) 1386–1397.

[98] F.Q. Liu, L. Wang, Z.G. Huang, C.Q. Li, W. Li, R.X. Li, et al., Amine-tethered adsorbents based on three-dimensional macroporous silica for CO2 capture from simulated flue gas and air, ACS Appl. Mater. Interfaces. 6 (2014) 4371–4381.

[99] J. Wang, H. Huang, M. Wang, L. Yao, W. Qiao, D. Long, et al., Direct capture of low-concentration CO2 on mesoporous carbon-supported solid amine adsorbents at ambient temperature, Ind. Eng. Chem. Res. 54 (2015) 5319–5327.

[100] M.A. Sakwa-Novak, C.W. Jones, Steam induced structural changes of a poly(ethylenimine) impregnated γ-alumina sorbent for CO2 extraction from ambient

air, ACS Appl. Mater. Interfaces. 6 (2014) 9245–9255.

[101] H. Sehaqui, M.E. Gálvez, V. Becatinni, Y. cheng Ng, A. Steinfeld, T. Zimmermann, et al., Fast and reversible direct CO2 capture from air onto all-polymer nanofibrillated cellulose—polyethylenimine foams, Environ. Sci. Technol. 49 (2015) 3167–3174.

[102] Z. Chen, S. Deng, H. Wei, B. Wang, J. Huang, G. Yu, Polyethylenimine-impregnated resin for high CO2 adsorption: An efficient adsorbent for CO2 capture from simulated flue gas and ambient air, ACS Appl. Mater. Interfaces. 5 (2013) 6937–6945.

[103] A. Kumar, D.G. Madden, M. Lusi, K. Chen, E.A. Daniels, T. Curtin, et al., Direct air capture of CO2 by physisorbent materials, Angew. Chemie - Int. Ed. 54 (2015) 1–7.

[104] Netzsch Simultaneous thermal analysis - method, technique, applications, STA 449 F1 Jupiter brochure, (2015). https://dcyd0ggl1hia3.cloudfront.net/media/thermal-analysis/brochures/STA_449_F3_E_0814.pdf?1426281751&Policy=eyJTdGF0ZW1lbnQiOlt7IlJlc291cmNlIjoiaHR0cHM6XC9cL2RjeWQwZ2dsMWhpYTMuY2xvdWRmcm9udC5uZXRcL21lZGlhXC90aGVybWFsLWFuYWx5c2lzXC9icm9jaHVyZXNcL1NUQV80N (accessed November 30, 2015).

[105] A.R. Kulkarni, D.S. Sholl, Analysis of equilibrium-based TSA processes for direct capture of CO2 from air, Ind. Eng. Chem. Res. 51 (2012) 8631–8645.

[106] A. Danon, P.C. Stair, E. Weitz, FTIR study of CO2 adsorption on amine-grafted SBA-15: Elucidation of adsorbed species, J. Phys. Chem. 115 (2011) 11540–11549.

[107] L.M. Hanssen, C. Zhu, Wavenumber standards for mid-infrared spectrometry, in: Handb. Vib. Spectrosc., 2002.

[108] J. Coates, R.A.M. Ed, J. Coates, Interpretation of infrared spectra, a practical approach, in: Encycl. Anal. Chem., 2000: pp. 10815–10837.

[109] IR spectroscopy tutorial: amines, University of Colorado, (2015). http://orgchem.colorado.edu/Spectroscopy/irtutor/aminesir.html (accessed November 2, 2015).

[110] J. Furukawa, E. Kobayashi, T. Wakui, Phosphorus-containing polystyrene derivatives as flame resistance, Polym. J. 12 (1980) 277–285.

[111] Q. Tai, L. Song, X. Lv, H. Lu, Y. Hu, R.K.K. Yuen, Flame-retarded polystyrene with phosphorus- and nitrogen-containing oligomer : preparation and thermal properties, J. Appl. Polym. Sci. 123 (2012) 770–778.

[112] Rohm and Haas Amberlite IRP69, (2006). http://www.dow.com/assets/attachments/business/process_chemicals/amberlite_and_duolite_pharmaceutical_grade_resins/amberlite_irp69/tds/amberlite_irp69.pdf (accessed November 12, 2015).

Appendix I - Summary of literature results

TABLE A-I Material characteristics of different CO_2 sorbent materials by matrix type. Equilibrium sorption capacities were the highest reported, not maximum capacities.

Index Nr.	Source	Matrix	Functionalization /functional group	Surface area (m^2/g)	c_{CO2} (ppm)	q_e ($mmol_{CO2}/g_{sorbent}$)	Amine loading ($mmol_N/g_{sorbent}$)	Amine efficiency ($mmolCO_2/mmolN$)
1	[1]	Zeolite	-	-	395	1.34	-	-
2	[1]	Zeolite	-	-	395	1.34	-	-
3	[1]	Zeolite	-	-	395	0.67	-	-
4	[1]	Zeolite	-	-	395	0.67	-	-
5	[2]	Zeolite	75% $LiOH \cdot H_2O$	13	1000	1.50	-	-
6	[2]	Zeolite	75% $LiOH \cdot H_2O$	17	1000	1.10	-	-
7	[2]	Mesoporous silica	PEI	-	400	2.36	10.50	0.225
8	[3]	Mesoporous silica	PEI+silane additive	-	400	2.26	10.70	0.211
9	[3]	Mesoporous silica	PEI+Ti-additive	-	400	2.19	10.50	0.209
10	[4]	Mesoporous silica	PEI+ 0.070 Zr/Si	647	400	0.85	8.33	0.102
11	[5]	Mesoporous silica	Aminoethylamino - propyltrimethoxy-silane	-	400	-	-	-
12	[5]	Mesoporous silica	Aziridine	234	400	1.00	5.30	0.189
13	[5]	Mesoporous silica	Aziridine	45	400	1.72	9.90	0.174
14	[6]	Mesoporous silica	3-aminopropyl-trimethoxysilane	237	400	1.10	2.70	0.407
15	[6]	Mesoporous silica	3-aminopropyl-trimethoxysilane	230	400	0.55	3.75	0.147
16	[6]	Mesoporous silica	(N-methylaminopropyl)-trimethoxysilane	344	400	0.20	2.41	0.083
17	[6]	Mesoporous silica	(N,N-dimethylaminopropyl) - trimethoxysilane	317	400	0.00	2.20	0.000
18	[7]	Silica gel	[N-(2-aminoethyl)-3-aminopropyl] trimethoxysilane	216	400-440	0.30	2.48	0.121
19	[7]	Silica gel	[N-(2-aminoethyl)-3-aminopropyl] trimethoxysilane	216	400-440	0.40	2.48	0.161
20	[7]	Silica gel	[N-(2-aminoethyl)-3-aminopropyl] trimethoxysilane	216	400-440	0.44	2.48	0.177

Index Nr.	Source	Matrix	Functionalization /functional group	Surface area (m^2/g)	c_{CO2} (ppm)	q_e ($mmol_{CO2}/g_{sorbent}$)	Amine loading ($mmol_N/g_{sorbent}$)	Amine efficiency ($mmolCO_2/mmolN$)
21	[7]	Silica gel	[N-(2-aminoethyl)-3-aminopropyl] trimethoxysilane	216	400-440	-	2.48	-
22	[8]	Fumed silica	50 w-% PEI	27	400-420	1.67	-	-
23	[9]	Macroporous silica	3-aminopropyl-trimethoxysilane	56	400	2.65	10.98	0.241
24	[9]	Macroporous silica	3-aminopropyl-trimethoxysilane	56	100000	3.86	10.98	0.352
25	[10]	Mesoporous carbon	55 w-% PEI	153	400	1.50	-	-
26	[10]	Mesoporous carbon	55 w-% PEI+5 w-% Span 80	109	400	2.25	-	-
27	[10]	Mesoporous carbon	55 w-% PEI	153	400	2.00	-	-
28	[10]	Mesoporous carbon	55 w-% PEI+5 w-% Span 80	109	400	2.40	-	-
29	[11]	Mesoporous alumina	37.2 w-% PEI	66	400	1.73	8.66	0.200
30	[11]	Mesoporous alumina	48.1 w-% PEI	29	400	1.95	11.20	0.174
31	[12]	Mesoporous alumina	PEI	97	400	1.71	8.40	0.204
32	[12]	Mesoporous alumina	PEI	97	400	1.71	8.40	0.204
33	[13]	PPN	EDA	-	400	0.15	-	-
34	[13]	PPN	EDA	-	400	0.15	-	-
35	[13]	PPN	DETA	-	400	1.04	-	-
36	[13]	PPN	DETA	-	400	1.04	-	-
37	[14]	Colloidal crystal	Quaternary ammonium hydroxide groups	-	400	0.57	2.30	0.248
38	[15]	PolyHIPE	Quaternary ammonium hydroxide groups+2 w-% silica+20 w-% Span 80	-	400	0.72	-	-
39	[16]	NFC	N-(2-aminoethyl)-3-aminopropylmethyl-dimethoxysilane	7	506	1.39	4.90	0.284
40	[17]	NFC	3-aminopropylmethyl-diethoxysilane	12	400-510	0.39	3.86	0.101
41	[17]	NFC	3-aminopropylmethyl-diethoxysilane	12	400-510	0.65	3.86	0.168
42	[17]	NFC	3-aminopropylmethyl-diethoxysilane	12	400-510	-	3.86	-

Index Nr.	Source	Matrix	Functionalization /functional group	Surface area (m^2/g)	c_{CO2} (ppm)	q_e ($mmol_{CO2}/g_{sorbent}$)	Amine loading ($mmol_N/g_{sorbent}$)	Amine efficiency ($mmolCO_2/mmolN$)
43	[18]	NFC	N-(2-aminoethyl)-3-aminopropylmethyl-dimethoxysilane	8	444-463	1.28	5.90	0.217
44	[18]	NFC	N-(2-aminoethyl)-3-aminopropylmethyl-dimethoxysilane	8	417-491	-	5.90	-
45	[18]	NFC	N-(2-aminoethyl)-3-aminopropylmethyl-dimethoxysilane	8	417-491	-	5.90	-
46	[19]	NFC	44 w-% PEI	8	400.00	2.20	10.00	0.220
47	[20]	MOF	N,N'-dimethylethylene-diamine (mmen)	70	390	2.05	-	-
48	[20]	MOF	N,N'-dimethylethylene-diamine (mmen)	70	390	2.05	-	-
49	[21]	MOF	Ethylenediamine (en)	1253	390	2.83	-	-
50	[22]	MOF	-	300	400	1.24	-	-
51	[23,24]	IER	Quaternary ammonium hydroxide/carbonate groups	2	440	0.86	-	-
53	[25]	Resin	Primary amine (phtalamide)	26	100000	1.55	7.50	0.207
54	[26]	Resin	50 w-% PEI	22	400	2.26	-	-

TABLE A-II Process conditions and cyclic performance of different CO_2 sorbent materials by matrix type. Sorption capacities before and after cycling experiments were either equilibrium capacities or working capacities. *Equations in section 3.1.4.

Index Nr.	Swing type	$T_{adsorption}$ (°C)	$T_{desorption}$ (°C)	q_0 ($mmol_{CO2}/g_{sorbent}$)	q_{end} ($mmol_{CO2}/g_{sorbent}$)	N_{cycles}	Selectivity calculation*	Selectivity	Purity (%)	Other
1	TSA	25	280	-	-	-	q_{CO2}/q_{N2}	1.6	60.0	-
2	TVA	25	240	-	-	-	q_{CO2}/q_{N2}	1.6	90.0	-
3	TSA	25	220	-	-	-	q_{CO2}/q_{N2}	3.0	55.0	-
4	TVS	25	220	-	-	-	q_{CO2}/q_{N2}	3.0	95.0	-
5	-	25	-	-	-	-	-	-	-	-
6	-	25	-	-	-	-	-	-	-	-
7	TSA	25	110	2.36	1.65	4	-	-	-	Desorption capacity reported
8	TSA	25	110	2.26	2.05	4	-	-	-	Desorption capacity reported
9	TSA	25	110	2.19	2.16	4	-	-	-	Desorption capacity reported
10	TSA+Ar flow	25	110	0.75	0.74	4	-	-	-	-
11	TSA	25	110	0.28	0.28	4	-	-	-	-
12	TSA	25	110	0.35	0.32	4	-	-	-	-
13	-	25	-	-	-	-	-	-	-	-
14	-	25	-	-	-	-	-	-	-	-
15	-	25	-	-	-	-	-	-	-	-
16	-	25	-	-	-	-	-	-	-	-
17	-	25	-	-	-	-	-	-	-	-
18	TVS	25	90	-	-	-	-	-	95.8	Dry air, desorption capacities reported
19	TCS	25	90	-	-	-			95.8	Dry air, desorption capacities reported
20	TCS	25	90	-	-	-	-	-	97.6	Humid air

Index Nr.	Swing type	$T_{adsorption}$ (^oC)	$T_{desorption}$ (^oC)	q_0 ($mmol_{CO2}/g_{sorbent}$)	q_{end} ($mmol_{CO2}/g_{sorbent}$)	N_{cycles}	Selectivity calculation*	Selectivity	Purity (%)	Other
21	TVS	25	90	0.18	0.18	40	-	-	-	Humid air. Average cycling capacity.
22	TSA+N_2 flow	25	85	1.42	1.42	4	-	-	4.0	-
23	-	50	-	-	-	-	-	-	-	-
24	TSA+Ar flow	50	110	3.86	3.78	120	-	-	-	-
25	-	25	-	-	-	-	-	-	11.0	-
26	TSA+N_2 flow	25	110	2.25	2.2	10	-	-	11.0	-
27	-	50	-	-	-	-	-	-	11.0	-
28	-	50	-	-	-	-	-	-	11.0	-
29	TSA+Ar flow	25	110	1.3	1.3	3	-	-	-	-
30	-	25	-	-	-	-	-	-	-	-
31	Steam	30	110	1.71	1.73	18	-	-	-	-
32	Steam	30	110	1.71	0.66	-	-	-	-	Cycling time 24 hours.
33	TSA	22	-	-	-	-	IAST(N_2)	5078	67.0	-
34	-	22	-	-	-	-	IAST(N_2&O_2)	5086	67.0	-
35	-	22	170	-	-	-	IAST(N_2)	3.8×10^{10}	99.9	Desorption T for working capacity of ~1 mmol/g
36	-	22	170	-	-	-	IAST(N_2&O_2)	3.6×10^{10}	99.9	Desorption T for working capacity of ~1 mmol/g
37	HS	-	-	0.25	0.24	15	-	-	-	-
38	-	-	-	0.7	0.6	5	-	-	-	-
39	TSA+Ar flow	25	90	0.695	0.695	20	-	-	-	40% humidity

Index Nr.	Swing type	$T_{adsorption}$ (^oC)	$T_{desorption}$ (^oC)	q_0 ($mmol_{CO2}/g_{sorbent}$)	q_{end} ($mmol_{CO2}/g_{sorbent}$)	N_{cycles}	Selectivity calculation*	Selectivity	Purity (%)	Other
40	TVS	20	-	-	-	-	-	-	95.6	20% humidity, desorption capacities reported
41	TVS	20	-	-	-	-	-	-	95.6	80% humidity, desorption capacities reported
42	TVS	20	95	0.421	0.421	10	-	-	95.6	40% humidity, desorption capacities reported
43	-	30	-	-	-	-	-	-	-	-
44	TVS	30	90	1.28	1.22	100	-	-	-	60% RH. Equilibrium capacities before & after cycling.
45	TVS	30	90	0.87	0.87	100	-	-	-	60% RH. Cycling capacity.
46	TSA+N_2 flow	25	85	2.2	2.15	5	-	-	-	-
47	TSA+N_2 flow	25	150	1.05	1.05	10	Eq. (11) (N_2)	49000.0	96.0	Dry air. Selectivity from gas with 20% O_2, 80% N_2.
48	TSA+N_2 flow	25	150	1.05	1.05	10	Eq. (11) (O_2)	27000.0	98.0	-
49	TSA+N_2 flow	25	150	2.83	2.66	5	Eq. (11) N_2	70000.0	97.0	-
50	TVS	25	50	-	-	4	Eq. (12) N_2	10500.0	-	-
51	HS	25	23	-	-	-	-	-	-	-
53	TSA+N_2 flow	50	120	1.18	1.18	18	-	-	-	Drying for 2h.
54	TSA+N_2 flow	25	100	2.26	2.22	5	-	-	-	-

Appendix II- Testing of linear correlation

Linear correlation of equilibrium capacity and amine loading (see App. I) of solid sorbents was tested in around 400ppm CO_2.

$$Y = B_0 + B_1 X \qquad \text{(A-3)}$$

Where
Y equilibrium capacity,
B_0 intercept,
B_1 slope,
X amine loading.

Equation (A-1) is the equation of linear curve tested. Significance level of 0.05 is selected.

Hypotheses: $H_0: B_1 = 0$

$H_a: B_1 \neq 0$

Linear regression analysis was conducted by MS Excel data analysis. The results are in Table III.

TABLE A-III Linear regression data gained from MS Excel data analysis conducted to test the linear correlation between equilibrium sorption capacity and amine loading of solid direct air capture sorbents.

B1	Standard error	t-value	P(t<11.45)
0.21458	0.018739	11.4506	9.73E-11

Because the P-value is smaller than 0.05, the null hypothesis is rejected. A significant linear correlation therefore exists between the two variables.

Appendix III- BET-BJH analysis

The sample conditions

TABLE A-IV Pre-treatment conditions and masses of samples used in BET-BJH analysis.

Sample	Resin	Pretreatment	Degasification	$m_{before\ degas}$/g	$m_{after\ degas}$/g
1	Resin 1	Drying at 120°C	60°C, 19h	0.2397	0.2321
2	Resin 2	Drying at 120°C	60°C, 43h	0.1988	0.1938
3	Resin 1	Drying at 90°C	90°C, 6h	0.0751	0.0717
4	Resin 2	Drying at 90°C	90°C, 17h	0.0896	0.0852

Examples of BET isotherms and BJH cumulative pore volume plots

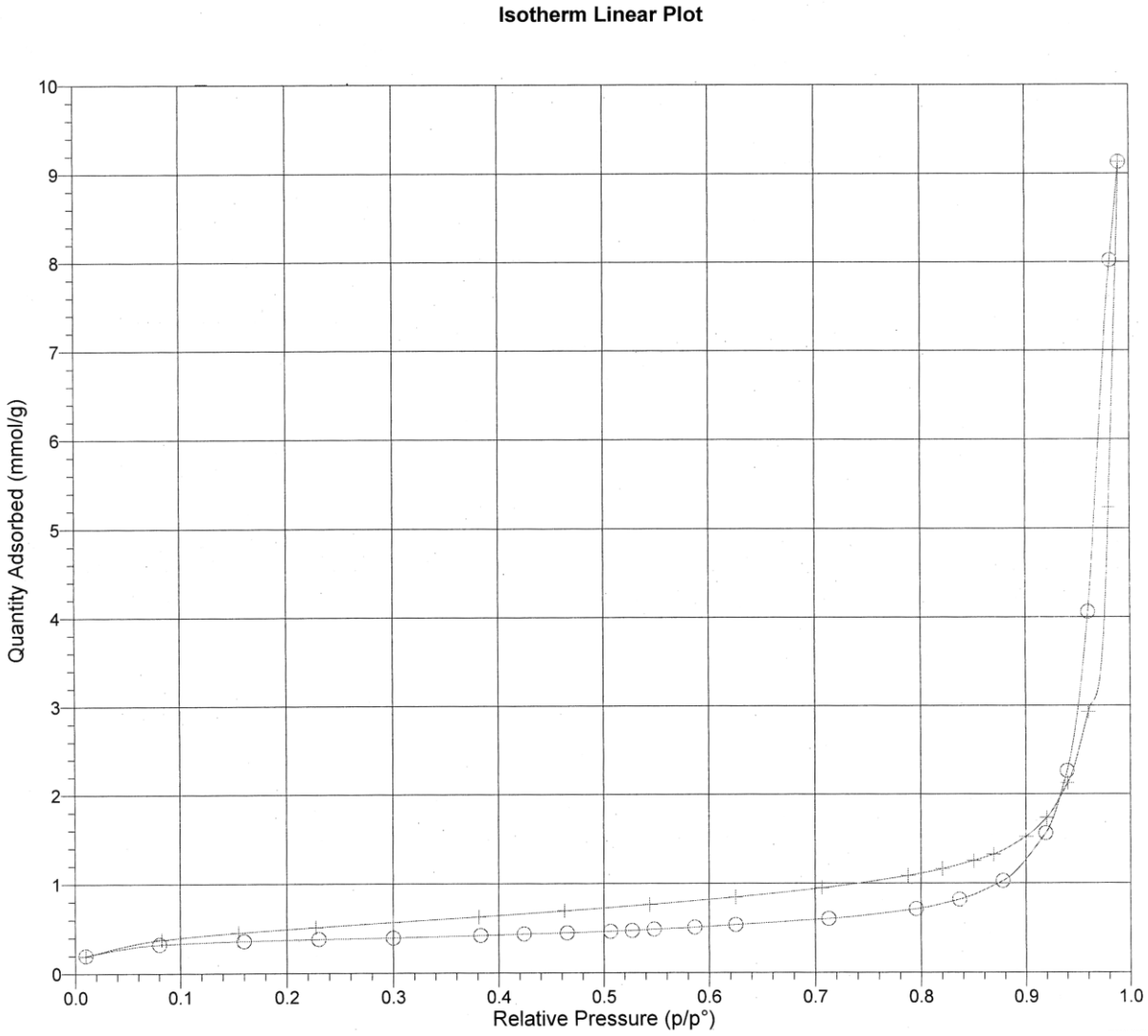

FIGURE A-1 The BET isotherm from the adsorption and desorption of N_2 at 77K on resin 2 dried at 90°C. The crosses correspond to data points in the adsorption phase, the circles correspond to data points in the desorption phase.

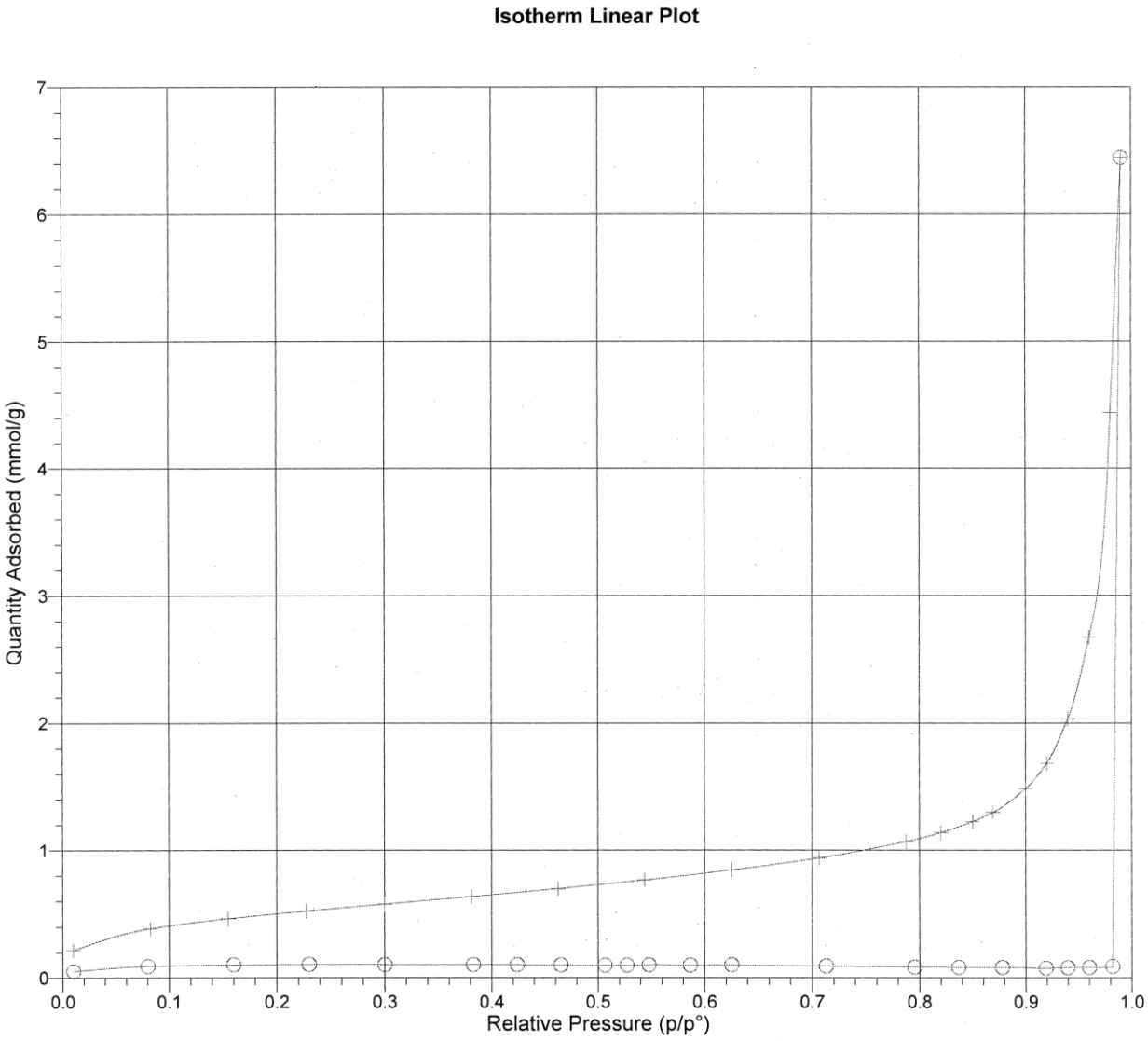

FIGURE A-2 The BET isotherm from the adsorption and desorption of N_2 at 77K on resin 2 dried at 120°C. The crosses correspond to data points in the adsorption phase, the circles correspond to data points in the desorption phase.

In Figure A-1 both adsorption and desorption curves follow similar BET isotherm pattern. In Figure A-2, adsorption curve follows BET isotherm but the desorption data points are near to zero values. The desorption for resin sample 2 does not follow BET isotherm and is thus unsuccessful.

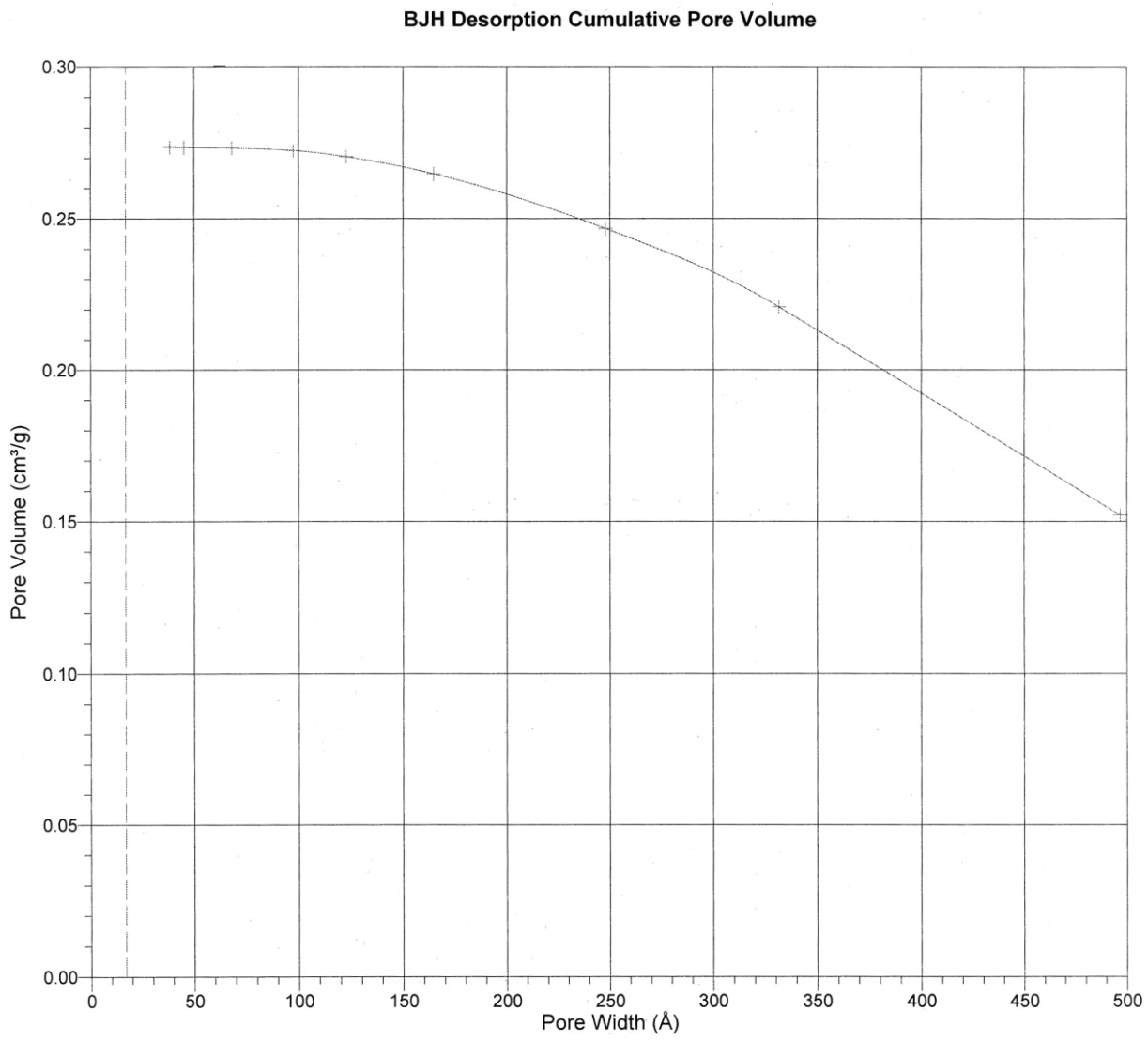

FIGURE A-3 The BJH cumulative pore volume from the desorption of N_2 at 77K on resin 2 dried at 90^{o}C.

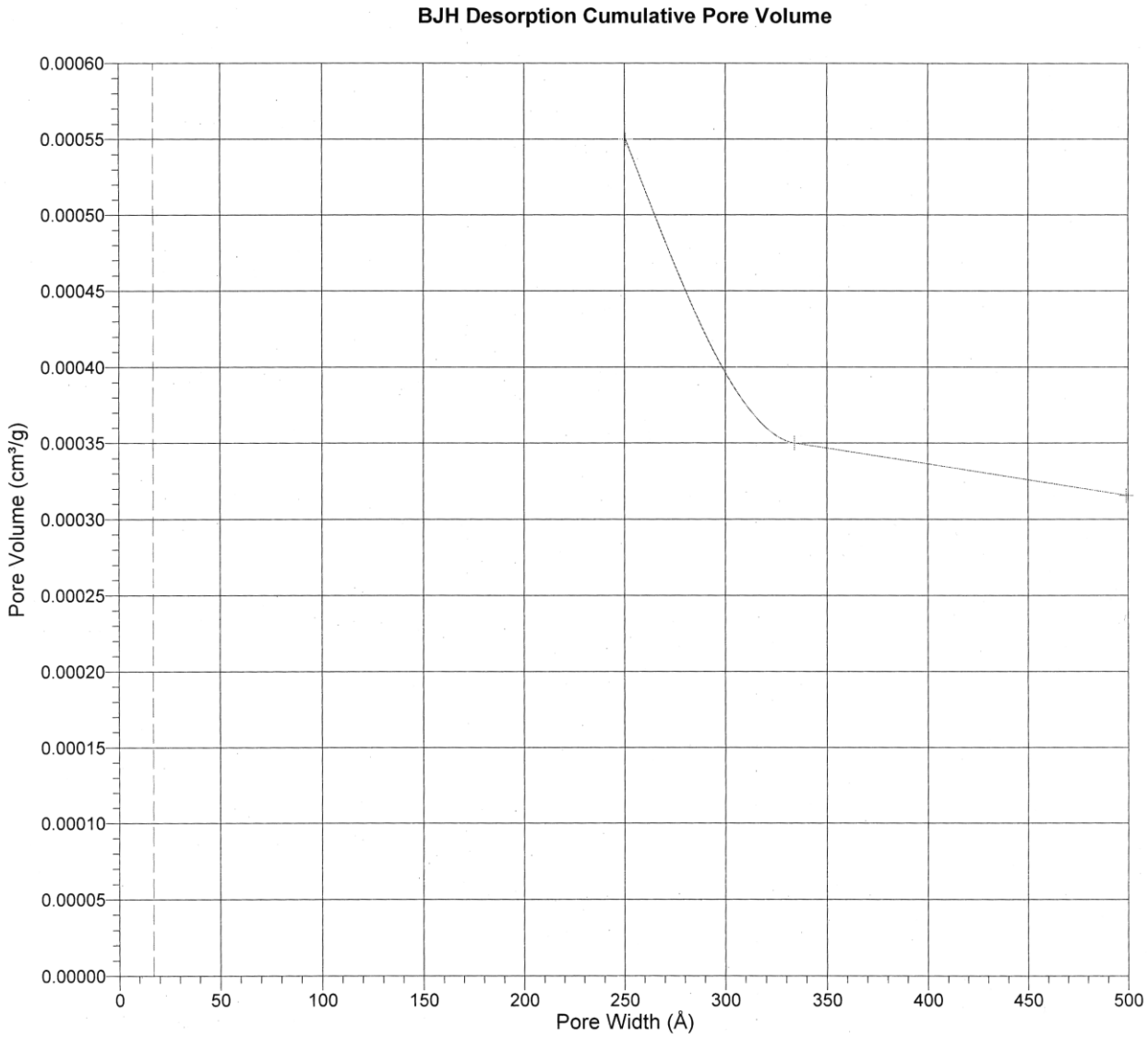

FIGURE A-4 The BJH cumulative pore volume from the desorption of N_2 at 77K on resin 2 dried at 120^{o}C.

In Figure A-3 the BJH desorption cumulative pore volume consists of multiple points and a reasonable plot was obtained. In Figure A-4 the corresponding plot has only 3 data points, which indicates that the experiment for sample 2 was not successful.

Appendix IV- The porosity evaluation

Specific gravity was determined to calculate the skeletal density of resin 1, which in turn could be used to determine porosity.

$$S.G. = \frac{S}{(W + S - SW)} \qquad \text{(A-2)}$$

Where
$S.G$ specific gravity,
S dry sample weighed to pycnometer,
W weight of water in pycnometer,
SW weight of sample and water in pycnometer.

Specific gravity was determined by Equation (2) from resin 1 in 3 separate measurements using a Gay-Lussac pycnometer. The results from the pycnometer measurements are in Table V.

TABLE A-V Masses of dry samples, water and dry samples plus water in pycnometer, and the gained specific gravities. The sample was resin 1, and water temperature was 20°C.

Measurement	S (g)	W (g)	SW (g)	S.G.
1	7.456	145.200	146.562	1.224
2	10.513	150.160	152.120	1.229
3	13.149	145.180	147.620	1.228

The mean of the specific gravities in Table V is 1.227. The density of water at 20°C is approximately 0.9982 g/cm^3. When these are multiplied, the skeletal density is

$$\rho_s = 1224.8 \text{ g/cm}^3$$

Cumulative pore volume of resin 1 corresponding to sample 1: $V_p = 0.0896\ cm^3/g$

The internal porosity of resin 1 thus:

$$\varepsilon_p = V_p \cdot \rho_s = 0.0896\ cm^3/g \cdot 1224.8 \text{ g/cm}^3 \approx 0.110$$

Appendix IV- FTIR peaks

TABLE A-VI List of peaks and wavenumber ranges used to analyse FTIR spectra. PS refers to polystyrene. RS corresponds to start of a wavenumber range and RE corresponds to the end of the range.

$1/\lambda/cm^{-1}$	Assigment	Species	Source	Other
540	-	PS	[27]	
698	-	PS	[27]	
842	-	PS	[27]	
906	-	PS	[27]	
1028	-	PS	[27]	
1069	-	PS	[27]	
1154	-	PS	[27]	
1181	-	PS	[27]	
1320	$NCOO^-$ skeletal vibration	carbamate	[25]	
1332	$NCOO^-$ skeletal vibration	carbamate	[28]	
1335	symmetric $NCOO^-$ bands	ionic carbamate	[29]	RS
1430	symmetric $NCOO^-$ bands	ionic carbamate	[29]	RE
1381	symmetric stretching $NCOO^-$	ionic carbamate	[30]	
1385	symmetric stretching $NCOO^-$	carbamate	[28]	
1412	σ CH_2…H	amines	[29]	
1439	symmetric stretching $NCOO^-$	carbamate	[28]	
1431	$NCOO^-$ skeletal vibration	carbamate	[25]	
1450	σ CH_2	amines	[29]	
1469	-	bicarbonate	[25]	
1480	NH deformation	ionic carbamate	[30]	
1482	$NCOO^-$ skeletal vibration	carbamate	[25]	
1484	$NH3^+$ symmetric deformation	NH_3^+	[30]	
1485	$NH3^+$ symmetric deformation	ionic carbamate	[29]	RS
1550	symmetric NH_3^+ deformation	ionic carbamate	[29]	RE
1493	-	PS	[27]	
1500	symmetric NH^+ deformation	ammonium ion	[28]	
1510	CHN group	bound carbamate	[29]	
1517	carbonyl stretch	carbamate & bicarbonate	[25]	
1549	-	bicarbonate	[25]	
1550	asymmetric stretching $NCOO^-$	carbamate	[28]	
1565	$NCOO^-$ stretching	carbamate	[25]	
1564	symmetric $NCOO^-$ bands	ionic carbamate	[29]	
1580	asymmetric NH_3^+ deformation	NH_3^+	[30]	
1583	-	PS	[27]	
1597	Bending NH	amines	[29]	
1601	-	PS	[27]	
1626	asymmetric NH_3^+ deformation	ammonium ion	[28]	

1625	NH_3^+ deformation	ionic carbamate	[29]	
1633	asymmetric NH_3^+ deformation	NH_3^+	[30]	
1643	Bending NH (no H bonding)	amines	[29]	
1680	C=O stretch	carbamic acid	[30]	RS
1700	C=O stretch	carbamic acid	[30]	RE
1688	C=O stretch	carbamic acid	[28]	
1714	C=O stretch	bound carbamate	[29]	
1802	-	PS	[27]	
1871	-	PS	[27]	
1944	-	PS	[27]	
2160	NH_3^+ asymmetric deformation and twisting	NH_3^+	[30]	
2338	NH_3^+ asymmetric deformation and twisting	NH_3^+	[30]	
2365	CO_2 asymmetric stretch	physisorbed linear CO_2	[30]	
2500	NH_3^+ symmetric stretch	ionic carbamate	[29]	
2850	-	PS	[27]	
2870	CH Stretch	amines	[29]	
2924	-	PS	[27]	
2935	CH Stretch	amines	[29]	
2958	CH Stretch	amines	[29]	
3001	-	PS	[27]	
3026	-	PS	[27]	
3060	-	PS	[27]	
3082	-	PS	[27]	
3104	-	PS	[27]	
3300	NH_2 symmetric stretch	amines	[30]	
1800	NH stretch, hydrogen-bonded	amines	[30]	RS
3300	NH stretch, hydrogen-bonded	amines	[30]	RE
3330	NH stretch	amines	[29]	RS
3400	NH stretch	amines	[29]	RE
3375	NH_2 symmetric stretch	amines	[30]	
3380	loss band NH stretch	ionic carbamate	[29]	
3440	NH stretch	ionic carbamate	[29,30]	RS
3450	NH stretch	ionic carbamate	[29,30]	RE
3650	Hydrogen-bonded hydroxyls	amines	[29]	RS
3740	Hydrogen-bonded hydroxyls	amines	[29]	RE
3748	isolated hydroxyls	amines	[29]	

Appendix V-Thermal degradation using STA

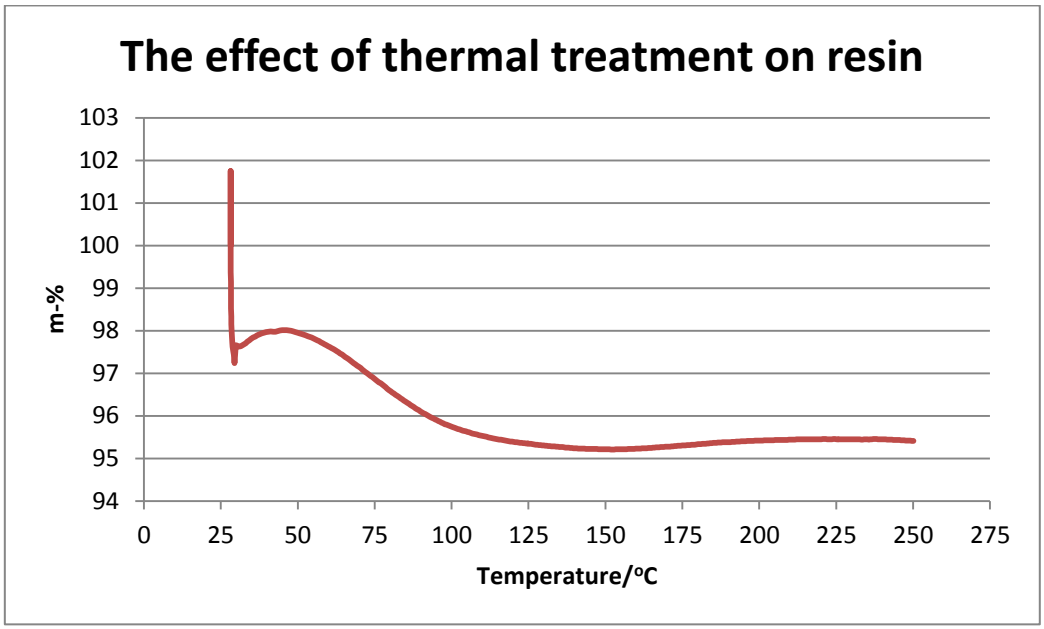

FIGURE A-1 The mass-% profile of resin 1 in N_2 flowing at 50 ml/min with increasing temperature.

Appendix VI-SEM-EDS analysis areas

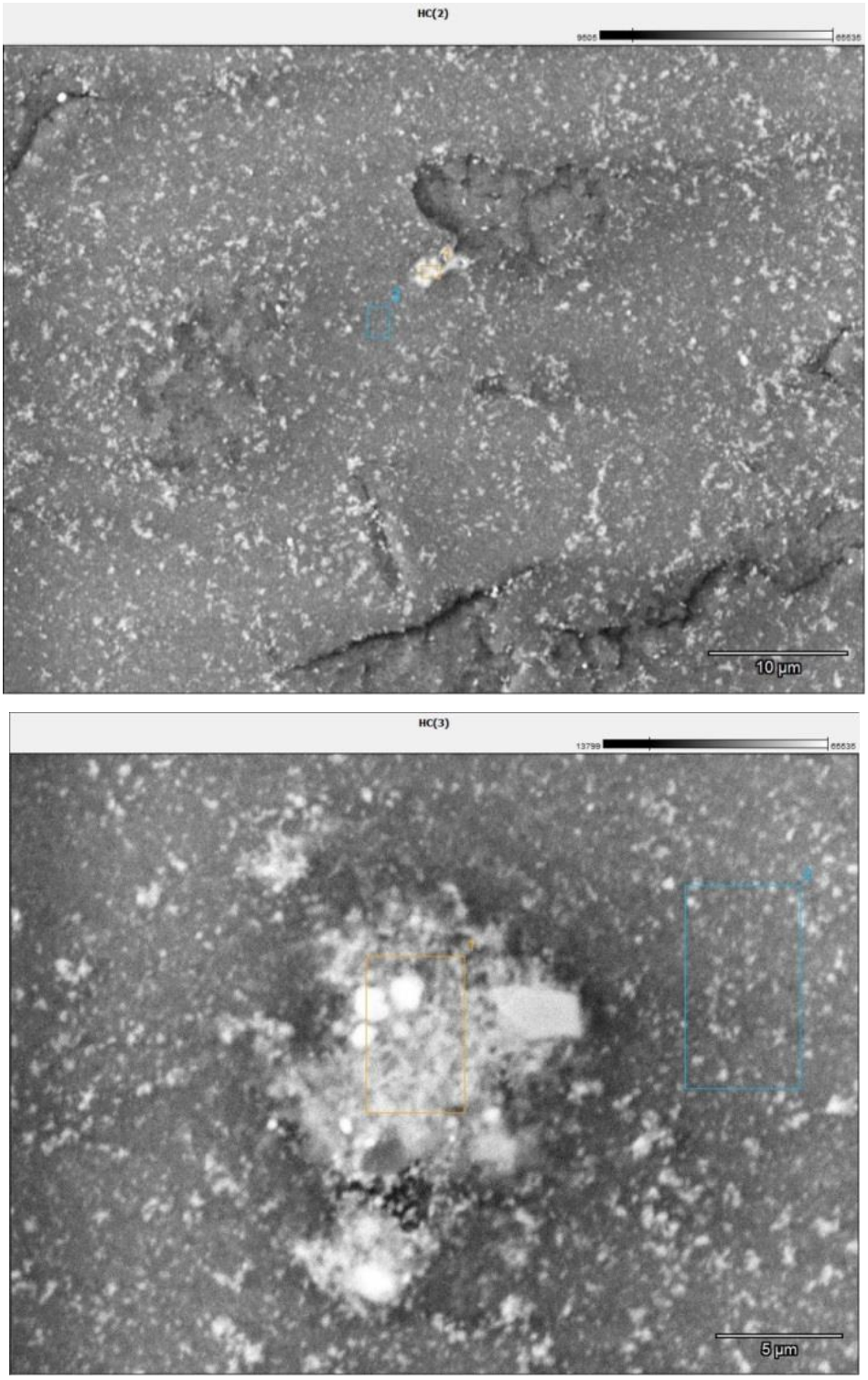

FIGURE A-2 The areas of resin 1 on which SEM-EDS was conducted. The upper figure corresponds to the first measurement area, and the lower to the second measurement area.

Appendix VII-STA adsorptions

Smoothening the N_2 adsorption mass profile

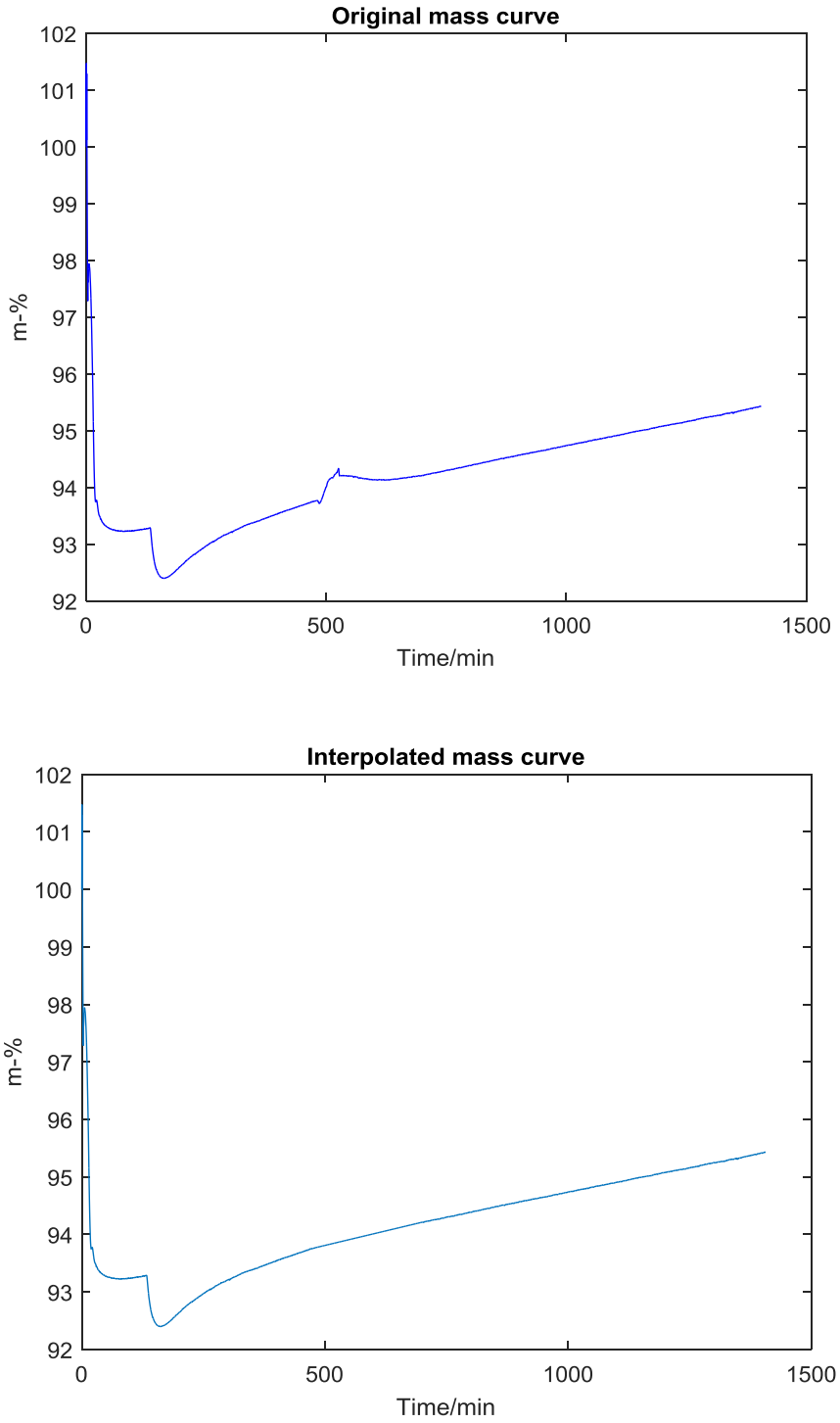

FIGURE A-3 The original mass-% profile gained with STA using only nitrogen at 50 ml/min on resin 1 in the upper figure. By interpolating the section in the range of 480-700 minutes, mass-% profile in the lower figure was gained.

Calculation of the adsorption capacity

The calculation procedures used to gain the adsorption capacity profiles are presented here. Sample tested at 25°C and 400ppm CO_2 with drying at 90°C is taken as an example. The final adsorption capacity after 20 hours of adsorption is calculated.

$$m_{sample} = 10.1mg$$

Interpolated nitrogen adsorption data (see Figure A-3) was first used to correct the STA mass-% profiles (Figure A-4), and so the mass-% change profiles were gained.

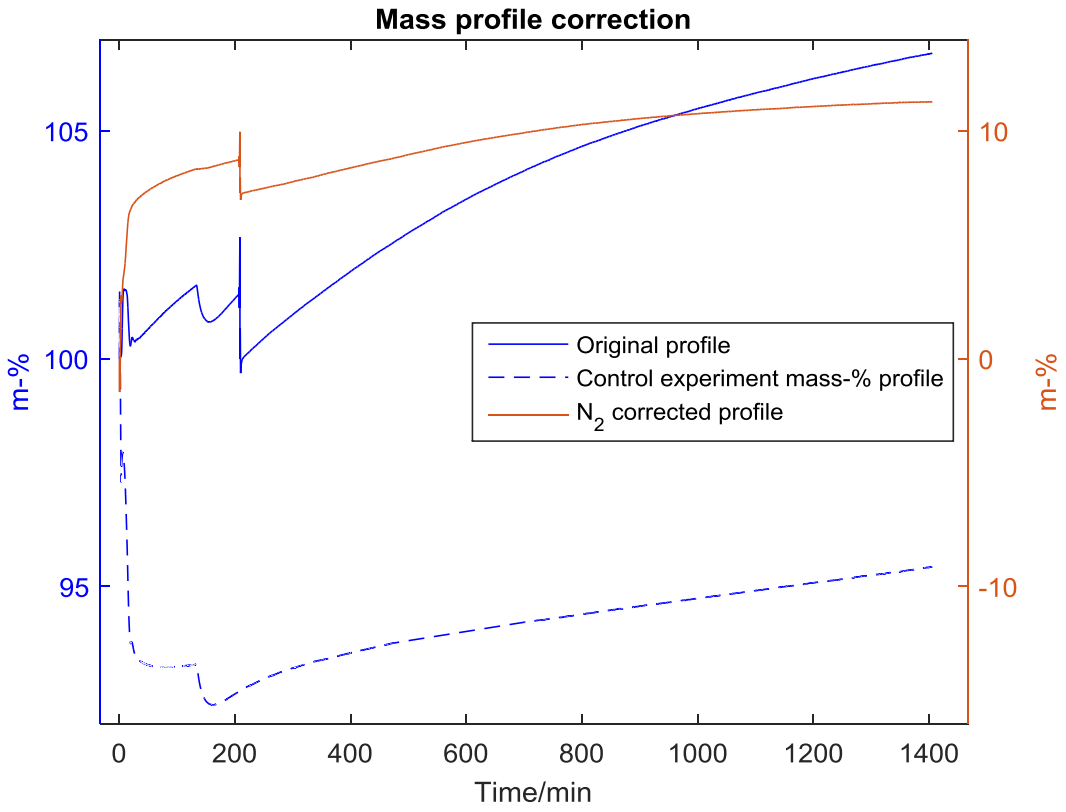

FIGURE A-4 Correction of STA mass-% profile with control experiment data. The corrected mass-% profile was gained by subtracting the control experiment data from the original data. The original mass-% profile was gained by using 400 ppm CO_2 at 50 ml/min on resin 1. Drying temperature was 90°C, and adsorption temperature was 25°C. The control experiment was conducted in similar conditions but with only N_2.

In Figure A-4, the point at which the data variation caused by CO_2 introduction is levelled is at

$$t = 215\ min\text{: } \Delta m(\%) = 7.27242\%$$

In Figure A-4, the point at which adsorption is stopped is at

$t = 1405.6\,min$: $\Delta m(\%) = 11.269\%$

Thus, the mass change caused by CO_2:

$$\Delta m(\%)_{CO_2} = 11.269\% - 7.27242\% = 3.99658\%$$

$$\Delta m_{CO_2} = \Delta m(\%)_{CO_2} \cdot m_{sample} = \frac{3.99658\%}{100\%} \cdot 10.1mg \approx 0.40365mg$$

The adsorption capacity is then:

$$q = \frac{\Delta m_{CO_2}}{M_{CO_2}} : m_{sample} = \frac{0.40365mg}{\frac{44.01g}{mol}} : 10.01mg = \frac{0.00040365g}{44.01\frac{g}{mol}} : 0.0101g \approx 0.000908\frac{mol}{g}$$

$$q = 0.908mmol/g$$

The conditions and maximum adsorption capacities in STA experiments

TABLE A-VII Summary of the pre-treatment of resin samples, conditions in the simultaneous thermal analysis, and the adsorption capacities calculated from the gained data. The mass-% changes of a sample in a control experiment with only N_2 flow were subtracted from the results. The pre-treatment, if any, was conducted in vacuum oven under 60-100mbar.

c_{CO2}	$t_{adsorption}$/h	$T_{pretreatment}$/^oC	T_{drying}/^oC	$T_{adsorption}$/^oC	q/(mmol$_{CO2}$/g$_{sorbent}$)
400ppm	24	120	120	25	0.753
400ppm	24	-	90	25	0.824
400ppm	20	90	90	25	0.908
400ppm	20	90	90	35	0.492
400ppm	20	90	90	50	0.046
1 %	2	90	90	25	1.073

References used in the appendices

[1] a S.M. Chong, X.S. Zhao, Functionalization of SBA-15 with APTES and characterization of functionalized materials, J. Phys. Chem. B. 107 (2003) 12650–12657.

[2] Y. Cho, J.Y. Lee, A.D. Bokare, S.B. Kwon, D.S. Park, W.S. Jung, et al., LiOH-embedded zeolite for carbon dioxide capture under ambient conditions, J. Ind. Eng. Chem. 22 (2014) 350–356.

[3] S. Choi, M.L. Gray, C.W. Jones, Amine-tethered solid adsorbents coupling high adsorption capacity and regenerability for CO2 capture from ambient air, ChemSusChem. 4 (2011) 628–635.

[4] Y. Kuwahara, D.Y. Kang, J.R. Copeland, N. a. Brunelli, S. a. Didas, P. Bollini, et al., Dramatic enhancement of CO2 uptake by poly(ethyleneimine) using zirconosilicate supports, J. Am. Chem. Soc. 134 (2012) 10757–10760.

[5] S. Choi, J.H. Drese, P.M. Eisenberger, C.W. Jones, Application of amine-tethered solid sorbents for direct CO2 capture from the ambient air, Environ. Sci. Technol. 45 (2011) 2420–2427.

[6] S. a. Didas, A.R. Kulkarni, D.S. Sholl, C.W. Jones, Role of amine structure on carbon dioxide adsorption from ultradilute gas streams such as ambient air, ChemSusChem. 5 (2012) 2058–2064.

[7] J.A. Wurzbacher, C. Gebald, A. Steinfeld, Separation of CO2 from air by temperature-vacuum swing adsorption using diamine-functionalized silica gel, Energy Environ. Sci. 4 (2011) 3584–3592.

[8] A. Goeppert, H. Zhang, M. Czaun, R.B. May, G.K.S. Prakash, G. a. Olah, et al., Easily regenerable solid adsorbents based on polyamines for carbon dioxide capture from the air, ChemSusChem. 7 (2014) 1386–1397.

[9] F.Q. Liu, L. Wang, Z.G. Huang, C.Q. Li, W. Li, R.X. Li, et al., Amine-tethered adsorbents based on three-dimensional macroporous silica for CO2 capture from simulated flue gas and air, ACS Appl. Mater. Interfaces. 6 (2014) 4371–4381.

[10] J. Wang, H. Huang, M. Wang, L. Yao, W. Qiao, D. Long, et al., Direct capture of low-concentration CO2 on mesoporous carbon-supported solid amine adsorbents at ambient temperature, Ind. Eng. Chem. Res. 54 (2015) 5319–5327.

[11] W. Chaikittisilp, H.J. Kim, C.W. Jones, Mesoporous alumina-supported amines as potential steam-stable adsorbents for capturing CO2 from simulated flue gas and ambient air, Energy and Fuels. 25 (2011) 5528–5537.

[12] M.A. Sakwa-Novak, C.W. Jones, Steam induced structural changes of a poly(ethylenimine) impregnated γ-alumina sorbent for CO2 extraction from ambient air, ACS Appl. Mater. Interfaces. 6 (2014) 9245–9255.

[13] W. Lu, J.P. Sculley, D. Yuan, R. Krishna, H.-C. Zhou, Carbon dioxide capture from air using amine-grafted porous polymer networks, J. Phys. Chem. 117 (2013) 4057–4061.

[14] H. He, M. Zhong, D. Konkolewicz, K. Yacatto, T. Rappold, G. Sugar, et al., Three-dimensionally ordered macroporous polymeric materials by colloidal crystal templating for reversible CO2 capture, Adv. Funct. Mater. 23 (2013) 4720–4728.

[15] H. He, W. Li, M. Lamson, M. Zhong, D. Konkolewicz, C.M. Hui, et al., Porous polymers prepared via high internal phase emulsion polymerization for reversible CO2 capture, Polym. (United Kingdom). 55 (2014) 385–394.

[16] C. Gebald, J.A. Wurzbacher, P. Tingaut, T. Zimmermann, A. Steinfeld, Amine-based nanofibrillated cellulose as adsorbent for CO2 capture from air, Environ. Sci. Technol. 45 (2011) 9101–9108.

[17] J.A. Wurzbacher, C. Gebald, N. Piatkowski, A. Steinfeld, Concurrent separation of CO2 and H2O from air by a temperature-vacuum swing adsorption/desorption cycle, Environ. Sci. Technol. 46 (2012) 9191–9198.

[18] C. Gebald, J. a. Wurzbacher, P. Tingaut, A. Steinfeld, Stability of amine-functionalized cellulose during temperature-vacuum-swing cycling for CO2 capture from air, Environ. Sci. Technol. 47 (2013) 10063–10070.

[19] H. Sehaqui, M.E. Gálvez, V. Becatinni, Y. cheng Ng, A. Steinfeld, T. Zimmermann, et al., Fast and reversible direct CO2 capture from air onto all-polymer nanofibrillated cellulose—polyethylenimine foams, Environ. Sci. Technol. 49 (2015) 3167–3174.

[20] T.M. McDonald, W.R. Lee, J. a. Mason, B.M. Wiers, C.S. Hong, J.R. Long, Capture of carbon dioxide from air and flue gas in the alkylamine-appended metal-organic framework mmen-Mg2(dobpdc), J. Am. Chem. Soc. 134 (2012) 7056–7065.

[21] W.R. Lee, S.Y. Hwang, D.W. Ryu, K.S. Lim, S.S. Han, D. Moon, et al., Diamine-functionalized metal–organic framework: exceptionally high CO2 capacities from ambient air and flue gas, ultrafast CO2 uptake rate, and adsorption mechanism, Energy Environ. Sci. 7 (2014) 744–751.

[22] O. Shekhah, Y. Belmabkhout, Z. Chen, V. Guillerm, A. Cairns, K. Adil, et al., Made-to-order metal-organic frameworks for trace carbon dioxide removal and air capture, Nat. Commun. 5 (2014) 4228–4234.

[23] T. Wang, K.S. Lackner, A. Wright, Moisture swing sorbent for carbon dioxide capture from ambient air, Environ. Sci. Technol. 45 (2011) 6670–6675.

[24] T. Wang, J. Liu, M. Fang, Z. Luo, A moisture swing sorbent for direct air capture of carbon dioxide: Thermodynamic and kinetic analysis, Energy Procedia. 37 (2013) 6096–6104.

[25] W.R. Alesi, J.R. Kitchin, Evaluation of a primary amine-functionalized ion-exchange resin for CO2 capture, Ind. Eng. Chem. Res. 51 (2012) 6907–6915.

[26] Z. Chen, S. Deng, H. Wei, B. Wang, J. Huang, G. Yu, Polyethylenimine-impregnated resin for high CO2 adsorption: An efficient adsorbent for CO2 capture from simulated flue gas and ambient air, ACS Appl. Mater. Interfaces. 5 (2013) 6937–6945.

[27] L.M. Hanssen, C. Zhu, Wavenumber standards for mid-infrared spectrometry, in: Handb. Vib. Spectrosc., 2002.

[28] M.A. Alkhabbaz, P. Bollini, G.S. Foo, C. Sievers, C.W. Jones, Important roles of enthalpic and entropic contributions to CO2 capture from simulated flue gas and ambient air using mesoporous silica grafted amines, J. Am. Chem. Soc. 136 (2014) 13170–13173.

[29] A. Danon, P.C. Stair, E. Weitz, FTIR study of CO2 adsorption on amine-grafted SBA-15: Elucidation of adsorbed species, J. Phys. Chem. 115 (2011) 11540–11549.

[30] Z. Bacsik, N. Ahlsten, A. Ziadi, G. Zhao, A.E. Garcia-bennett, B. Martin-Matute, et al., Mechanisms and kinetics for sorption of CO2 on bicontinuous mesoporous silica modified with n-propylamine, Langmuir. 27 (2011) 11118–11128.